

**Spontaneous Imbibition and Imbibition Oil Recovery in Tight
Formations**

by

Ali Javaheri

A thesis submitted in partial fulfillment of the requirements for the degree of

Master of Science

in

Petroleum Engineering

Department of Civil and Environmental Engineering

University of Alberta

© Ali Javaheri, 2017

Abstract

Advances in the development of unconventional resources have led to a surge in North American oil production. For example, tight oil production has pushed the U.S. crude supply to over 9% of world total production. Therefore, petrophysical characterization of such low-permeability rocks, has become increasingly important for petroleum engineers. Properties such as porosity, permeability, pore throat size, and wettability are of high importance for evaluating production from tight oil formations. This study has two parts. In first part, we measure and analyze spontaneous imbibition of water and oil into five twin core plugs drilled from the cores of a well drilled in the Montney Formation, an unconventional oil and gas play in Western Canadian Sedimentary Basin (WCSB). We characterize the samples by measuring the mineralogy using XRD (x-ray diffraction), total organic carbon content, porosity, and permeability. In order to quantify wettability of the core plugs, we define two wettability indices for the oil phase based on the slope and equilibrium values of water and oil imbibition curves. We observe that the two indices decrease by increasing neutron porosity and gamma ray parameters measured by wireline logging tools. Our results demonstrate that porosity is a key parameter controlling the fluid uptake of tight rock core samples from the Montney formation. Furthermore, we propose a decoupling scheme for pore-network characterization of core plugs based on their porosity and permeability. In second part, we apply dual-core imbibition (DCI) method on several Montney core plugs and introduce imbibition-recovery (IR) trio to investigate the recovery mechanisms in rocks with dual-wettability pore network. We comparatively analyze the spontaneous imbibition data from the first part and the recovery data of the second part in one imbibition recovery trio (oil imbibition, brine imbibition, and imbibition oil recovery). For each twin set, the oil recovery curve follows the trend of brine imbibition curve, and the final oil recovery is always less than the equilibrated water uptake of dry samples. This observation indicates that water can only access the hydrophilic part of the pore network initially saturated with oil. Finally, we introduce a porosity-based model to analyze recovery data.

ACKNOWLEDGEMENTS

It is with tremendous gratitude that I acknowledge the support and help of my supervisor Dr. Hassan Dehghanpour for his valuable guidance and encouragement through the learning process of this master thesis. He has always been accessible and willing to help me with my research. His kindness and encouragement will be engraved on my mind.

I also acknowledge James Wood for his useful discussion and guidance. I am also thankful to Engineering Technologist Todd Kinnee for his help and assistance in conducting laboratory experiments.

Contents

| | |
|---|-----------|
| Chapter 1 | 1 |
| Wettability: A comparative study on standard methods..... | 1 |
| Wettability | 1 |
| Methods to Measure Wettability | 1 |
| Quantitative Wettability Measurement Methods | 2 |
| Qualitative Wettability Measurement Techniques | 8 |
| Summary..... | 10 |
| Dual core imbibition (DCI) method | 11 |
| Summary..... | 15 |
| References..... | 17 |
| Chapter 2 | 19 |
| Tight Rock Wettability and Its Relationship to | 19 |
| Other Petrophysical Properties | 19 |
| Abstract..... | 19 |
| Introduction..... | 19 |
| Materials | 21 |
| Methodology | 27 |
| Results and Discussions | 29 |
| Conclusions..... | 41 |
| Nomenclature | 42 |
| Reference | 45 |
| Chapter 3 | 52 |
| Application of imbibition transient analysis in pore network characterization of tight rocks | 52 |
| Abstract..... | 52 |
| Introduction..... | 53 |
| Materials | 54 |
| Results, Models and Discussions..... | 59 |
| Conclusions..... | 71 |
| References..... | 72 |
| Chapter 4 | 74 |
| Investigating Imbibition Oil Recovery in Dual-Wettability Media: A Montney Case Study | 74 |
| Abstract..... | 74 |

| | |
|---|-----|
| Introduction | 75 |
| Materials | 77 |
| Methodology, Results and Discussions | 86 |
| Conclusions | 101 |
| References | 103 |
| Chapter 5 | 106 |
| Conclusions | 106 |

List of Figures

Chapter 1

| | |
|--|----|
| Figure 1 - Schematics of (a) oil-wet and (b) water-wet states of wettability on a microscopic level..... | 9 |
| Figure 2 - Contact angle measurement by sessile drop method..... | 11 |
| Figure 3 - Contact angle measurement by modified sessile drop method..... | 12 |
| Figure 4 - Spontaneous imbibition of water and displacement of oil by the rock sample..... | 13 |
| Figure 5 - Forced imbibition of water by rock sample in the Amott method..... | 15 |
| Figure 6 - Spontaneous imbibition of oil and displacement of water by the rock sample..... | 16 |
| Figure 7 - Forced imbibition of oil by rock sample in the Amott method..... | 17 |
| Figure 8 - USBM wettability test capillary curve neutral wet rock sample..... | 17 |
| Figure 9 – Affinity chart (left), Contact angle test (right)..... | 18 |
| Figure 10 – Spontaneous imbibition setup for DCI method (left), spontaneous imbibition results from DCI method (right)..... | 20 |
| Figure 11- Recovery plots during recovery tests. Recovered oil is captured at different times, (a) $t=0$ Hrs, (b) $t=60$ Hrs, (c) $t=180$ Hrs..... | 22 |
| Figure 12 - Imbibition recovery graph-trio consists of three curves. Oil spontaneous imbibition curve, brine spontaneous imbibition curve and recovery curve, plotted versus time..... | 23 |
| Figure 13 – Forced imbibition setup..... | 26 |
| Figure 14 – Forced imbibition recovery factor versus porosity (a), Recovery factors for a sample with porosity=0.03 at versus pressure (b)..... | 27 |

Chapter 2

| | |
|--|----|
| Figure 1. Geochemical log for the zone of interest..... | 32 |
| Figure 2. Location of the samples in the zone of interest..... | 33 |
| Figure 3. Illustration of the experimental set-up for oil and brine imbibition into twin core plugs..... | 34 |
| Figure 4. Brine (A) and oil (B) droplets equilibrated on rock surface at the presence of air..... | 36 |

| | |
|--|----|
| Figure 5. Normalized imbibed volume of brine and oil versus time. O and B represent oil and brine, respectively..... | 38 |
| Figure 6. Multivariate scatterplots for five variables: I_w , I_o , NPOR, GR and MICP porosity..... | 40 |
| Figure 7. I_w and Clay content histograms for all five samples..... | 41 |
| Figure 8. Oil and brine imbibition profiles versus square root of time..... | 43 |
| Figure 9. WI_o^{eq} versus other petrophysical properties..... | 46 |
| Figure 10. m_w versus m_o for the five twin plugs..... | 48 |
| Figure 11. WI_o^{sl} versus other petrophysical properties..... | 50 |

Chapter 3

| | |
|--|----|
| Figure 1. Twin imbibition cells showing oil and brine imbibing into twin core plugs..... | 63 |
| Figure 2. Imbibed mass of brine and versus with time and square root of time..... | 64 |
| Figure 3. Brine spontaneous imbibition profile for MTW6..... | 65 |
| Figure 4. Schematics for imbibition characterization..... | 67 |
| Figure 5. Schematics for spontaneous imbibition into type I and type II pore networks..... | 68 |
| Figure 6. Schematics of the decoupling model for MT-6..... | 70 |
| Figure 7. Pore size distribution of four Rock samples..... | 72 |
| Figure 8. SEM images for MT-6..... | 74 |

Chapter 4

| | |
|--|----|
| Figure 1. Contact angle of oil droplet in brine at the surface of rock sample (a). Contact angle of brine droplet in oil at the presence of rock sample (b)..... | 84 |
| Figure 2. Affinity chart with data points from four set of core plugs from Montney formation. Horizontal axis represents contact angle of oil droplet in brine at the surface of rock sample. Vertical axis represents contact angle of brine droplet in oil at the presence of rock sample..... | 85 |
| Figure 3. Schematics of spontaneous oil and brine imbibition into one set of twin plug. The weight gain of the plugs is constantly measured by a precision digital weight..... | 86 |
| Figure 4. Spontaneous oil and brine imbibition (volumetric) versus time for the four sets of twin plugs..... | 87 |

| | |
|--|----|
| Figure 5. Multivariate scatterplots for the three variables: Porosity, Permeability and Median pore throat size..... | 88 |
| Figure 6. Multivariate scatterplots for logarithm of three variables: Porosity, Permeability and Median pore throat size..... | 89 |
| Figure 7. Brine and oil spontaneous imbibition data on a logarithmic scale versus time..... | 90 |
| Figure 8. Recovery setup for imbibition recovery tests. Oil saturated plugs are placed in brine and brine saturated plugs are placed in oil..... | 90 |
| Figure 9. (a) recovered oil covering the top surface of MT2 (b) recovered oil covering the top surface of MT3 in laminas (c) recovered oil along a fracture line of MT5 at after t=10 days (d) recovered oil along a fracture line of MT5 after t=20 days..... | 91 |
| Figure 10. Recovery plots during recovery tests. Recovered oil is captured at different times, (a) t=0 Hrs, (b) t=60 Hrs, (c) t=180 Hrs..... | 92 |
| Figure 11. Imbibition recovery graph-trio consists of three curves. Oil spontaneous imbibition curve, brine spontaneous imbibition curve and recovery curve, plotted versus time..... | 94 |
| Figure 12. Imbibition recovery graph-trios for the four twin plugs..... | 95 |

List of Tables

| | |
|--|----|
| Table 1. Wettability state corresponding to different index values..... | 16 |
| Table 2. Summary of wettability measurement techniques..... | 20 |
| Table 3. Advantages and Disadvantages of DCI method..... | 27 |
| Table 1. Clay and TOC content of the five twin plugs..... | 32 |
| Table 2. Porosity and permeability of the five twin plugs..... | 33 |
| Table 3. Minerology of the five twin plugs obtained from XRD analysis..... | 33 |
| Table 4. Brine properties..... | 37 |
| Table 5. Oil properties. | 37 |
| Table 6. The measured values of Total GR, spectra gamma ray, NPOR, MICP porosity, I_w , I_o , WI_o^{eq} for the five twin plugs. | 42 |
| Table 7. The equilibrium values of normalized imbibed volume of oil and brine and the slopes of oil and brine imbibition data versus square root of time. | 47 |
| Table 1. Clay, TOC content, Porosity and permeability of twin plugs. | 64 |
| Table 2. Brine properties. | 64 |
| Table 3. Oil properties. | 65 |
| Table 4. Summary of decoupling scheme. | 74 |
| Table 1. Clay and TOC content of the four twin plugs. | 81 |
| Table 2. Porosity and permeability of the four twin plugs. | 81 |
| Table 3. XRD minerology analysis measured of the four binary pairs. | 82 |
| Table 4. Brine properties. | 83 |
| Table 5. Oil properties. | 83 |

Chapter 1

Wettability: A comparative study on standard methods

Wettability

Wettability is defined as preference of one fluid to spread on a solid surface in the presence of other immiscible fluids [1]. From a practical point of view, wettability can be described as the relative affinity of a surface to be coated by a certain fluid when other fluids are present [2]. Wettability phenomena can well be understood by investigating the intermolecular interactions between the fluids and the solids [3]. Wettability studies are widely carried out on reservoir rocks due to its significance in oil production in the oil industry. Wettability, is one of major factors that control saturation distribution and fluid flow within porous media [3]. Subsequently, wettability effects alters other petrophysical properties such as capillary pressure, relative permeability, waterflood behavior, electrical and geochemical properties [7-9].

Methods to Measure Wettability

Over time, numerous methodologies have been developed by industry and academia to establish sound protocols to evaluate wettability of rocks. All techniques developed, have categorized wettability of rocks in to three major classes: 1. Oil-wet: is the state of the rock when oil, in company of other fluids (i.e. water), preferentially covers the rock surface. This results in most of the rock surface be covered by oil, as seen in Figure 1(a).

2. Water-wet: is the state of the rock when water, in presence of other fluids (i.e. oil), preferentially covers the rock surface. This results in most of the rock surface be covered by water, as seen in Figure 1(b).

3. Neutral wet: is the state when the rock surface does not have any specific affinity to get covered by either water or oil.



Figure 1 - Schematics of (a) oil-wet and (b) water-wet states of wettability on a microscopic level.

Classifying wettability into distinct categories is relatively inadequate since wettability is not homogeneous and hence covers a wide spectrum. Within such spectrum we can define different variety of other wettability classes such as: mixed wettability, fractional wettability and speckled wetting [5]. We refer to a rock surface as mixed wet when part of the rock surface is covered with oil and some part with water [6]. Fractional wettability is defined as when a fraction of the rock surface is wetted by a fluid, either oil or water [7]. Speckled wetting refers to a phenomena when oil is trapped in pore throats rather than being spread on the surface of the pores [9]. Most of developed wettability methodologies define characterize rock affinity towards oil or brine either quantitatively or qualitatively. One major hurdle with all these techniques is their inability of *in situ* evaluation of the rock surface wettability while the wettability is occurring in real time [10].

Quantitative Wettability Measurement Methods

Quantitative methods of measuring wettability quantify affinity of a rock surface towards oil or brine by associating a numerical value to the affinity of that rock. The most applied quantitative method is contact angle measurements [5]. Amott and the United States Bureau of Mines (USBM) are among methods which are the most commonly and traditionally used techniques in the petroleum industry. However, all these techniques are best suited for characterizing uniform wetting [5].

Contact Angle Method

Contact angle, by definition, is the angle between the fluid-solid interfaces in a single phase fluid-smooth solid system [5]. In theory, the degree of wettability can be determined by contact angle measurements for the solid-water-oil system [11]. Moreover, the contact angle method is regarded as the best wettability measurement method when pure fluids and artificial cores are used because there is no possibility of surfactants or other compounds altering the wettability. The two methods used in the petroleum industry, to measure contact angles, are the sessile drop method and the modified sessile drop method [12]. The sessile drop method allows the measurement of the contact angle with the help of a capillary tube. A drop of the fluid, formed at the end of the tube, is brought in contact with the reservoir surface. The droplet is allowed to age on the surface and the contact angle is measured, as seen in Figure 2 [12].

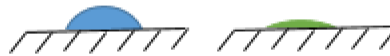


Figure 2 - Contact angle measurement by sessile drop method.

In the modified sessile drop method, the contact angle is measured by placing an oil drop between two crystals so that it contacts a large surface area. After the oil/crystal interface has aged for a few days, the two crystals are displaced parallel to each other, as seen in Figure 3 [12].

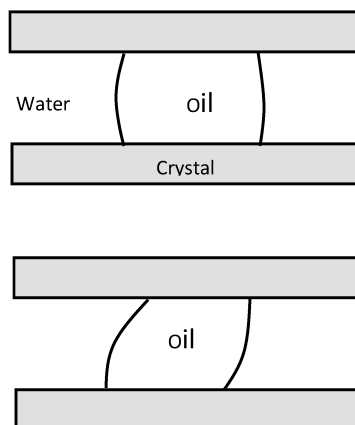


Figure 3 - Contact angle measurement by modified sessile drop method.

As the crystals are displaced, the oil drop shifts and brine adsorbs on a portion of the surface, previously covered by oil. The contact angle measured, as indicated in Figure 3, is referred to as the water advancing contact angle [6]. If the measured contact angle is found to be less than 90 degrees, the rock is regarded as water-wet. If the angle is found equal to 90 degrees, it is regarded as neutral wet and when it is greater than 90, the solid is considered to be oil-wet [5-6]. Contact angle measurements have a few limitations that make it unviable to use for actual reservoir rocks. Specifically speaking, contact angle measurements cannot take into account surface roughness, heterogeneity and complex geometry of the reservoir rock. Additionally, it cannot provide any information regarding the presence or absence of permanently attached organic coatings on the reservoir rocks. The apparatus needs to be very clean and even trace amounts can alter the contact angle [12]. Prior to making measurements, the rock's surface needs to be smooth and often requires drastic treatments such as polishing [5, 16]. A liquid drop, on a surface, can have many different stable contact angles and there is no standard reference to compare the values with [5, 12]. Due to the surfactants in crude, a significant length of time is needed for a contact angle to reach equilibrium [12,13,14]. Furthermore, the required length of equilibration time cannot be reproduced in the lab which leads to reproducibility issues with this measurement technique of wettability [5].

Amott Method

The Amott method was invented in 1959 and since then, it has been an industrial method of measuring wettability [16]. It is a macroscopic means of measuring wettability based on measurements of amounts of fluids that are spontaneously and forcibly imbibed by a rock sample [6]. Initially, oil-saturated rock sample is placed in water where it spontaneously imbibes water and displaces oil, as seen in Figure 4

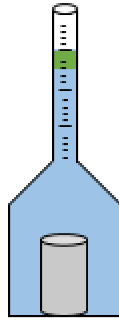


Figure 4 - Spontaneous imbibition of water and displacement of oil by the rock sample.

The sample is then forced to imbibe water by flowing water fluid through the rock sample. As water flows through the sample, it is absorbed by the rock sample and water, stored in the pores, is displaced. The process continues until no more oil is observed to be displaced, as seen from Figure 5, [10].

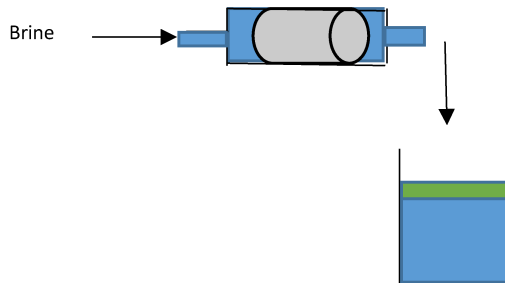


Figure 5 - Forced imbibition of water by rock sample in the Amott method.

The Amott wettability index water ratio (I_w) is then calculated by Equation 1:

$$I_w = \frac{V_a}{V_a + V_b} \quad (1)$$

Where, V_a represents the volume of oil displaced due to spontaneous imbibition of water, and V_b represents the additional volume of oil displaced due to forced imbibition of water. The experiment is then reversed where the rock sample is placed in oil to determine the amount of oil spontaneously imbibed and water

displaced by the rock sample [15]. The rock sample is then forced to absorb additional oil by forced imbibition [10].

The Amott wettability index oil ratio (I_o) is then calculated by Equation 2:

$$I_o = \frac{V_c}{V_c + V_d} \quad (2)$$

Where, represents the volume of water displaced due to spontaneous imbibition of oil, and represents the additional volume of water displaced due to forced imbibition of oil. If is greater than 0, the rock sample is water wet. Additionally, if the is greater than 0, the rock sample is oil wet. At the end of this experiment, the Amott wettability index is calculated, as expressed in Equation 3.

$$W_{IA} = I_w - I_o \quad (3)$$

Table 1 summarizes the values of the indices mentioned above [6].

Table 1. Wettability state corresponding to different index values.

| Index | Oil wet | Neutral wet | Water wet |
|----------|--------------|-------------|------------|
| I_w | 0 | 0 | >0 |
| I_o | >0 | 0 | 0 |
| W_{IA} | -1.0 to -0.3 | -0.3 to 0.3 | 0.3 to 1.0 |

Amott-Harvey Method

The Amott-Harvey method is similar to the Amott method with the addition of a pre-treatment. Before conducting the Amott test, the rock sample is centrifuged under brine and then under crude oil to reduce the initial water imbibition [18].

United States Bureau of Mines (USBM) Method

The USBM method, invented by Erle Donaldson in 1969, is a macroscopic mean of measuring wettability using capillary pressure curves [4]. In contrast to the Amott test, the USBM technique calculates the work required to imbibe oil and water instead of the volumes displaced [6]. Rock samples are initially saturated with brine under vacuum and then placed in oil in a glass core holder. The sample is centrifuged until no more brine can be displaced. The rock sample is then placed in brine in a new core holder filled with brine, inverted and centrifuged. From the amount of oil displaced at each constant speed, measured with a stroboscope, the USBM test capillary pressure curve can be obtained, as seen in Figure 6 [4].

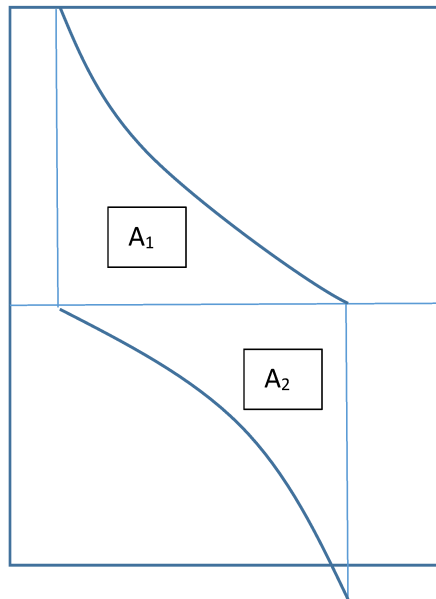


Figure 6 - USBM wettability test capillary curve neutral wet rock sample.

A limitation with the USBM method is that the rock sample can only be defined strictly by oil-wet, water-wet or neutral wet, indicated by -1, 1 or 0, respectively.

Qualitative Wettability Measurement Techniques

Qualitative wettability measurement techniques state the wettability of a reservoir rock without giving any numerical value that could indicate the degree of wettability. The common techniques include imbibition rates method, microscopic examination method, flotation method, nuclear magnetic resonance (NMR) method and dye adsorption method [6, 12, 19].

Imbibition Rates Method

Imbibition rates method is the most commonly used qualitative method because it gives a quick but rough idea without the need of complex machinery. Simply, the rock sample, at irreducible water saturation (pores filled with water held by capillary forces that will not flow), is initially submerged in brine underneath a graduated cylinder. The imbibition rates and volumes of oil displaced by brine are measured. If the rates are high, this demonstrates a strong water-wet state of wettability. On the contrary, if no water is imbibed, the rock can be regarded as oil-wet or neutrally-wet. The test can be reversed, where rock sample can be driven with oil saturation and submerged in oil. The imbibition apparatus needs to be inverted with the graduated cylinder below the rock sample. If the rock sample imbibes oil at a high rate, the rock is regarded to be oil-wet. If it does not imbibe any fluid from both tests, it can be regarded as neutrally-wet. The limitation to imbibition method is that the imbibition rates depend not solely on wettability but also on relative permeability, viscosity, fluid/fluid interfacial tension (IFT), pore structure and initial saturation core [12].

Microscopic Examination Method

In the microscopic observation method, the interaction between the fluids and the rock matrix is observed. Based on the affinity, the rock's state of wettability is determined [6]. Grains of rock sample are observed microscopically in an oil-water system. If the rock is strongly water-wet, the water surrounds the grain as

a thin film while the residual oil rests on this thin film. If the system is strongly oil-wet, the oil forms a thin film surround the grain with water resting above the film, as seen earlier in Figure 1. If, both, oil and water are found in contact with the rock surface, the rock is regarded to be neutral wet. The microscopic examination method is of particular importance, in the petroleum industry, when studying wettability reversals due to alkaline flooding. When a chemical is injected into the rock-water-oil system, a microscope is used to follow wettability changes that would help determine the effectiveness of the chemical for EOR applications [12].

Flotation Method

Flotation method is a fast method to determine wettability of rocks. Yet, it is effective for strongly wetted systems only [12]. It is performed by distributing grains of the reservoir rock at the water-oil interface [6]. If the grains remain afloat and suspended at the oil-water interface, they are regarded as oil-wet. However, if they settle at the bottom, the rock is regarded to be water-wet.

Nuclear Magnetic Resonance (NMR) Method

The Nuclear Magnetic Resonance method was proposed in 1956 to study fractional wettability. This method uses a parameter known as ‘nuclear thermal relaxation time’. It is defined to be the time used to measure the fractional wettability and is used as a basis to determine the state of wettability. In order to measure this relaxation time, the rock sample is first exposed to a strong magnetic field which makes the nuclei of the water hydrogen atoms, residing in the pores of the rock, line up with the field. The rock is then exposed to a much weaker magnetic field where the hydrogen nuclei relax and adjust to the new field. The time it takes for these nuclei to relax is known as nuclear magnetic relaxation time. The use of nuclear magnetic relaxation times to measure wettability is based on the observation that the surfaces of the porous media can significantly reduce the relaxation time. Based on this observation, regions are categorized as oil-wet

and water-wet since oilwet surfaces cause a smaller reduction in relaxation time than the water-wet ones [12].

Dye Adsorption Method

The dye adsorption method has been found to be quite successful in measuring fractional wettability in packed columns filled with rock sample and mixture of oil and water [12]. A dye is added to such a column and the adsorption behavior of the dye is observed [6]. If the rock is water-wet, it will adsorb the dye. However, if it is oil-wet, it will not.

Summary

Table 2 summarizes all the advantages and limitations of each wettability measurement technique.

Table 2. Summary of wettability measurement techniques.

| Wettability measurement technique | Advantages | Disadvantages |
|-----------------------------------|---|---|
| Contact angle | -Accurate -Simple | -Surface heterogeneity can effect reading -Cannot provide information regarding organic coatings -Impurities can effect reading |
| Ammot-Harvey | -reliable | -Not very effective to measure neutral wettability -No validity as an absolute measure |
| USBM | -Reliable | - No validity as an absolute measure |
| Imbibition rate | -Quick -Simple | -Not very accurate -Imbibition rate does not solely depend on wettability but also other factors |
| Microscopic examination | -In situ wettability alteration can be observed | -Based on affinity with no degree of wettability measured |
| Floatation | -Quick | -Sensitivity to only strongly-wetted systems |
| NMR | -Ability to study fractional wettability | -Require expensive equipment and tools |
| Dye adsorption | -Quick | -Not very accurate |

| | | |
|--|--|--|
| | -Simple -Cost effective -Ability to study fractional wettability | |
|--|--|--|

Dual core imbibition (DCI) method

In this section we introduce dual core imbibition method as an alternative to the quantitative and qualitative methods described in previous section to analyze affinity of shale rock samples to reservoir fluids (oil, brine). DCI is composed of three complementary stages to evaluate rock-fluid interaction between samples cored from zone of interest and reservoir fluids.

Contact angle test

In the first stage we measure solid/fluid/air contact angles and solid/fluid/fluid contact angles. We present solid/fluid/fluid contact angle results in an affinity chart. Figure 7, represents an affinity chart with data points from six core samples from Montney formation. Horizontal axis represents contact angle of oil droplet in brine at the surface of rock sample. Vertical axis represents contact angle of brine droplet in oil at the presence of rock sample. The robustness of the affinity chart is in its ease of application in

- 1- Visualizing and assessing affinity of rock samples cored from a specific zone of interest to reservoir fluids or fracturing fluids.
- 2- Comparing affinity of several zones of interest to reservoir fluids or fracturing fluid in one single chart.
- 3- Comparing and evaluating affinity of rock samples from one zone of interest to different fracturing fluids of interest. This can help engineers to pick the right fluid with the optimum affinity by comparing results in one single plot.

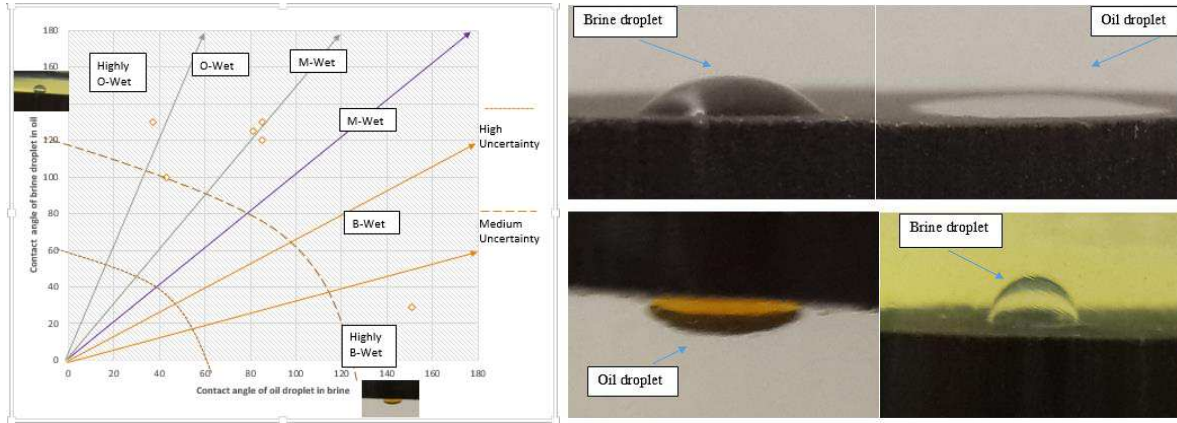


Figure 7 – Affinity chart (left), Contact angle test (right).

Spontaneous imbibition tests

We evaluate the wetting affinity of five sets of twin core-plugs from the Montney formation by measuring spontaneous imbibition and equilibrium contact angle. One plug of each pair is placed in reservoir oil and the other in reservoir brine, and the weight change is measured periodically. Figure 8 represents the setup we used in this stage.

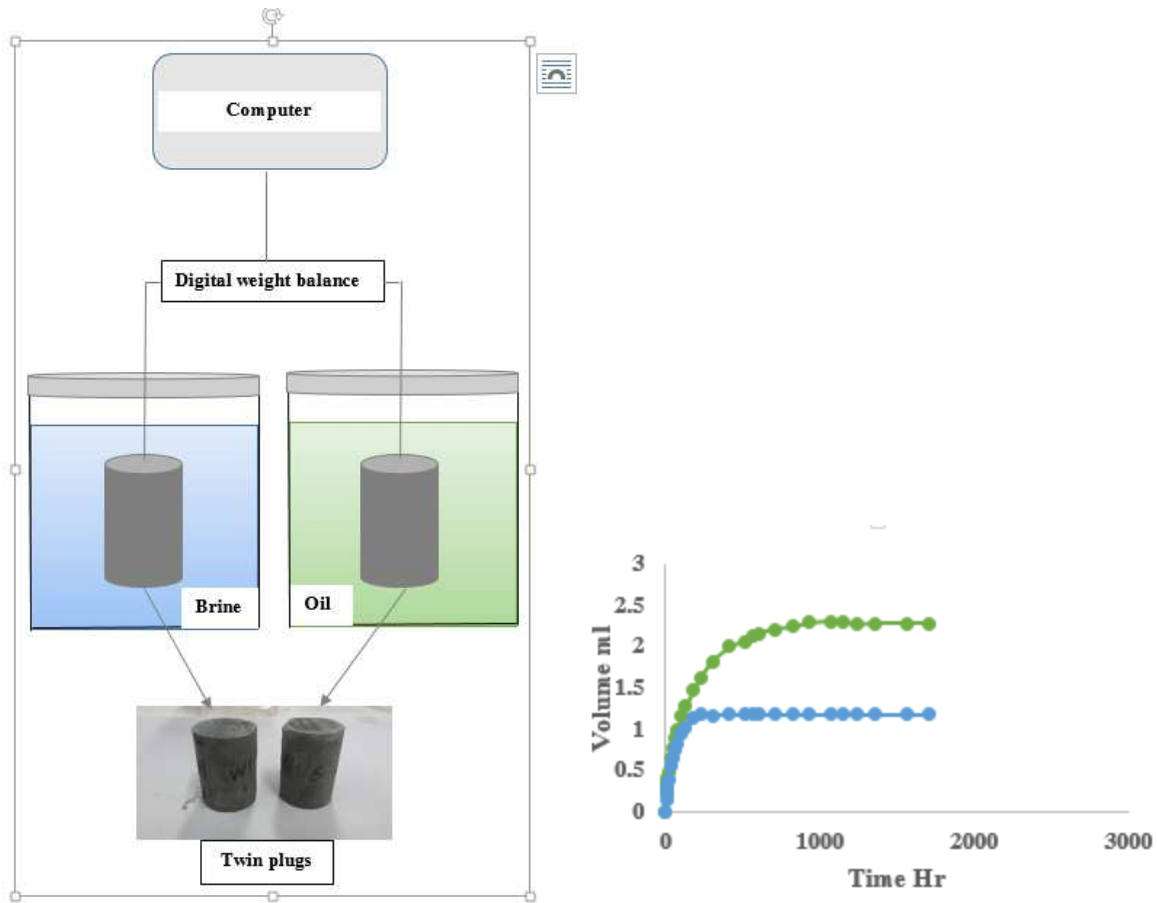


Figure 8– Spontaneous imbibition setup for DCI method (left), spontaneous imbibition results from DCI method (right).

Recovery test

Figure 9 represents the method we obtained recovery plots by putting oil saturated samples from previous stage in an Amott cell and record recovered oil with time.

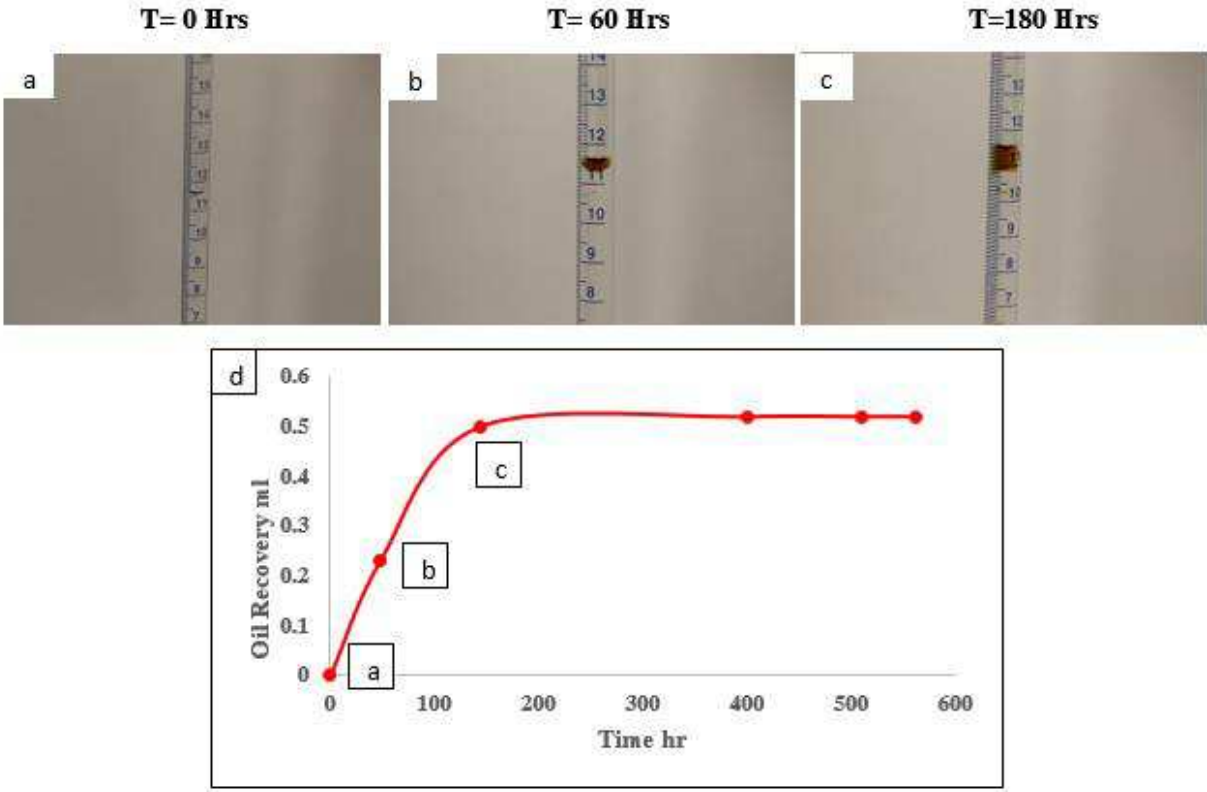


Figure 9- Recovery plots during recovery tests. Recovered oil is captured at different times, (a) $t=0$ Hrs, (b) $t=60$ Hrs, (c) $t=180$ Hrs.

Next, we comparatively analyze the spontaneous imbibition data from previous stage and the recovery data in one imbibition-recovery trio (oil imbibition, brine imbibition, imbibition oil recovery). Figure 10 represents an imbibition-recovery trio for one set of twin plug.

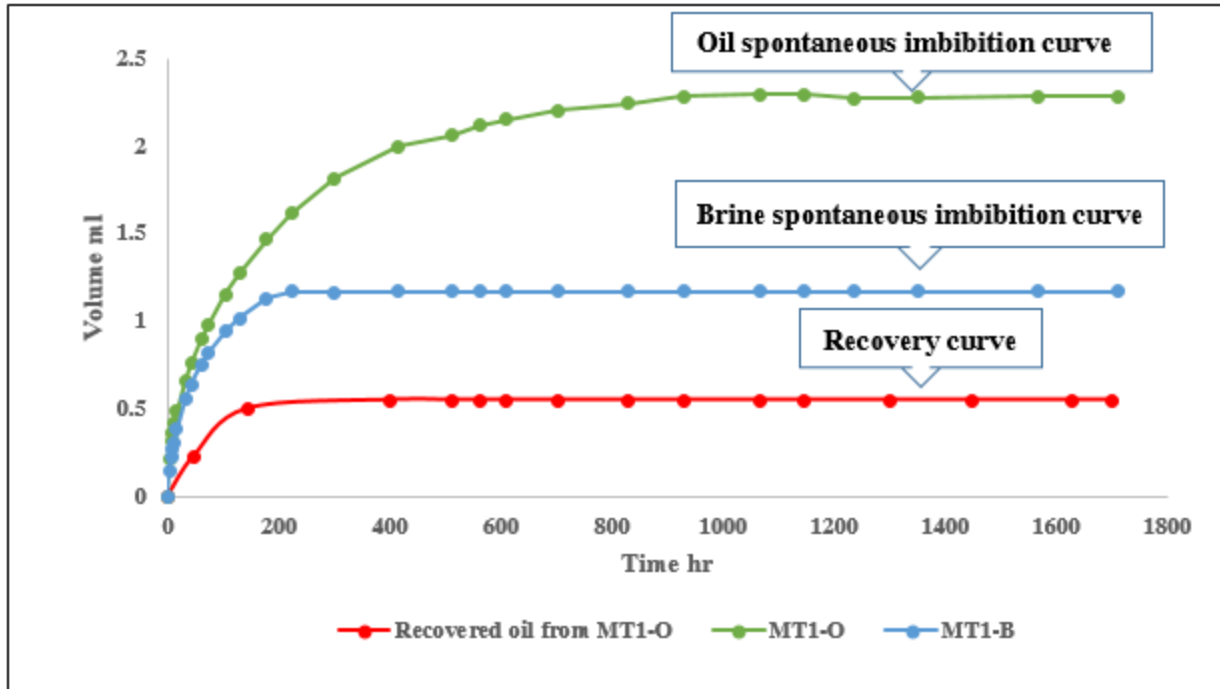


Figure 10 - Imbibition recovery graph-trio consists of three curves. Oil spontaneous imbibition curve, brine spontaneous imbibition curve and recovery curve, plotted versus time.

Summary

Table 3, Summarizes advantages and disadvantages of DCI method according to the previous four stages described.

Table 3. Advantages and Disadvantages of DCI method.

| Advantages | Disadvantages |
|---|--|
| <ul style="list-style-type: none"> - Able to characterize mixed-wet/dual wet core samples. - Provides insight on flow and recovery of fluids in core samples. - Reliable | <ul style="list-style-type: none"> - Time consuming specially in spontaneous imbibition stage, can take months for very low-permeable rock samples. - Samples might not reach equilibrium during spontaneous imbibition stage. |

| | |
|--|--|
| <ul style="list-style-type: none">- Can provide information regarding organic coating, clay.- Can provide information on role of fractures/ micro-fractures in fluid suction and ultimate recovery. | <ul style="list-style-type: none">- Samples might breakdown or wear out during tests due to relatively high soaking time period or forced flood. |
|--|--|

References

- [1] S. Kim, M. Boudh-Hir, and G. Mansoori, "The role of asphaltene in wettability reversal," presented at the 65th SPE Annual Technical Conference and Exhibition, New Orleans, LA, 1990.
- [2] S. Ghedan, C. Canbaz, D. Boyd, G. Mani, and M. Haggag, "Wettability profile of a thick carbonate reservoir by the new rise in core wettability characterization method," presented at the Abu Dhabi International Petroleum Exhibition and Conference, Abu Dhabi, UAE, 2010.
- [3] V. Bortolotti, P. Macini, and F. Srisuriyachai, "Wettability index of carbonatic reservoirs and EOR: laboratory study to optimize alkali and surfactant flooding," presented at the International Oil and Gas Conference and Exhibition in China, Beijing, China, 2010.
- [4] E. Donaldson, R. Thomas, and P. Lorenz, "Wettability determination and its effect on recovery efficiency," *SPE Journal*, vol. 9, no. 1, pp. 13-20, 1969.
- [5] C. Agbalaka, A. Dandekar, S. Patil, S. Khataniar, and J. Hemsath, "The effect of wettability on oil recovery: a review," presented at the SPE Asia Pacific Oil and Gas Conference and Exhibition, Perth, Australia, 2008.
- [6] P. Glover. Class Lecture, Topic: "Wettability." Department of Geology and Petroleum Geology, University of Aberdeen, Scotland, UK, Feb. 20, 2001.
- [7] I. Fatt and W. A. Klikoff, "Effect of fractional wettability on multiphase flow through porous media," *Journal of Petroleum Technology*, vol.11, no.10, pp.71-76, Oct.1959.
- [8] K. K. Mohanty and S. J. Salter, "Multiphase flow in porous media: III oil mobilization, transverse dispersion, and wettability", presented at SPE Annual Technical Conference and Exhibition, San Francisco, CA, 1983.
- [9] W. C. Lyons, "Reservoir engineering," in *Standard Handbook of Petroleum and Natural Gas Engineering*, vol.2. Houston, TX: Gulf Publishing Company, 1996, pp.3- 344.
- [10] B. Zinszner and F. M. Pellerin, "Chapter 1-2 Fluid recovery and modelling: dynamic properties," in *A Geoscientist's Guide to Petrophysics*. France, Editions Technip, 2007, ch. 1, sec. 2, pp.169-170.

- [11] J. Newcombe, J. McGhee and M. J. Rzasa, "Wettability versus displacement in water flooding in unconsolidated sand columns," *Petroleum Transactions*, AIME, vol. 204, pp. 227-232, 1955. Paper presented at Petroleum Branch Fall Meeting, New Orleans, Oct. 2-5, 1955.
- [12] W. G. Anderson, "Wettability literature survey – Part 2: wettability measurement," *Journal of Petroleum Technology*, vol.38, no. 11, pp.1246-1262, Nov. 1986.
- [13] Yarveicy, H., & Javaheri, A."Application of Lauryl Betaine in enhanced oil recovery: A comparative study in micromodel." *Petroleum*.2017.
- [14] Yarveicy, H., & Haghtalab, A."Effect of amphoteric surfactant on phase behavior of hydrocarbon-electrolyte-water system-an application in enhanced oil recovery." *Journal of Dispersion Science and Technology* just-accepted .2017.
- [15] M. S. Celik and P. Somasundaran, "Wettability of reservoir minerals by flotation and correlation with surfactant adsorption," presented at the SPE 5th International Symposium on Oilfield and Geothermal Chemistry, Stanford, CA, 1980.
- [16] E. Amott, "Observations relating to the wettability of porous rock," *Petroleum Transactions*, AIME, vol. 216, pp. 156–162, 1959. Paper presented at Fall Meeting of Los Angeles Basin Section, Los Angeles, Calif., Oct. 16-17, 1958.
- [17] A. Y. Dandekar, "Interfacial tension and wettability," in *Petroleum Reservoir Rock and Fluid Properties*, 1st ed. Boca Raton: Taylor & Francis Group LLC, 2013, ch. 7, p. 144.
- [18] A. A. Abe, "Relative permeability and wettability implications of dilute surfactants at reservoir conditions," M.S. thesis, Louisiana State Univ., Baton Rouge, LA, 2005.
- [19] M. K. Zahoor, M. N. Derahman and M. H. Yunan, "Wettability – interpreting the myth," *NAFTA*, vol. 60, no. 6, pp. 367-369, 2009.

Chapter 2

Tight Rock Wettability and Its Relationship to Other Petrophysical Properties

Abstract

Optimizing hydraulic fracturing operations requires understanding the interactions of fracturing fluids with unconventional tight rocks. In particular, a possible recovery mechanism is imbibition of fracturing fluid into the rock matrix and the subsequent expelling of oil into the fracture system. Therefore, it is important to understand and model the wettability of such rocks.

In this paper, we measure and analyze spontaneous imbibition of water and oil into five twin core plugs drilled from the cores of a well drilled in the Montney Formation, an unconventional oil and gas play in Canada. We characterize the samples by measuring the mineralogy using XRD (x-ray diffraction), total organic carbon content, porosity, and permeability. Interestingly, the equilibrated water uptake of the five samples is similar, while, their oil uptake increases by increasing the core porosity (φ) and permeability (k). We define two wettability indices for the oil phase based on the slope and equilibrium values of water and oil imbibition curves (WI_o^{sl} and WI_o^{eq} , respectively). Both WI_o^{sl} and WI_o^{eq} increase by increasing φ and k , with WI_o^{sl} showing a stronger correlation. This observation suggests that part of the pore network has a stronger affinity to oil than to water. We also observe that the two indices decrease by increasing neutron porosity and gamma ray parameters measured by wireline logging tools. The samples with higher gamma ray and neutron porosity are expected to have more clay content, and thus less effective φ and k .

Introduction

Advances in the development of unconventional resources have led to a surge in North American oil production. For example, tight oil production has pushed the U.S. crude supply to over 10% of world total

production [1]. Tight oil is conventional oil that is found within reservoirs with very low permeability [2]. Tight oil is of high quality and requires very little refinement [3]. Petrophysical characterization of such low-permeability rocks, that were once considered non-reservoir, now has become increasingly important for petroleum engineers. Properties such as porosity, pore throat size [4], and wettability [5-7] are of high importance for evaluating production from tight oil formations. Among these properties, rock wettability towards different fluids is of utmost importance since the formation is exposed to non-reservoir fluids (i.e. slick water) during and after the fracturing process.

Different methods have been developed to evaluate rock wettability. Equilibrium contact angle measurement, Amott wettability index [8], USBM method [12], spontaneous imbibition [9-11] hysteresis of the relative permeability curves [13] and nuclear magnetic relaxation (NMR) [14, 15] are the most common methods to measure wettability of core rock samples towards different fluids. Conventional methods such as Amott and USBM need to be applied with extreme caution to evaluate wettability of low-permeability rocks [16]. Fragility of rock samples at high pressures can cause errors during forced displacement tests in the laboratory.

Recently, NMR technology has been applied to evaluate the wettability of tight rocks [17, 18]. NMR logging has also been applied by wireline companies for in-situ measurement of reservoir wettability, which due to high operational costs and technical difficulties comes along with a set of challenges. Interpreting and processing NMR signals from unconventional rocks is more challenging compared with those from conventional rocks [19]. Tight rocks are usually composed of total organic carbon (TOC) which tends to be hydrophobic and clays which are hydrophilic [20]. It is challenging to interpret the NMR signals from organic-rich formations and formations with high clay content. Moreover, as pore size decreases, the error associated with NMR measurement increases.

The long-term objective of this work is to evaluate the wettability of tight formations by interpreting open-hole log data such as neutron porosity and gamma ray. In this paper, we investigate the existence of possible correlations between the wettability of the Montney core plugs and other petrophysical properties including

porosity, permeability, and commonly-measured downhole logs of neutron porosity and gamma spectra. The rest of this article consists of three sections and concluding remarks. Section II presents rock and fluid properties, and Section III describes the methodology used in conducting wettability tests. Section IV presents and discusses the relationships between the imbibition/wettability results and other petrophysical data.

Materials

Rock properties

The core plugs are dry-cut from the cores of the Montney Formation in the zone of 2100-2200 m. The plugs are well-preserved and uncontaminated. Montney Formation is a stratigraphical unit of Lower Triassic age in the Western Canadian Sedimentary Basin in British Columbia and Alberta [2, 21]. The formation is composed of siltstone and dark grey shale, with dolomitic siltstone in the base and fine grained sandstone towards the top [2, 22]. Clay and TOC content of the core samples are listed in Table 1. The clay content does not vary much and the amount of total organic carbon is very low. The clays are mainly composed of chlorite, illite and mica. Table 2 lists the porosity and permeability of the rock samples. The results of XRD analysis of the samples are listed in Table 3. The core plugs are mainly composed of quartz, k-feldspar, plagioclase, dolomite and clay. The clays are composed of illite, mica and chlorite.

Table 1. Clay and TOC content of the five twin plugs.

| Rock number | Depth (m) | Clay content (wt %) | TOC content (wt %) |
|-------------|-----------|---------------------|--------------------|
| MT-1 | 2144 | 13.1 | 0.2 |
| MT-2 | 2149 | 12.3 | 0.24 |
| MT-3 | 2174 | 13.2 | 0.32 |
| MT-4 | 2192 | 12.3 | 0.44 |
| MT-5 | 2196 | 12 | 0.47 |

Table 2. Porosity and permeability of the five twin plugs.

| Rock number | Depth (m) | Porosity | Permeability (mD) |
|--------------------|------------------|-----------------|--------------------------|
| MT-1 | 2144 | 0.045 | 49E-05 |
| MT-2 | 2149 | 0.031 | 4E-05 |
| MT-3 | 2174 | 0.046 | 56E-05 |
| MT-4 | 2192 | 0.030 | 3E-05 |
| MT-5 | 2196 | 0.04 | 43E-05 |

Table 3. Minerology of the five twin plugs obtained from XRD analysis.

| Mineralogy | MT-1 | MT-2 | MT-3 | MT-4 | MT-5 |
|----------------------------------|-------------|-------------|-------------|-------------|-------------|
| <i>Non clay (wt %)</i> | | | | | |
| Quartz | 40.4 | 44.8 | 41.6 | 43.1 | 42.5 |
| Anhydrite | 0.8 | 0.5 | 0.4 | 0.0 | 0.8 |
| K-Feldspar | 12.1 | 10.0 | 14.9 | 12.8 | 11.7 |
| Plagioclase | 15.1 | 10.9 | 14.0 | 11.6 | 13.9 |
| Calcite | 3.0 | 5.7 | 0.0 | 2.0 | 0.0 |
| Dolomite & Fe-Dolomite | 14.0 | 14.2 | 14.5 | 16.5 | 20.6 |
| Pyrite | 1.5 | 1.5 | 1.4 | 1.7 | 1.8 |
| Marcasite | 0.0 | 0.0 | 0.0 | 0.0 | 0.0 |
| <i>Relative clay data</i> | | | | | |
| Total Clay (wt %) | 13.1 | 12.3 | 13.2 | 12.3 | 17.2 |
| Illite & Mica | 56.3 | 52.3 | 64.6 | 58.0 | 62.2 |
| Chlorite | 43.8 | 47.7 | 35.4 | 42.0 | 37.8 |

| | | | | | |
|----------|-------|-------|-------|-------|-------|
| Sum Bulk | 100.0 | 99.9 | 100.0 | 100.0 | 100.0 |
| Sum Clay | 100.1 | 100.0 | 100.0 | 100.0 | 100.0 |

Geochemical logs [23] can be obtained through Rock-Eval equipment, which burns a crushed sample of rock at 600°C. The Rock-Eval analyzer consists of a flame ionization detector and two IR (infra-red) detector cells. The free hydrocarbons (S_1) are determined from an isothermal heating of the sample at 340 °C. These hydrocarbons are measured by the flame ionization detector. The temperature is then increased from 340 to 640 °C. Hydrocarbons are then released from the kerogen and measured by the flame ionization detector creating the S_2 peak. The temperature at which S_2 reaches its maximum rate of hydrocarbon generation is referred to as T_{max} . The CO_2 generated from the oxidation step in the temperature range of 340 to 580°C is measured by the IR cells and is referred to as S_3 peak. The geochemical log [24] of the zone of interest where the samples are cored is presented in Figure 1. According to S_2 value (mg HC/g), oil potential is poor (less than 1mg HC/g). Also according to the hydrogen index (S_2/TOC), the zone lies in the gas window. In order to reduce the effects of heterogeneity, the twin plugs are cut as close to each other as possible. Average distance between the plugs of each twin set is 5 cm.

Figure 2 shows the location of the core plugs on the total gamma ray and uranium free gamma ray logs. The concentration of radioactive elements in sedimentary rocks depends on the source of sediment's materials, and their chemical characteristics as well as the conditions of deposition [25]. A gamma-ray spectrometer can be used to measure the abundance of uranium; together with the mostly detrital potassium and thorium. This produces the bulk of the natural radioactivity, and hence gamma radiation in rocks.

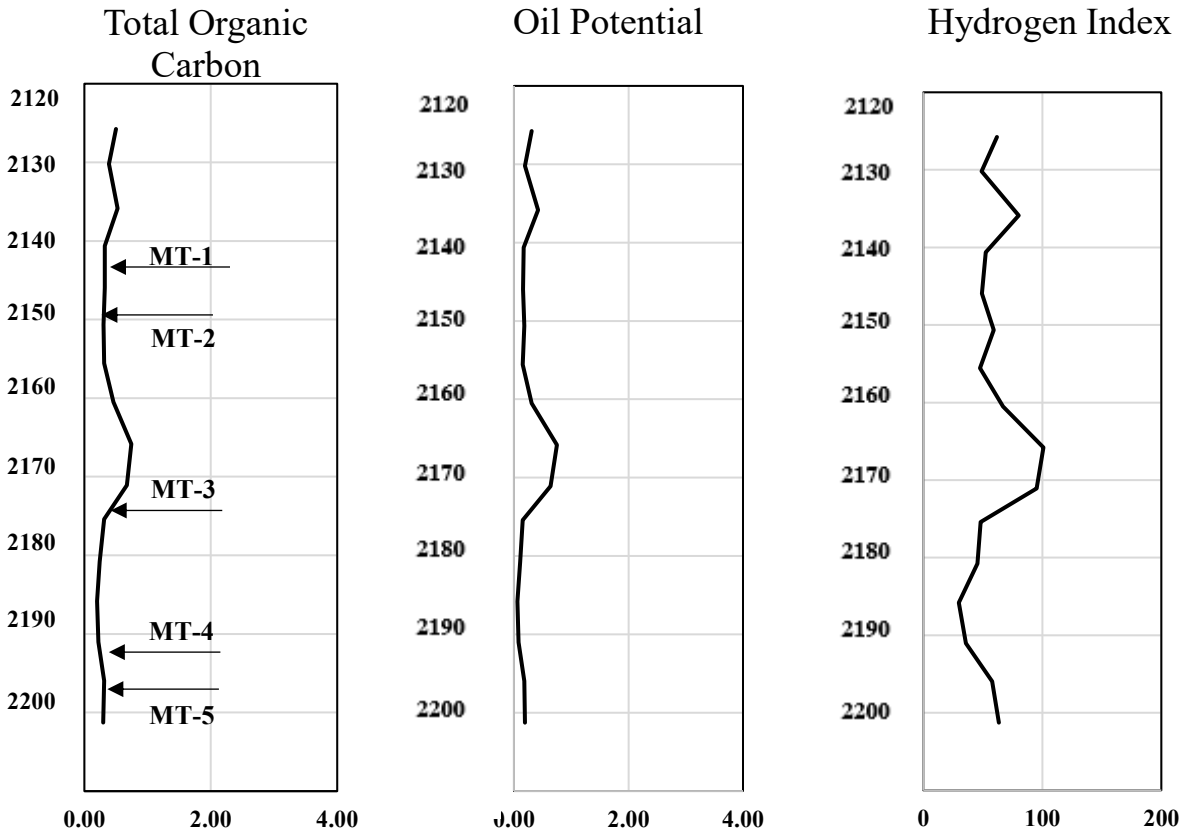


Figure 1. Geochemical log for the zone of interest.

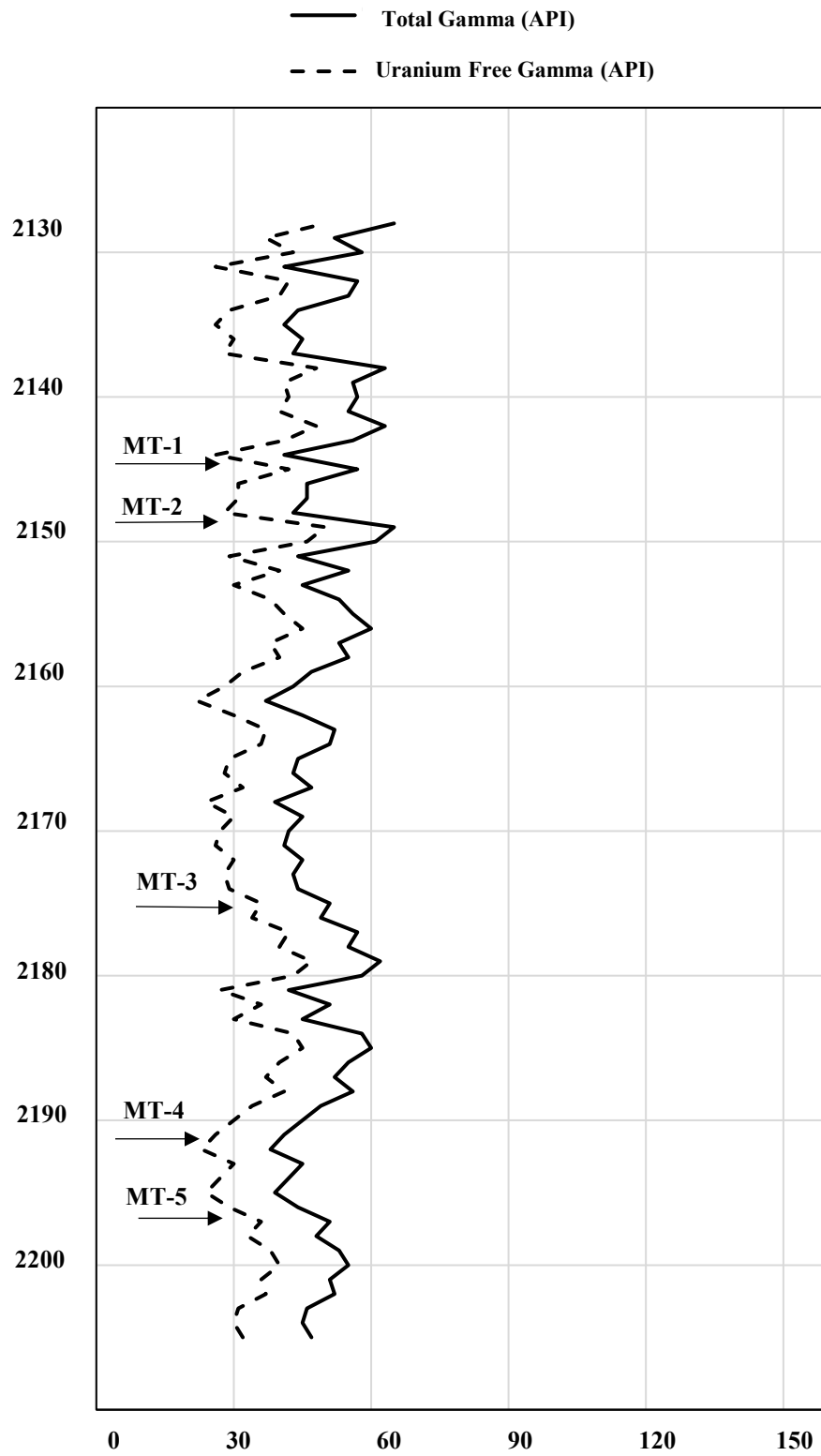


Figure 2. Location of the samples in the zone of interest.

Fluid properties

Reservoir brine and oil are used as aqueous and oleic phases, respectively, for investigating the wetting affinity of the samples, and their properties are listed in Tables 3 and 4. The brine is highly saline water with the total dissolved solids of 126-130 gr/L and the total hardness of 22 gr/L which is relatively high due to dissolution of CaCO₃ salt. The brine is neutral in terms of alkalinity. The oil is light with API of 45.07, and is low in sulphur content 0.0796 gr/gr which shows the oil is of high quality and requires little refinement.

Table 4. Brine properties.

| Property | Quantity |
|--|----------|
| Total Dissolved Solids (mg/L)-Measured | 126000 |
| Total Dissolved Solids (mg/L)-Calculated | 130000 |
| Relative Density | 1.101 |
| Surface Tension (mN/m) | 67 |
| Refractive Index | 1.356 |
| Conductivity (uS/cm) | 159000 |
| Resistivity (ohm-m) @25 ⁰ C | 0.06 |
| Total Hardness as CaCO ₃ (mg/L) | 22000 |
| Total Alkalinity as CaCO ₃ (mg/L) | 110 |
| Observed pH | 6.89 |
| H ₂ S Spot Test | Absent |
| Viscosity (cP) | 1.18 |

Table 5. Oil properties.

| Property | Quantity |
|--|----------|
| Density of Clean oil @15 ⁰ C (ASTM D5002) | 1 |
| Relative Density | 0.8014 |
| API | 45.07 |
| Surface tension (mN/m) | 28 |
| Absolute Density (m ³ /kg) | 800.7 |
| Total Sulphur (mass percent) ASTM D4294 | .0796 |
| Pour Point (⁰ C) ASTM D97/D5853 | <-35 |
| Viscosity (cP) | 1.84 |

Methodology

We conduct a series of comparative oil/water imbibition tests on several plugs, which were dry-cut from the Montney formation cores. The samples are characterized by measuring mineral concentration, TOC content, porosity, and permeability. Overall, 10 samples (5 twin plugs) are tested. Figure 3 shows the procedure for conducting the co-current spontaneous imbibition tests. One plug of each twin set is placed in a cell partly filled with brine and the other plug is placed in a cell partly filled with oil. Only the bottom face of the plugs is exposed to the imbibing fluid. The weight of each plug is measured periodically with time and recorded. The experiments are halted once the mass gain of each sample reaches to the equilibrium conditions.

The general procedure for the imbibition tests is as follows:

- 1- Dry cut twin plugs using nitrogen for comparative oil and water imbibition tests.

- 2- Place each plug into an imbibition cell and make sure one face of the plug is exposed to the imbibing fluid.
- 3- Seal the imbibition cell to avoid liquid evaporation and measure the weight gain periodically.

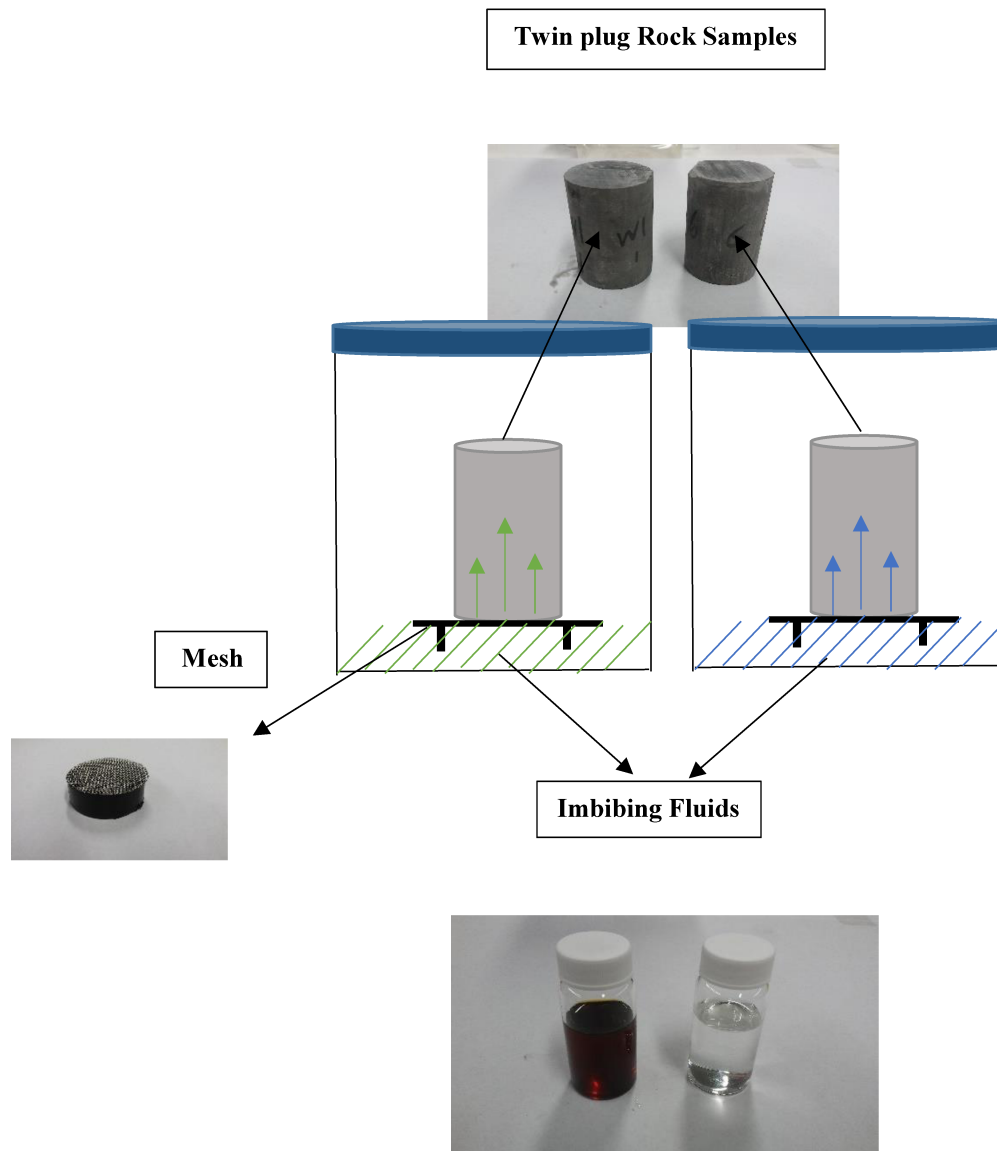


Figure 3. Illustration of the experimental set-up for oil and brine imbibition into twin core plugs.

Results and Discussions

Contact angle

Contact angle tests are done on all twin pairs. Samples are first polished, then washed with acetone and then air-dried before conducting the tests. Acetone helps to remove dirt from the surface and clean it, hence making the contact angle results more representative. The equilibrated oil and brine droplets, shown in Figures 4A and 4B, suggest that the affinity of the samples to oil is higher than that to brine. Oil droplet completely spreads on the rock surface while brine partially wets the sample.

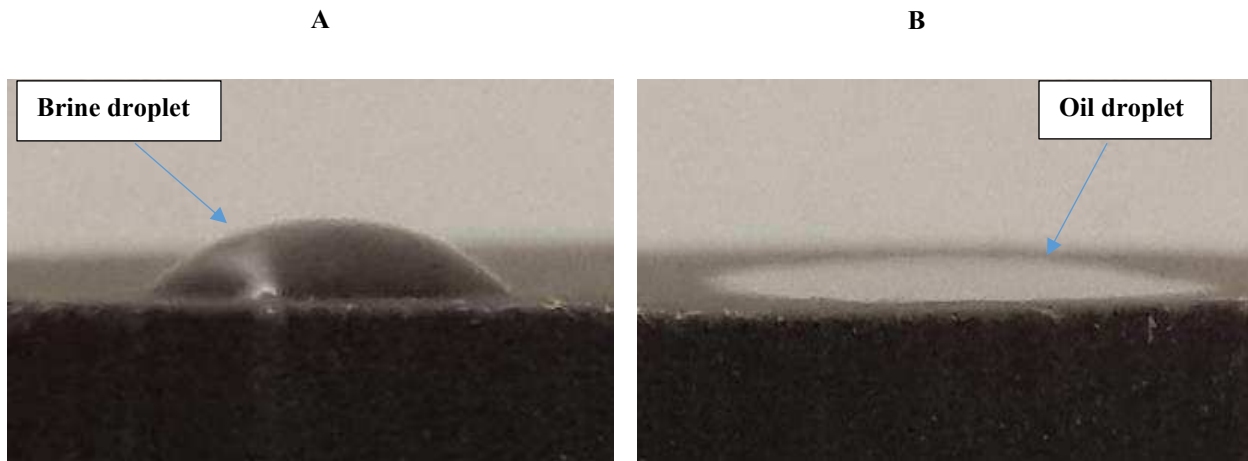
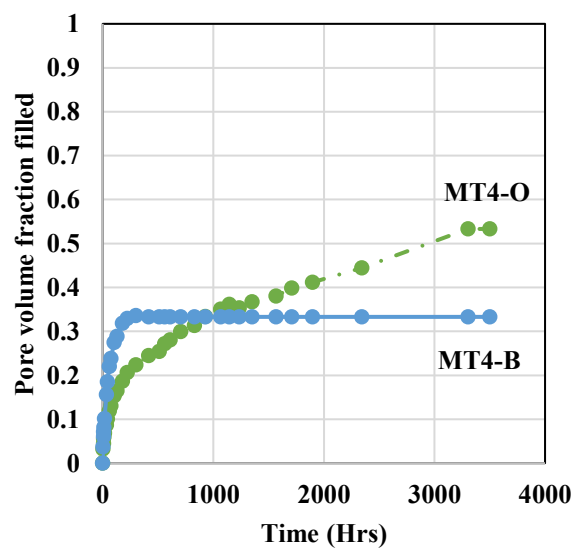
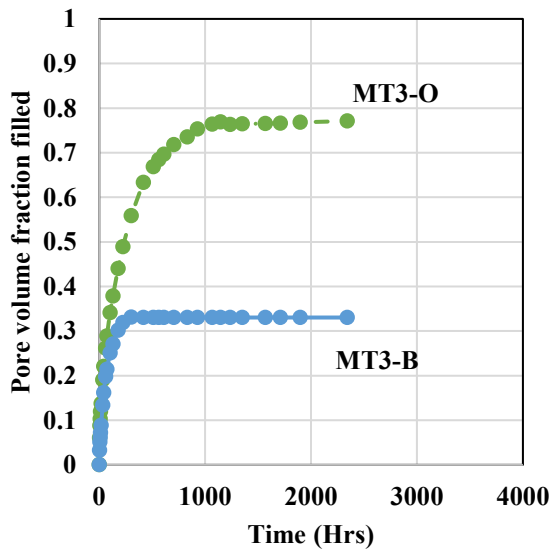
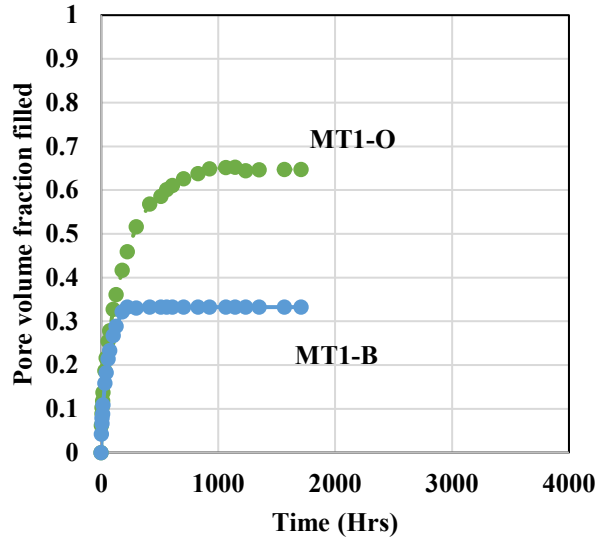
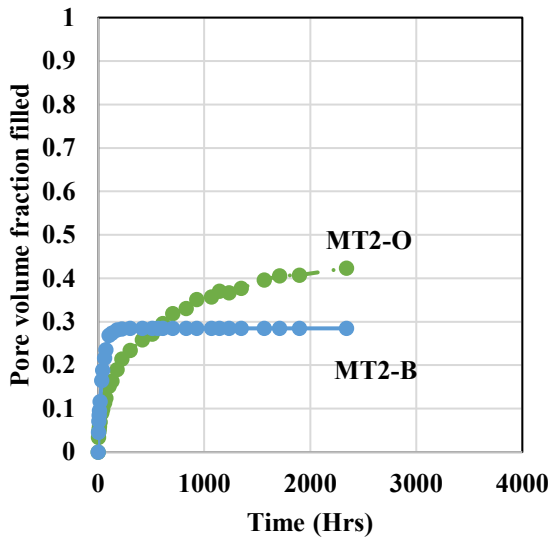


Figure 4. Brine (A) and oil (B) droplets equilibrated on rock surface at the presence of air.

Spontaneous imbibition

Normalized imbibed oil (I_o) and brine (I_w) are defined as the imbibed volume of oil and brine divided by the rock pore volume. The volume of oil and brine imbibed are calculated by dividing the total imbibed mass by the fluid density. The pore volume is obtained from mercury injection capillary pressure (MICP) laboratory data. Since MICP cannot capture the very small pores in the rock samples, the pore volume and the normalized imbibed volume are expected to be underestimated and overestimated, respectively.

Imbibition data for the five twin plugs are plotted in Figure 5. We observe consistently that the oil curves reach to the equilibrium later than brine, but the total imbibed volume of oil is significantly higher than that of brine. The general trend is that brine imbibes faster than oil for all samples but the brine imbibition profiles plateau earlier than oil profiles.



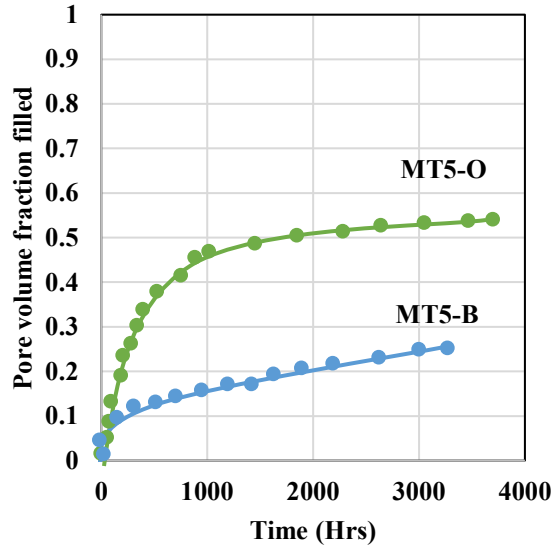


Figure 5. Normalized imbibed volume of brine and oil versus time. O and B represent oil and brine, respectively.

Multivariate scatterplots of imbibition results and other petrophysical data

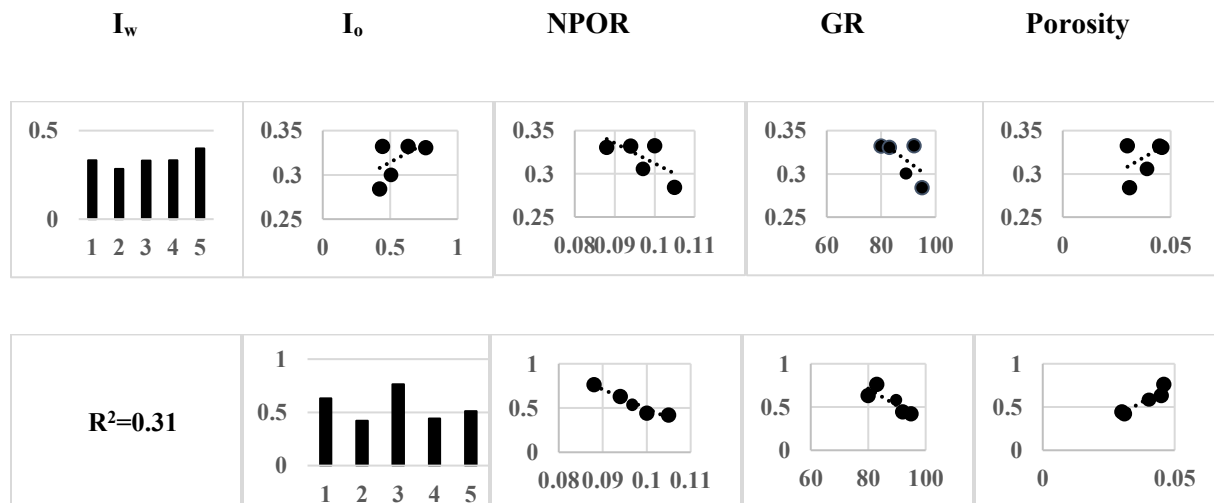
Table 5 lists the values of total GR, spectra gamma ray, NPOR (neutron porosity), MICP (mercury injection capillary pressure) porosity, I_w (normalized imbibed volume of water), I_o (normalized imbibed volume of oil), and WI_o^{eq} , which is the wetting affinity index of oil, defined as normalized imbibed volume of oil over the sum of normalized imbibed volume of water and oil.

Table 6. The measured values of Total GR, spectra gamma ray, NPOR, MICP porosity, I_w , I_o , WI_o^{eq} for the five twin plugs.

| Measurements | MT-1 | MT-2 | MT-3 | MT-4 | MT-5 |
|----------------|------|------|------|------|------|
| Total GR (API) | 80 | 95 | 83 | 92 | 90 |
| Uranium (PPM) | 3 | 4.5 | 3.1 | 3.7 | 3.6 |
| Thorium (PPM) | 7 | 8 | 7.5 | 8.5 | 8.1 |

| | | | | | |
|------------------|-------|-------|-------|-------|-------|
| Potassium (FRAC) | 0.027 | 0.031 | 0.028 | 0.031 | 0.03 |
| NPOR | 0.094 | 0.105 | 0.088 | 0.1 | 0.095 |
| MICP porosity | 0.045 | 0.031 | 0.046 | 0.03 | 0.04 |
| I_w (vol %) | 0.33 | 0.28 | 0.33 | 0.33 | 0.30 |
| I_o (vol %) | 0.63 | 0.42 | 0.76 | 0.44 | 0.51 |
| WI_o^{eq} | 0.65 | 0.59 | 0.69 | 0.57 | 0.63 |

Figure 6 shows multivariate scatterplots of the five variables I_w , I_o , NPOR, GR and porosity. Each variable can be positively or negatively related to the remaining variables, and the strength of that relationship is quantified by the R^2 values corresponding to each cross plot, displayed on its transverse side. Diagonal plots are univariate histograms of the five variables, off-diagonal scatterplots are bivariate cases. Using bivariate scatterplots, one can investigate the relationships between pairs of variables. The results show that I_o versus MICP porosity and also I_o versus NPOR give the strongest correlations. This suggests that the samples with higher porosity exhibit a higher oil uptake. In Figure A1 of the Appendix, we plot versus porosity the values of NPOR, GR, Uranium, Thorium and Potassium contents. Interestingly, we do not observe significant correlations between I_w and other parameters, mainly due to insignificant variability of I_w measurements.



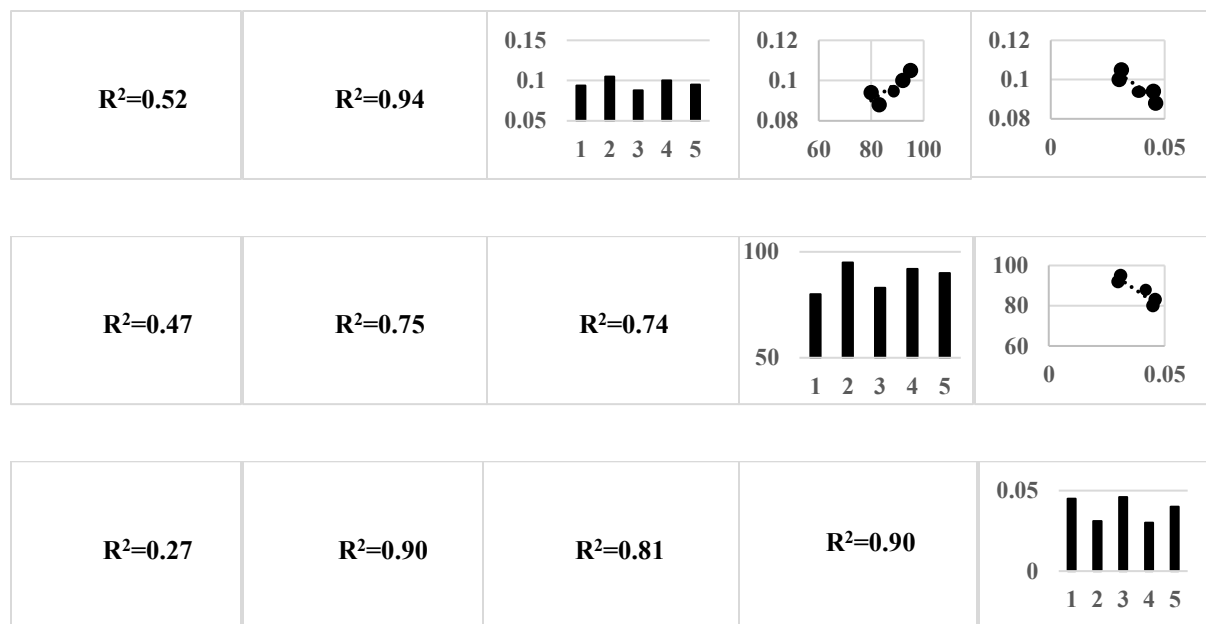


Figure 6. Multivariate scatterplots for five variables: I_w , I_o , NPOR, GR and MICP porosity.

Normalized imbibed volume of oil versus porosity and log data

Figure A1 of Appendix shows I_o versus Porosity, NPOR, GR, and concentrations of Pottassium, Thorium and Uranium content. According to the plots, I_o increases with increase of porosity and decreases with increase of the log data. The best correlation is observed for I_o versus NPOR and porosity. The change in clay content of the samples is not significant and the TOC content of the samples is relatively low (0.2-0.44). We believe that the reason for observed correlations with the log data and I_o is due to the natural correlations between porosity and log data. According to figure A3, all gamma ray measurements (potassium, thorium and uranium) decrease with porosity and as evident from figure A1 (a), there is a linear correlation between I_o and porosity. Therefore, the normalized oil index decreases with increase of spectral gamma ray and neutron porosity data.

Normalized imbibed volume of brine versus porosity and log data

Figure A2 of Appendix shows I_w versus NPOR, GR, and concentrations of Potassium, Thorium and Uranium. According to the plots, I_w varies only slightly with the change of the log parameters. In other words, the water uptake of the five plugs are very similar.

Figure 7 compares the values of I_w and clay content for the five samples. There is only very small variations in the clay content, and clays are known to be associated with water uptake [26], hence the water uptake of the samples are expected to be very similar. However, Figures A1 and A2, show that oil uptake of the samples is relatively higher and has more variations compared with their brine uptake.

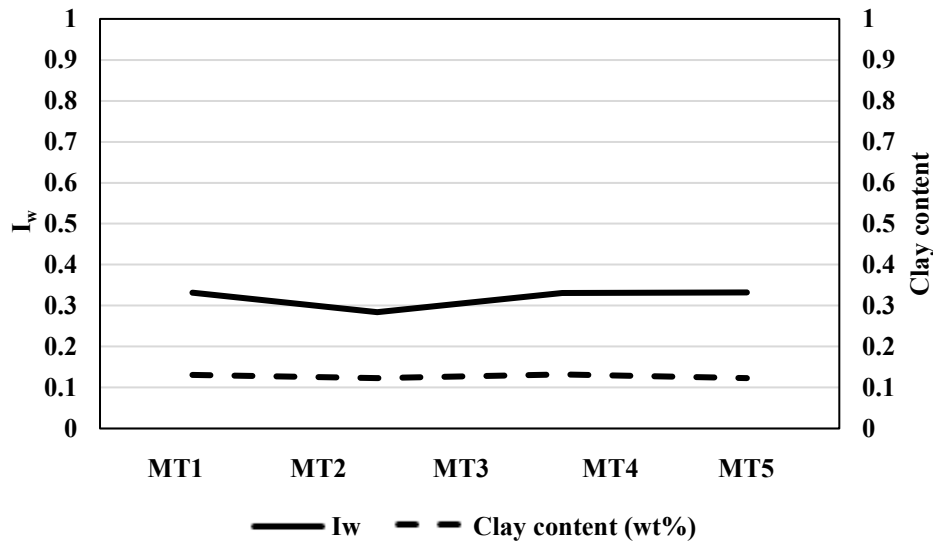


Figure 7. I_w and Clay content histograms for all five samples.

Wettability Index

In order to parameterize oil and brine uptake of the core plugs, we define two sets of affinity indices: slope affinity index (WI_o^{sl} , WI_w^{sl}) and equilibrium affinity index (WI_o^{eq} , WI_w^{eq}).

1. Slope affinity index

In Figure 8, we plot oil and brine imbibition versus square root of time. According to Handy's model (Handy, 1960) the total imbibed mass should be proportional to the square root of time:

$$M = \sqrt{\frac{2 A \phi \rho^2 K S_{wf} P_c}{\mu}} \sqrt{t} \quad (1)$$

Where M is the imbibed wetting fluid mass, ρ is fluid density, ϕ is the porosity, A is the cross-sectional area of the core plug, P_c is capillary pressure and t is the imbibition time. The imbibed volume (V) is given by

$$V = \sqrt{\frac{2 A \phi K S_{wf} P_c}{\mu}} \sqrt{t} \quad (2)$$

Figure 8 shows the imbibed volume versus square root of time for both oil and brine. As evident from the plots, imbibed volume increases linearly with square root of time and finally reaches plateau, representing the equilibrium conditions. We refer to the slope of the linear section of each curve m_w and m_o for brine and oil, respectively. The ratio of the slopes is given by

$$m = \frac{m_o}{m_w} = \sqrt{\frac{A_o \phi_o K_o S_{wf_o} P_{c_o} \mu_w}{A_w \phi_w K_w S_{wf_w} P_{c_w} \mu_o}} \quad (3)$$

Here, ϕ is core porosity, S_{of} and S_{wf} are saturations at the imbibition front, K_o and K_w are effective permeabilities, μ_o and μ_w are viscosities, P_{c_o} and P_{c_w} are capillary pressures for oil and brine, respectively. We assume that P_c can be approximated by Young-Laplace relationship, $P_c = \frac{2\sigma \cos \theta}{r}$, and for simplicity, we ignore the pore size distribution and tortuosity of oil and brine flow networks (Cai and Yu, 2011). The imbibition results suggest that water imbibes only into a fraction of the pore network. Therefore, we expect that $\phi S_{wf} < \phi S_{of}$ and $K_w < K_o$. Using the equilibrated values of imbibed oil and brine volumes, we assume $\left(\frac{\phi S_{of}}{\phi S_{wf}}\right) \approx \left(\frac{I_o}{I_w}\right)$ and by considering the Kozney-Carman correlation (Carrier, 2003), we assume

that $\frac{K_o}{K_w} \approx \left(\frac{\theta S_{of}}{\theta S_{wf}} \right)^2$. I_o and I_w are the equilibrated values of normalized imbibed volume for oil and brine, respectively. Finally, Eq. 3 can be simplified to

$$m = \sqrt{\left(\frac{I_o}{I_w} \right)^3 \frac{\cos\theta_o \sigma_o \mu_w}{\cos\theta_w \sigma_w \mu_o}} \quad (4)$$

Here, we assumed that the average pore radius (r) for oil and brine imbibition are relatively close. Since twin plugs are used in our experiments, we assume $A_o = A_w$. Rearranging Eq. 4 gives

$$\frac{\cos\theta_o}{\cos\theta_w} = m^2 \frac{\sigma_w \mu_o}{\sigma_o \mu_w} \left(\frac{I_w}{I_o} \right)^{1.5} \quad (5)$$

Finally, we define the following wettability indices for oil and brine:

$$WI_o^{sl} = \frac{\cos\theta_o}{\cos\theta_w} \quad (6)$$

$$WI_w^{sl} = \frac{\cos\theta_w}{\cos\theta_o} \quad (7)$$

$$WI_o^{sl} * WI_w^{sl} = 1 \quad (8)$$

The values of m and $\frac{I_w}{I_o}$ can be obtained from oil and brine imbibition profiles. Table 6 lists the values of m , I_o , I_w , and WI_o^{sl} .

2. Equilibrium affinity index

To compare the affinity of the core plugs to oil and brine, we also use the wettability indices defined by Lan et al. (Lan et al., 2015):

$$WI_o^{eq} = \frac{I_o}{I_w + I_o} \quad (9)$$

$$WI_w^{eq} = \frac{I_w}{I_w + I_o} \quad (10)$$

$$WI_w^{eq} + WI_o^{eq} = 1 \quad (11)$$

Eqs. 9 and 10 quantify the capacity of the samples to imbibe oil and brine, respectively. Eqs. 6 and 7 quantify the affinity of the pore surface to oil and brine, respectively, during imbibition process. Combined analyses of the two sets of indices provide useful insight in rock-fluid interactions.

Table 7. The equilibrium values of normalized imbibed volume of oil and brine and the slopes of oil and brine imbibition data versus square root of time.

| | I_w | m_o ($m^3s^{0.5}$) | m_w ($m^3s^{0.5}$) | m | WI_o^{sl} |
|------|-------|---------------------------|---------------------------|------|-------------|
| MT-1 | 0.63 | 0.33 | 0.1 | 1 | 4 |
| MT-2 | 0.42 | 0.28 | 0.02 | 0.28 | 0.31 |
| MT-3 | 0.76 | 0.33 | 0.1 | 1.11 | 4.9 |
| MT-4 | 0.44 | 0.33 | 0.03 | 0.5 | 1 |
| MT-5 | 0.51 | 0.30 | 0.77 | 1 | 3.5 |

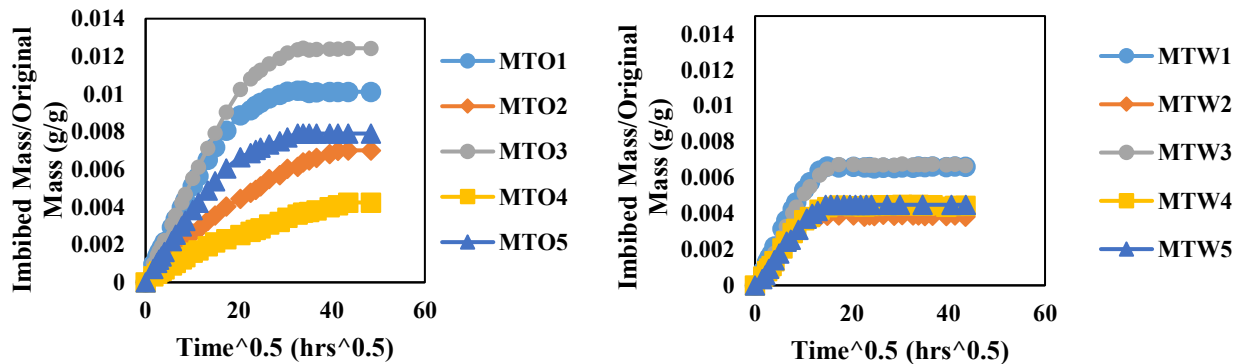


Figure 8. Oil and brine imbibition profiles versus square root of time.

WI₀^{eq} versus other petrophysical data

Figure 9 shows WI₀^{eq} versus porosity and permeability, NPOR, GR. Figure A4 of Appendix, shows correlation between MICP porosity and permeability. Figure A4, indicates that porosity and permeability of the plugs once plotted on a logarithmic scale follow a perfectly linear trend. According to figure 9, WI₀^{eq} increases with increasing porosity and permeability and decreases with increasing NPOR and GR. These results indicate that at higher NPOR and GR readings the twin plugs have less affinity towards oil. The samples with higher values of GR reading and NPOR are expected to have higher clay content.

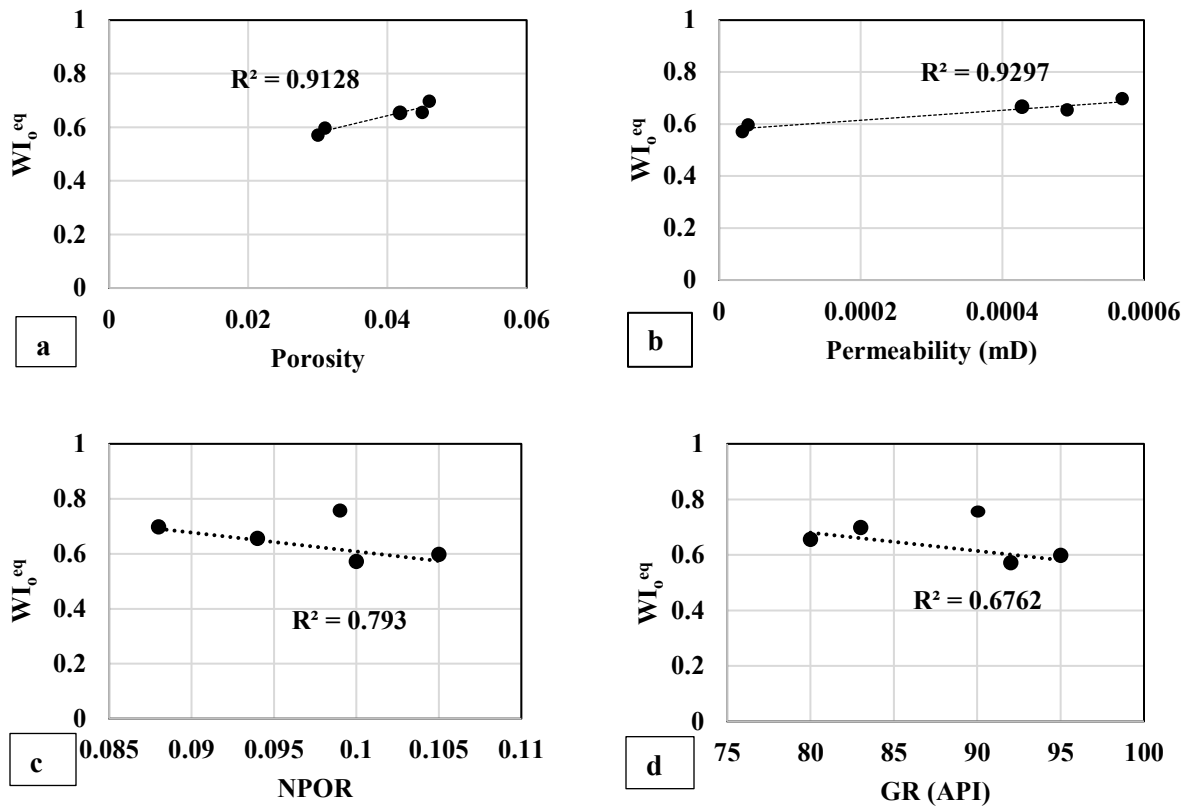


Figure 9. WI₀^{eq} versus other petrophysical properties.

WI_o^{sl} versus other petrophysical data

Figure 10 represents m_w (slope of brine imbibition versus square root of time) versus m_o (slope of oil imbibition versus square root of time). In general, m_o and m_w are positively correlated. The two samples with higher values of m_o and m_w have higher values of porosity and permeability. Therefore, the results indicate the effect of rock porosity and permeability on the imbibition rate.

Figure 11 represents WI_o^{sl} versus porosity and permeability, NPOR, GR. WI_o^{sl} represents the preferential affinity of the samples to oil over brine, and according to the plots, WI_o^{sl} increases with increasing porosity and permeability and decreases with increasing NPOR and GR.

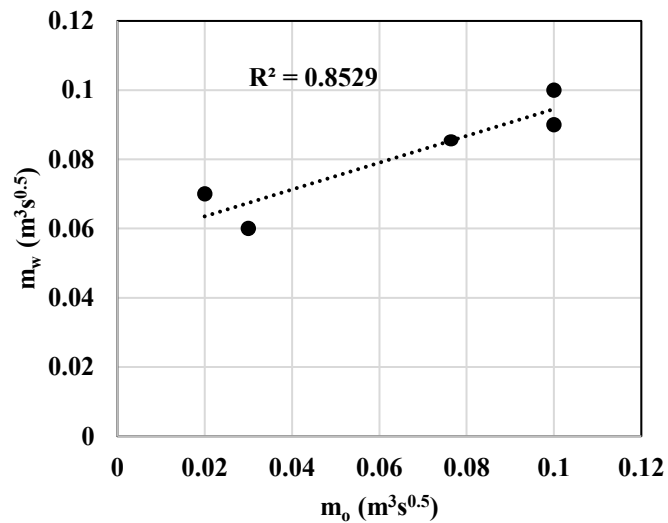


Figure 10. m_w versus m_o for the five twin plugs.

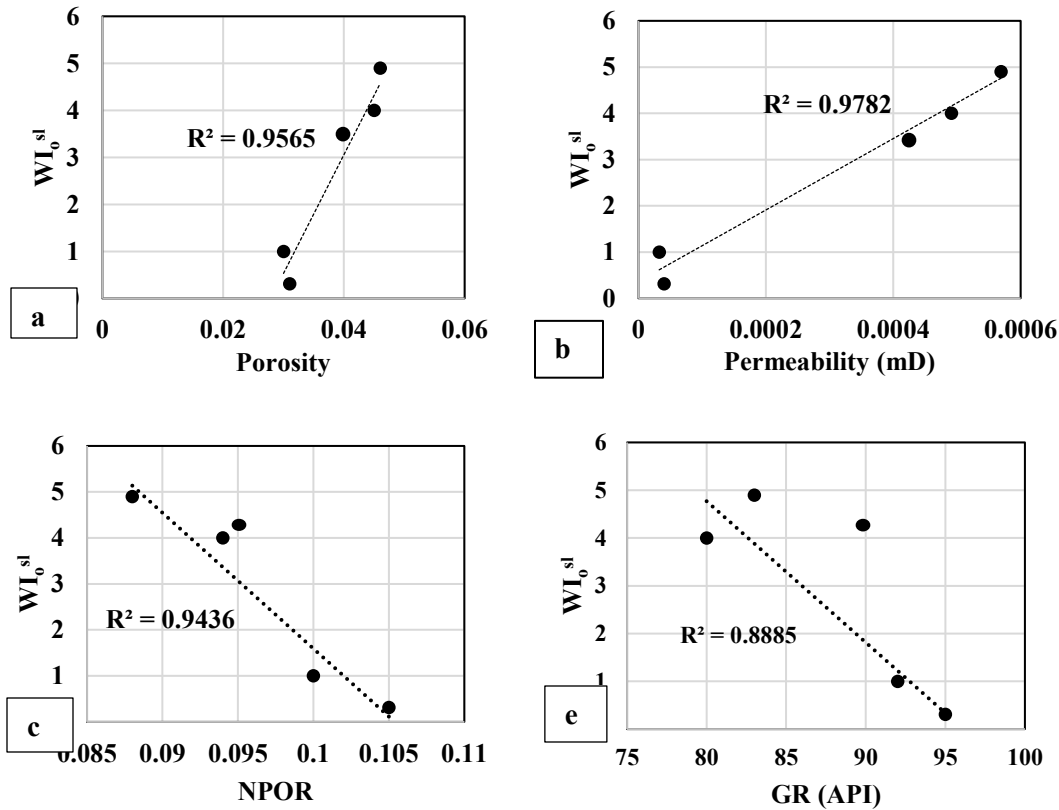


Figure 11. WI_0^{sl} versus other petrophysical properties.

Summary of Results and Discussions

In this paper, we investigate spontaneous imbibition of oil and brine into five binary core samples from the Montney formation. The samples are cored from 2100-2200m depth and have relatively low clay (11-13 wt %) and very low TOC (0.02- 0.05). Contact angle measurements indicate samples are oil wet. This observation is supported by spontaneous imbibition results. Normalized imbibed oil volume, I_o (0.42- 0.76), is generally higher than normalized imbibed brine volume, I_w (0.3- 0.33). In order to characterize the samples more precisely, we plot multivariate scatterplots for five variables I_w , I_o , NPOR, GR and MICP porosity. The results suggest that porosity is implicit to fluid uptake of the core samples. Although I_o increases with increasing porosity and decreases with increasing the GR and NPOR logs, I_w remains relatively constant. For further analysis of oil and brine uptake of the plugs, we defined two sets of affinity

indices: slope affinity index (WI_o^{sl} , WI_w^{sl}) and equilibrium affinity index (WI_o^{eq} , WI_w^{eq}). WI_o^{eq} increases with increasing porosity and permeability, and decreases with increasing NPOR and GR. These results indicate that at higher NPOR and GR readings the twin plugs have less affinity towards oil. The samples with higher values of GR reading and NPOR are expected to have higher clay content. Similarly, WI_o^{sl} increases with increasing porosity and permeability, and decreases with increasing NPOR and GR. In general, the positive correlations between WI_o^{sl} and porosity/permeability are stronger than that between WI_o^{eq} and porosity/permeability. Overall, the results suggest that that part of the pore network has a stronger affinity to oil than to water.

Protocol Limitations

The approach presented in this paper has a number of limitations due to some measurement uncertainties:

Log data: Usually, log resolution is 2 feet. If the depth of the cored samples falls between each measured data point, statistical approaches [28-30] need to be applied in order to estimate the data at the unknown sampled location.

MICP porosity data: Lab porosities measured through mercury porosimetry may be underestimated for tight and shale rocks. The mercury injection pressure may not be high enough to overcome the threshold capillary pressure for small pores, and that results in underestimation of porosity.

Imbibition data: The twin plugs are cored as close as possible but there still remains some degree of heterogeneity which may lead to some differences in the petrophysical properties of the twin plugs. In addition, phase trapping due to snap-off during the imbibition process was not considered in this work.

Conclusions

In this research, we measured oil and brine uptake of five twin plugs cored from the Montney formation. First, we parametrized imbibed quantities of oil and brine into each twin set. We defined two sets of affinity indices: slope affinity index and equilibrium affinity index. Through multivariate scatterplots, we

investigated correlations between indices and other petrophysical properties such as porosity, permeability, gamma spectra and neutron porosity logs. The following results are inferred after analyzing experimental results:

- 1- In general, oil imbibes slower than brine in the samples, but finally reaches to equilibrium with a higher value compared to brine.
- 2- Both slope affinity and equilibrium affinity indices for the oil phase increase by increasing ϕ and k , with slope affinity showing a stronger correlation. This observation suggests that part of the pore network has a stronger affinity to oil than to water.
- 3- Air-liquid contact angle results suggest that the samples are preferentially oil-wet, as oil fully spreads on the rock surface while brine partially wets the surface.

Overall, this study demonstrates that porosity is a key parameter controlling the fluid uptake of tight rock core samples from the Montney formation. We also observed useful correlations between rock wettability and neutron porosity and spectral gamma ray logs. Such correlations can be applied for quick evaluation of rock wettability by using the commonly-available open-whole logs.

Nomenclature

A = Surface area, m^2

A_o = Surface area, m^2

A_w = Surface area, m^2

I_o = Normalized oil volume

I_w = Normalized brine volume

K = Permeability, m^2

K_o = Permeability, m^2

K_w = Permeability, m^2

m_o = Oil imbibition profile versus square root of time slope

m_w = Brine imbibition profile versus square root of time slope

M = Mass, kg

P_c = Capillary pressure, Psi

P_{co} = Oil capillary pressure, Psi

P_{cw} = Brine capillary pressure, Psi

S_{wf} = Saturation at front

S_{wfo} = Oil saturation at front

S_{wfw} = Brine saturation at front

T = time, s

V = Volume, m^3

WI_o^{eq} = Wetting affinity index of oil

WI_w^{eq} = Wetting affinity index of oil

WI_o^{sl} = Slope wetting affinity index of oil

WI_w^{sl} = Slope wetting affinity index of oil

μ = viscosity, $Kg\ m^{-1}\ s^{-1}$

μ_o = Oil viscosity, $Kg\ m^{-1}\ s^{-1}$

μ_w = Brine viscosity, $Kg\ m^{-1}\ s^{-1}$

ϕ = Porosity

ϕ_o = Oil porosity

ϕ_w = Brine porosity

Acknowledgement

We thank Encana Corporation for providing the rock samples and petrophysical data, and NSERC (Natural Science and Engineering Research Council of Canada) for supporting this work.

Reference

- [1] M.F. Aloulou Fawzi, Meg Coleman, Tight oil production pushes U.S. crude supply to over 10% of world total, in: I.S. Analysis (Ed.), 2014.
- [2] North American Light Oil, in, Natural Resources Canada.
- [3] Understanding Tight Oil, in: C.S.f.U. Resources (Ed.).
- [4] P.H. Nelson, Pore-throat sizes in sandstones, tight sandstones, and shales in, AAPG Bulletin, 2009, pp. 329-340.
- [5] O. Kai, Shidong, Overview of nanofluid for EOR and its effect on wettability, NTNU, (2013).
- [6] Marthe, Investigation of Nanoparticle Effect on Wettability and Interfacial tension, NTNU, (2013).
- [7] E. Ghanbari, H. Dehghanpour, The fate of fracturing water: A field and simulation study, Fuel, 163 (2016) 282-294.
- [8] E. Amott, Observations relating to the wettability of porous media, AIME, (1959) 156-162.
- [9] H. Dehghanpour, Q. Lan, Y. Saeed, H. Fei, Z. Qi, Spontaneous imbibition of brine and oil in gas shales: effect of water adsorption and resulting microfractures, Energy & Fuels, 27 (2013) 3039-3049.
- [10] Q. Lan, E. Ghanbari, H. Dehghanpour, R. Hawkes, Water loss versus soaking time: spontaneous imbibition in tight rocks, Energy Technology, 2 (2014) 1033-1039.
- [11] N.R. Morrow, Wettability and its effect on oil recovery, J. Petrol. Technol., (1990) 1476-1484.
- [12] E.C. Donaldson, Thomas, R.D., Lorenz, P.B., Wettability determination and its effect on recovery efficiency, Soc. Petrol. Eng., (1969) 13-20.
- [13] S.C. Jones, Roszelle, W.O., Graphical techniques for determining relative permeability from displacement experiments, J. Petrol. Technol., (1978) 807-817.
- [14] R.J.S. Brown, Fatt, I., Measurements of fractional wettability of oil fields' rocks by the nuclear magnetic relaxation method, in: Fall Meeting of the Petroleum Branch of AIME, Los Angeles, 1956.
- [15] E.O. Odusina, C.H. Sondergeld, C.S. Rai, NMR study of shale wettability, in: Canadian Unconventional Resources Conference, Society of Petroleum Engineers, 2011.

- [16] N. Morrow, S. Ma, X. Zhou, X. Zhang, Characterization of wettability from spontaneous imbibition measurements, in: Annual Technical Meeting, Petroleum Society of Canada, 1994.
- [17] W. Anderson, Wettability literature survey-part 2: Wettability measurement, Journal of Petroleum Technology, 38 (1986) 1,246-241,262.
- [18] R. Freedman, N. Heaton, M. Flaum, G. Hirasaki, C. Flaum, M. Hürlimann, Wettability, saturation, and viscosity from NMR measurements, SPE Journal, 8 (2003) 317-327.
- [19] B.J. Washburn KE, A new laboratory approach to shale analysis using NMR relaxometry, in: The SPE conference at Unconventional Resources Technology Conference, Denver, CO, USA., 2013.
- [20] A. Borysenko, B. Clennell, R. Sedev, I. Burgar, J. Ralston, M. Raven, D. Dewhurst, K. Liu, Experimental investigations of the wettability of clays and shales, Journal of Geophysical Research: Solid Earth, 114 (2009).
- [21] A. Habibi, M. Binazadeh, H. Dehghanpour, D. Bryan, G. Uswak, Advances in Understanding Wettability of Tight Oil Formations, in: SPE Annual Technical Conference and Exhibition, Society of Petroleum Engineers, 2015.
- [22] D.R. Kendall, Sedimentology and stratigraphy of the lower Triassic Montney formation, Peace River Basin, subsurface of northwestern Alberta, University of Calgary, 1999.
- [23] K. Peters, Guidelines for evaluating petroleum source rock using programmed pyrolysis, AAPG bulletin, 70 (1986) 318-329.
- [24] M.M. Herron, Geochemical classification of terrigenous sands and shales from core or log data, Journal of Sedimentary Research, 58 (1988).
- [25] K. Rankama, and Sahama, T. G., Geochemistry, University of Chicago Press, (1950).
- [26] Q. Lan, H. Dehghanpour, J. Wood, H. Sanei, Wettability of the Montney tight gas formation, SPE Reservoir Evaluation & Engineering, (2015).
- [27] L. Handy, Determination of effective capillary pressures for porous media from imbibition data, Trans. AIME, 219 (1960) 75-80.

[28] Yarveicy, H., & Ghiasi, M. M.. "Modeling of gas hydrate phase equilibria: Extremely randomized trees and LSSVM approaches." *Journal of Molecular Liquids* (2017).

[29] Yarveicy, H., Moghaddam, A. K., & Ghiasi, M. M.. "Practical use of statistical learning theory for modeling freezing point depression of electrolyte solutions: LSSVM model." *Journal of Natural Gas Science and Engineering* 20 (2014): 414-421.

[30] Ghiasi, M. M., Yarveicy, H., Arabloo, M., Mohammadi, A. H., & Behbahani, R. M.. "Modeling of stability conditions of natural gas clathrate hydrates using least squares support vector machine approach." *Journal of Molecular Liquids* 223 (2016): 1081-1092.

Appendix

Figures A1 and A2 represent I_o and I_w versus NPOR, GR, and concentrations of potassium, thorium and uranium.

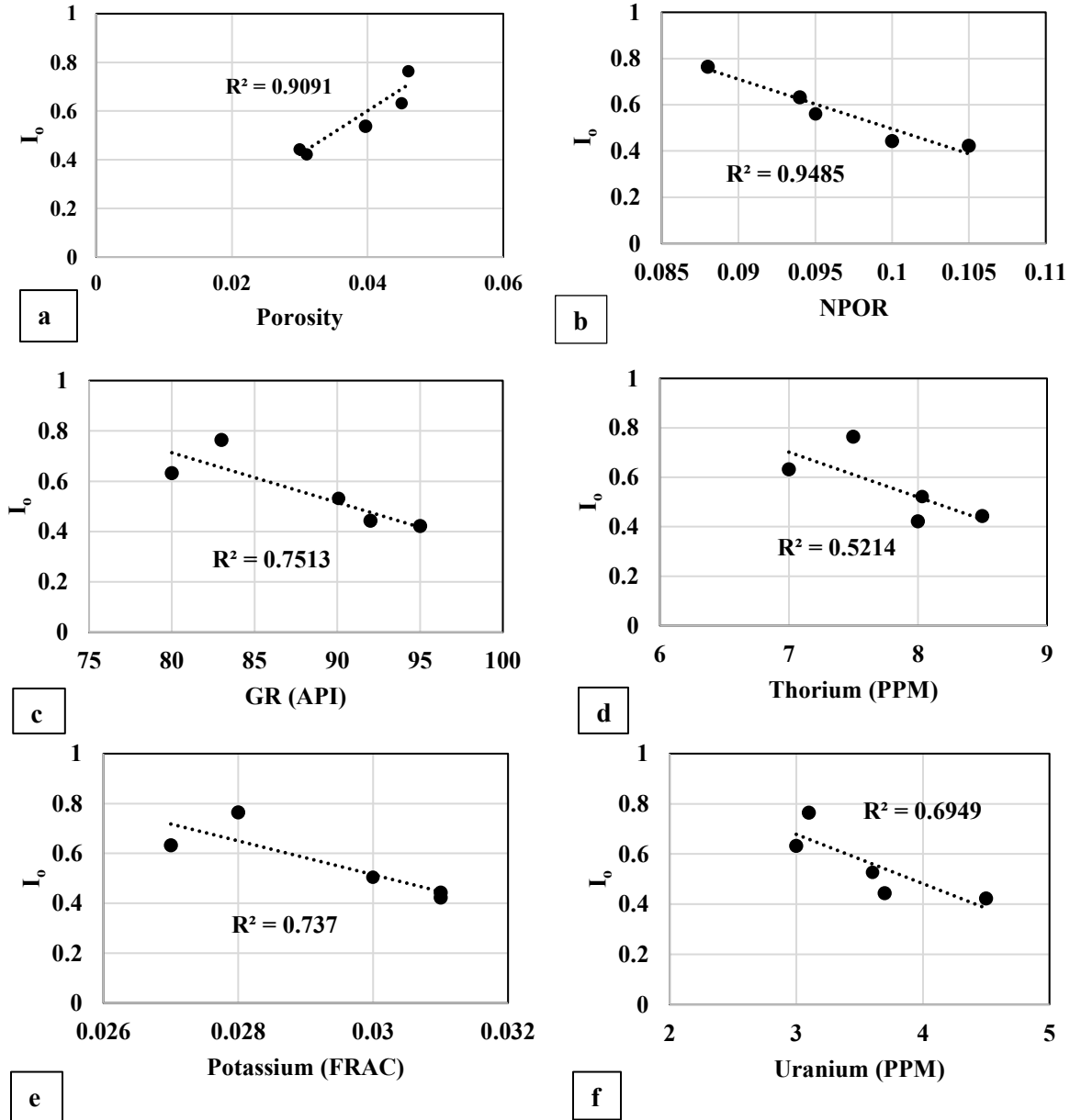


Figure A1. I_o versus log measurements.

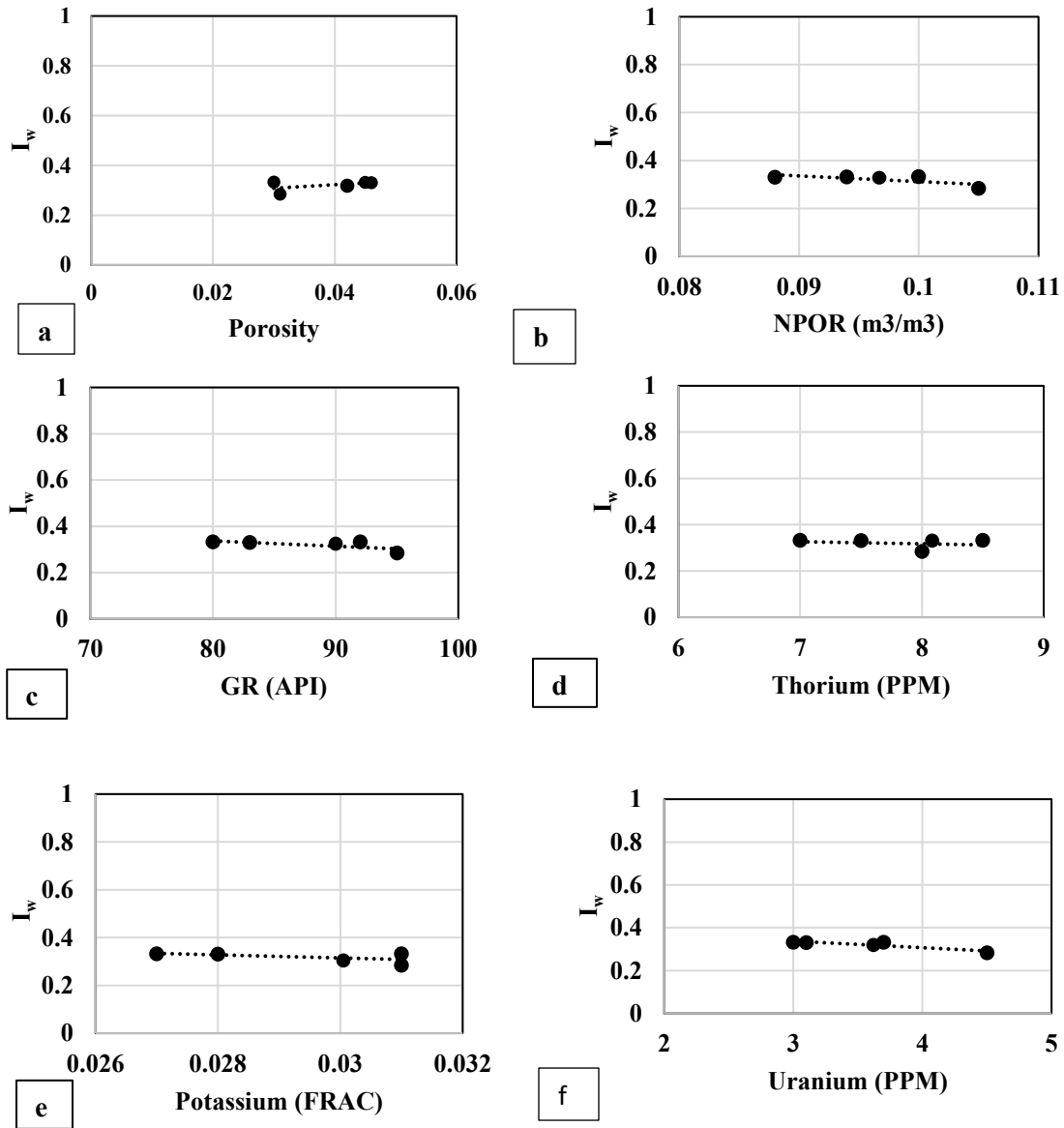
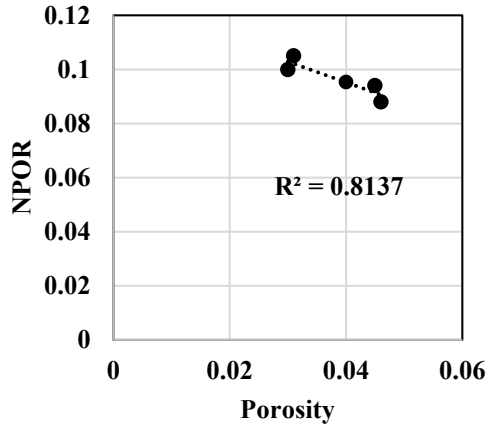
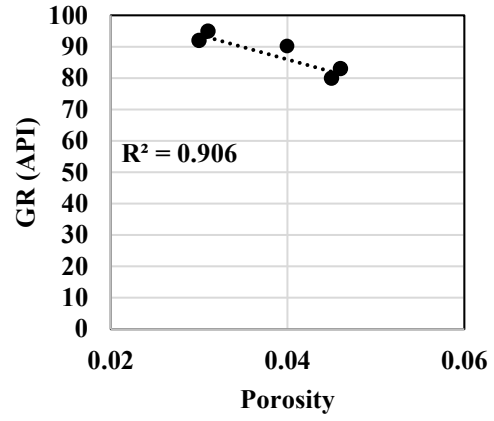


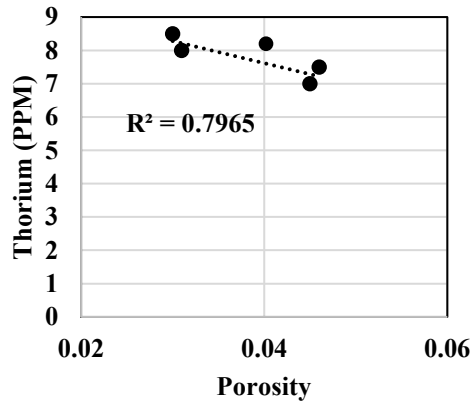
Figure A2. I_w versus log measurements



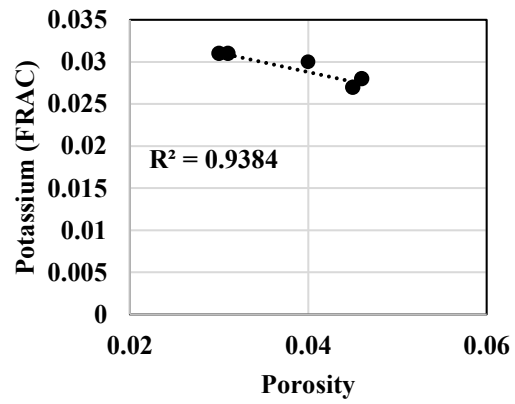
a



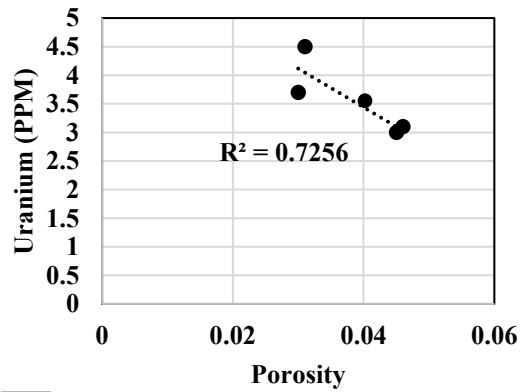
b



c



d



e

Figure A3. Log measurements versus porosity.

Figure A3 shows the log measurements versus MICP porosity. Figure A4, represents correlation between logarithm of porosity and permeability of the five data points. Since the samples are cored from a fine-grained formation, the correlation is linear. Hence, all log measurements in figure 8 versus permeability follow power law curve.

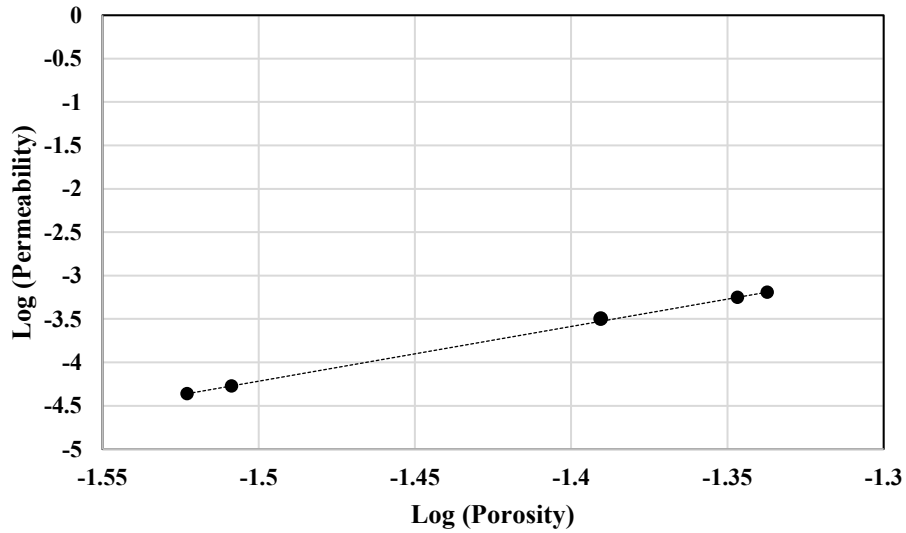


Figure A4. Log (Permeability) versus Log (Porosity).

Chapter 3

Application of imbibition transient analysis in pore network characterization of tight rocks

Abstract

Unconventional rock formations have complex pore networks in terms of pore/grain size, inter/intra-pore connectivity and organic content. In this paper, we apply a novel imbibition transient analysis method for characterize pore network of tight rocks based on spontaneous imbibition data. First, we conduct systematic co-current spontaneous imbibition experiments on five pairs of rock samples cored from the Montney Formation using reservoir oil and brine. Weight gain of the samples are recorded with time. Next, we plot spontaneous imbibition profiles for both brine and oil versus time and square root of time. Two different type of trends are observed. In one trend, two major regions are observed: imbibition profiles increase linearly when plotted versus square root of time and plateau. In another trend, three major regions are observed: imbibition profile increases linearly first then at some point the slope lowers and finally reaches plateau. Based on the spontaneous imbibition profiles, we categorized the pore network of these samples into type I and type II. We propose a decoupling scheme to characterize both types of imbibition profiles. The decoupling model assumes that a type I imbibition profile occurs when mainly one pore network dominates fluid flow in the rock pore-network. On the other hand, the model assumes that type II imbibition profile is the result of imbibition in both inter and intra pore networks. Hence, two different slopes are observed in the imbibition profile. Investigation of the pore size distribution profiles, SEM images, and elemental maps confirms that two different slopes in type II imbibition profiles and subsequently duality in fluid flow originates from duality in pore network of the rock sample. The results of this study indicates pore-network complexities can influence fluid flow.

Introduction

Recent advances in horizontal drilling and hydraulic fracturing have brought unconventional resources as viable hydrocarbon reserves across the world [1]. Upon drilling, 3-5 million gallons of water may be injected to fracture the horizontal well [2, 3]. Sometimes, the well is then closed to promote imbibition of the fracturing fluid into the matrix (soaking period). The well is then opened to allow recovery of fracturing fluid (i.e flowback period) and subsequent production. A major concern regarding hydraulic-fracturing process for the development of unconventional formations is that water based fracturing fluid injected into the formation gets retained and only 10-30% of the injected fluid recovers back to the surface during flowback [4, 5]. Factors responsible for retention of slick water in the reservoir formation are still poorly understood. Gravity segregation in fractures [6-8], water retention in secondary fractures[4], spontaneous imbibition of fracturing fluid into the rock matrix [9-12] and subsequent fractures caused by capillary suction of the imbibed fluid [13-16] are thought to be responsible for inefficient water recovery. Although higher water retention by the formation might lead to higher recovery [17-19], huge amounts of unrecoverable water retained in unconventional formations can add up to operational costs and cause environmental and seismic anomalies.

Accurate pore-network characterization and rock/fluid interaction [21,22] can be beneficial for optimum hydraulic fracturing operations. Unconventional rocks have complicated pore-networks composed of cracks, larger intergranular pores compared with smaller intragranular pores ranging in size from microns to nanometers [20, 23]. Fine-grained reservoirs can contain a variety of pore types: inter-granular, intra-granular, fracture, intra-kerogen, and intra-pyrobitumen/char, the last two 'organic-hosted' pores are more obvious at higher maturities [24]. Loucks demonstrated that unconventional rocks have two different sets of pore network systems [23]. One kerogen-covered organic matter pores, and the other pore-networks composed of inter/intra particle. Although unconventional rocks have a very complex pore network, studies on the role of these complexities in fluid flow/uptake and mechanisms that control the imbibition behavior of the ultra-low permeability rocks is scarce.

In this paper, we study the role of inter/intra pore system in spontaneous imbibition of tight-oil rock samples cored from the Montney Formation via spontaneous imbibition in twin core plugs. Based on the observed oil and brine imbibition plots, we propose a decoupling theory to characterize the pore-network of ultra-low permeable tight rocks. Pore size distribution of the rock samples and SEM images are also reported to support the proposed decoupling theory.

Experiments

We measured the spontaneous imbibition of oil and brine in tight samples from Montney formation. Core plugs are characterized by measuring clay and TOC content, permeability and porosity. Physical properties of reservoir oil and brine are measured as well.

Materials

Five twin plugs are selected from a well in the Montney Formation in the zone of 2100-2200 m.

Core plugs

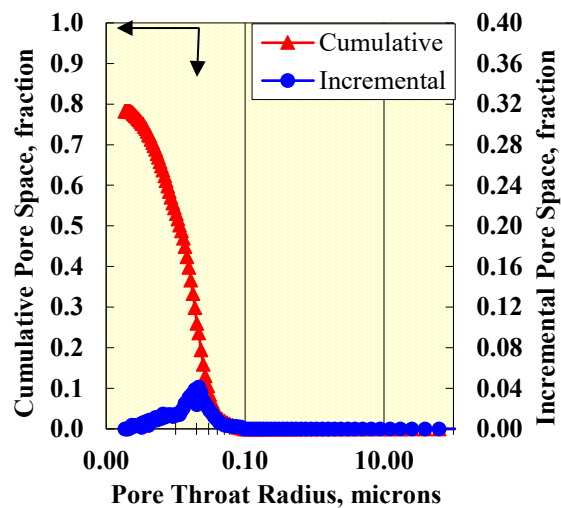
Petrophysical properties of the selected Montney plugs are listed in Table 1. Montney Formation is a stratigraphical unit of Lower Triassic age in the Western Canadian Sedimentary Basin [25] which crosses through a large area of British Columbia, trending northwest from the Alberta border to Fort St. John [26]. Montney Formation is one of the major economically feasible plays in North America [27]. The formation is composed of siltstone and dark grey shale, with dolomitic siltstone in the base and fine grained sandstone towards the top [28]. The formation thickness reaches to 320 m in some locations is divided into upper and lower Montney. In general, water saturation at reservoir condition is less than 50% in the upper Montney and less than 30% in the lower Montney [29].

Five pairs twin plugs were selected for this study. The cores were drilled using a dry-cut machine and supercooled nitrogen gas as lubricant. The samples were stored at ambient conditions for several weeks prior to the imbibition experiments. Depth, clay and TOC content, porosity, and permeability of the core samples are listed in Table 1. The clay content is within 12.3-14.0% and the amount of total organic carbon is very low (0.20-0.55%).

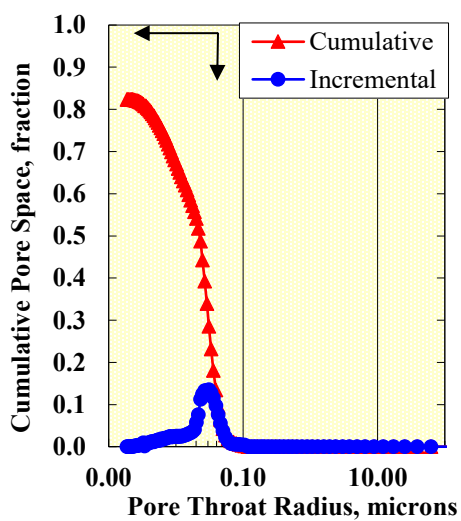
Table 1. Clay, TOC content, Porosity and permeability of twin plugs.

| Rock number | Depth (m) | Clay (wt %) | TOC (wt %) | Porosity | Permeability (mD) |
|-------------|-----------|-------------|------------|----------|-------------------|
| MT1 | 2144 | 13.1 | 0.2 | 0.045 | 49E-05 |
| MT2 | 2149 | 12.3 | 0.24 | 0.031 | 4E-05 |
| MT3 | 2174 | 13.2 | 0.32 | 0.046 | 56E-05 |
| MT4 | 2192 | 12.3 | 0.44 | 0.030 | 3E-05 |
| MT5 | 2196 | 14.0 | 0.55 | 0.036 | 1.26E-04 |

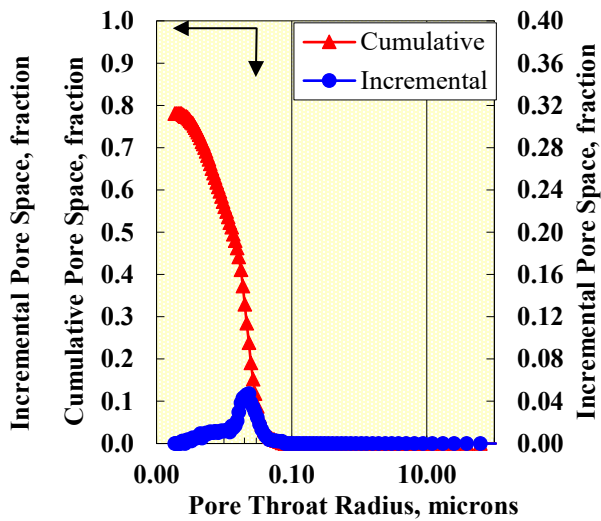
Figure 1 shows pore-throat size distributions of MT1 (a), MT2 (b), MT3 (c), MT4 (d) and MT5 (e). International Union of Pure and Applied Chemistry (IUPAC) [28] suggests pores can be categorized according to their pore-throat size as: micropores (< 2 nm), mesopores (2 nm < pores <50 nm) and macropores: (> 50 nm). According to this classification and Figure 1, all tested samples have a considerable volume (70-80%) of their pore space in mesopores.



(a)



(b)



(c)

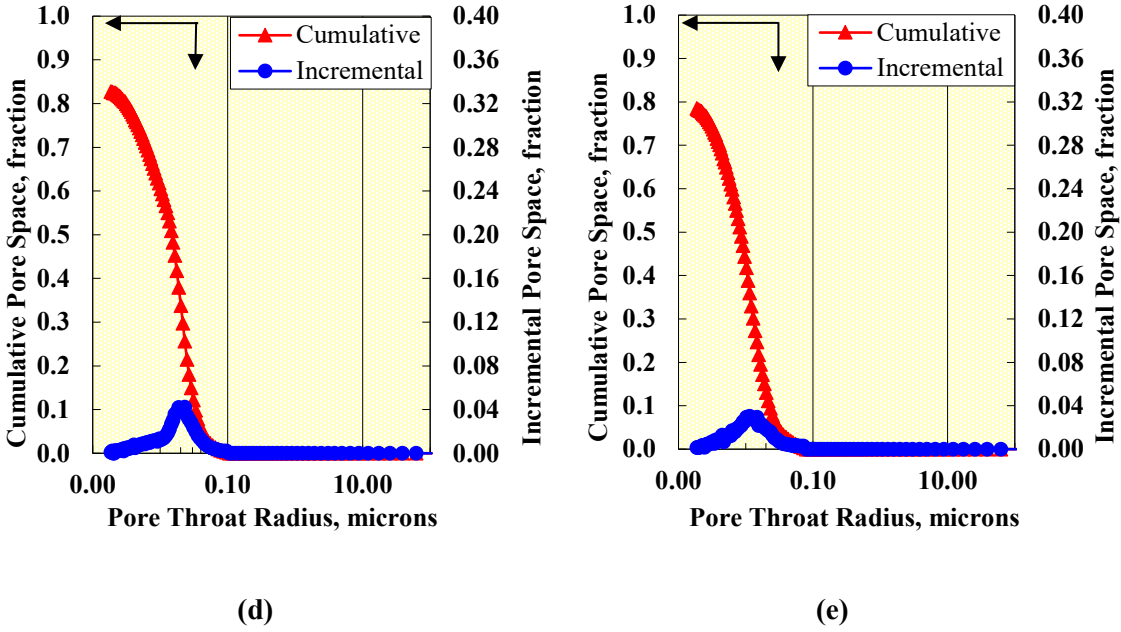


Figure 1. Pore-throat size distribution of five rock samples (a) MT1 (b) MT2 (c) MT3 (d) MT4 (e) MT5.

The distributions show all samples have considerable volume of their pore space in mesopores.

Fluids

Reservoir brine and oil were used as imbibing aqueous and oleic phases, respectively. Physical properties of brine and oil are listed in Table 3 and Table 4 respectively. The brine is highly saline water with measured total dissolved solids of 126g/L and the total hardness of 22g/L. The brine is almost neutral in terms of alkalinity. The oil is light with API=45.07, and is low in sulphur content (0.0796 wt%).

Table 2. Physical properties of brine

| Property | Quantity |
|--|----------|
| Total Dissolved Solids (g/L)-Measured | 126 |
| Total Dissolved Solids (g/L)-Calculated | 130 |
| Relative Density | 1.101 |
| Surface Tension (mN/m) | 67 |
| Refractive Index | 1.356 |
| Conductivity ($\mu\text{S}/\text{cm}$) | 159000 |
| Resistivity ($\Omega\text{-m}$) @25 $^{\circ}\text{C}$ | 0.06 |

| | |
|--|--------|
| Total Hardness as CaCO ₃ (mg/L) | 22000 |
| Total Alkalinity as CaCO ₃ (mg/L) | 110 |
| Observed pH | 6.89 |
| H ₂ S Spot Test | Absent |
| Viscosity (cP) | 1.18 |

Table 3. Physical properties of oil

| Property | Quantity |
|--|----------|
| Density of Clean oil @15 ⁰ C (ASTM D5002) | 1 |
| Relative Density | 0.8014 |
| API | 45.07 |
| Surface tension (mN/m) | 28 |
| Total Sulphur (mass percent) ASTM D4294 | 0.0796 |
| Pour Point (⁰ C) ASTM D97/D5853 | <-35 |
| Viscosity(cP) | 1.84 |

Experimental Procedure

Comparative oil/brine spontaneous imbibition tests are done on five sets of twin plugs dry-cut from formation cores. The general procedure for the imbibition tests is as follows:

- 1- The original weight of each plug is measured using a precision digital balance.
- 2- One plug of each twin set is placed in a cell partly filled with brine and the other plug is placed in a cell partly filled with oil. As shown in Figure 2, only the bottom face of the plugs is exposed to the imbibing fluid.
- 3- The top of the imbibition cell is sealed using an impermeable cap to avoid liquid evaporation.
- 4- The weight of each plug is measured periodically and recorded. Once the spontaneous imbibition process reaches equilibrium experiments are stopped.

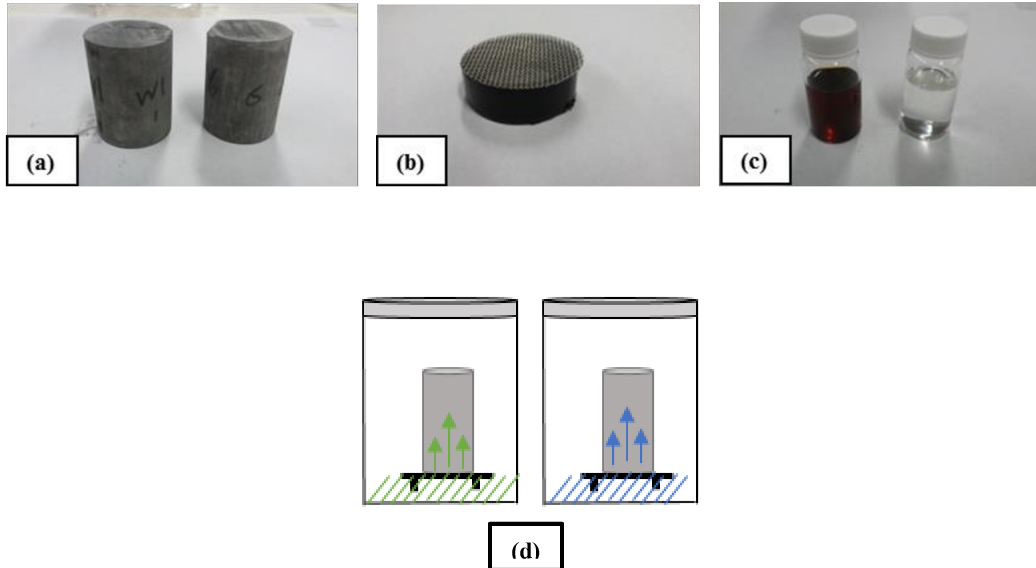


Figure 2. The materials used for the imbibition tests: (a) twin core plugs, (b) mesh and rubber stand, and (c) oil and brine samples. Twin imbibition cells showing oil and brine imbibing into twin plugs (d).

Results, Models and Discussions

In this section we discuss the experimental results and analyze role of pore-network complexities on brine and oil spontaneous imbibition of tight rock sandstone.

Spontaneous imbibition

Imbibed mass over original mass for MT1, MT2, MT3, MT4 and MT5 core samples are plotted versus time in Figure 3a and 3b respectively. Oil and brine imbibition profiles for the samples versus square root of time are plotted in Figures 3c and 3d respectively. As can be seen in Figures 3c and 3d, imbibition profiles once plotted versus square root of time increases linearly and then reaches equilibrium and plateau. In contrast, sample MT5 shows a different trend. This sample keeps imbibing oil/brine during the time course of the experiment with two different slopes in the imbibition profiles versus square root of time. For example, as can be seen from Figure 4, brine imbibition in sample MTB5 increases linearly at the early time. After 130 hrs, when the fluid front reaches the top of the sample, the sample keeps imbibing fluid and an inflection point appears on the imbibition profile after which the imbibition progresses with a reduced slope. A similar trend is observed for oil imbibition into the MT5.

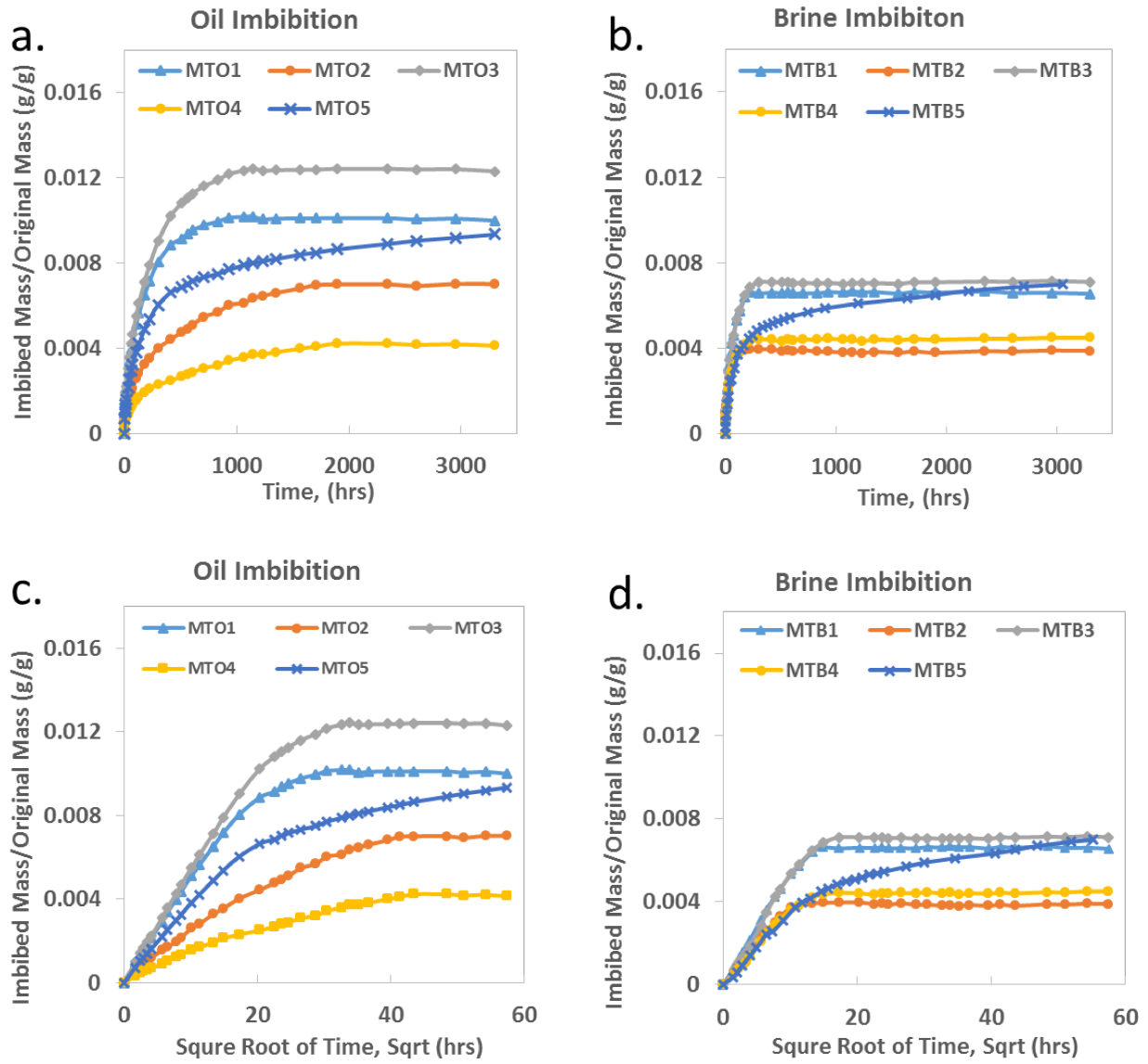


Figure 3. Imbibed mass of oil (a. and c.) and brine (b. and d.) versus time (a. and b.) and square root of time (c. and d.).

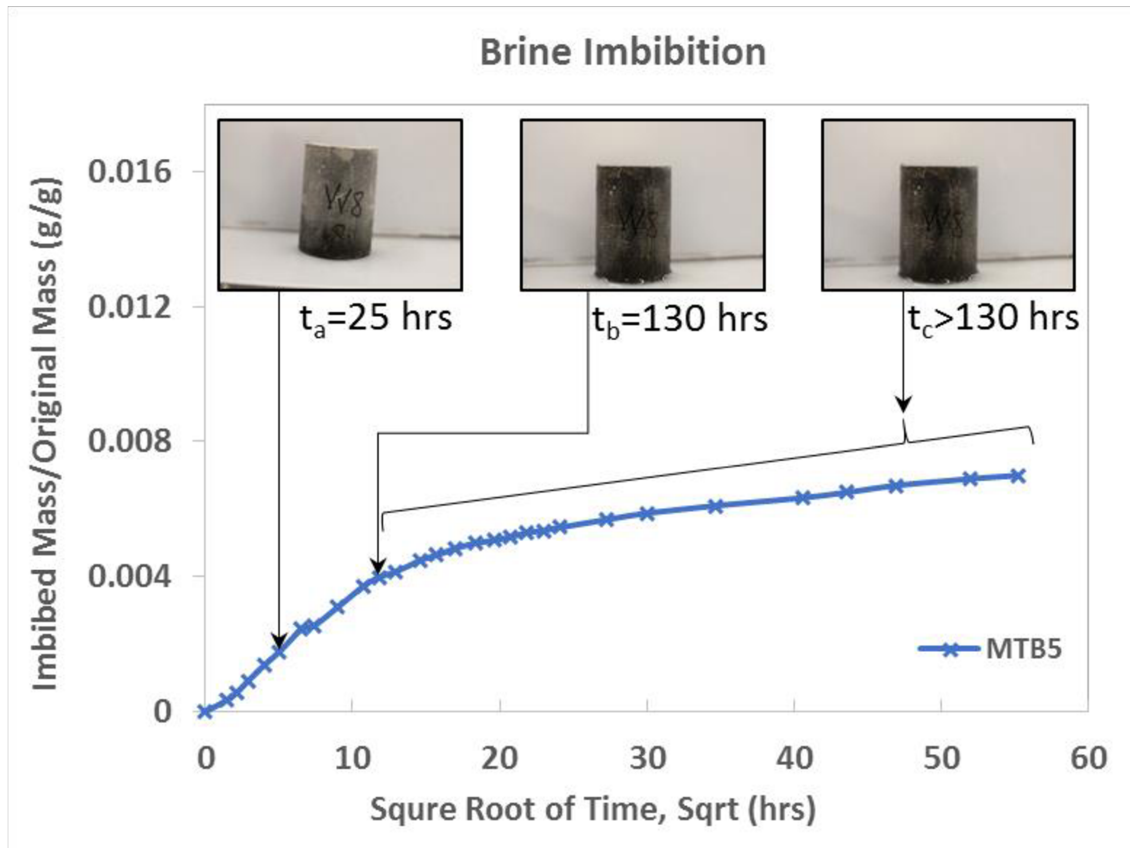


Figure 4. Brine spontaneous imbibition profile versus square root of time for MTB5. The plot shows a break point at 11.4 hr^2 (130 hrs) where the slope changes to a lower value.

Pore size distribution

Figure 5 represents mercury injection capillary pressure (MICP) data of the rock samples. According to this classification all samples have a considerable volume of their pore space in mesopores. MICP plots of all samples are composed of a bell-shaped part and a tail part. The bell-shaped part mainly represents the inter pore space and the tail part mainly represents the tail part.

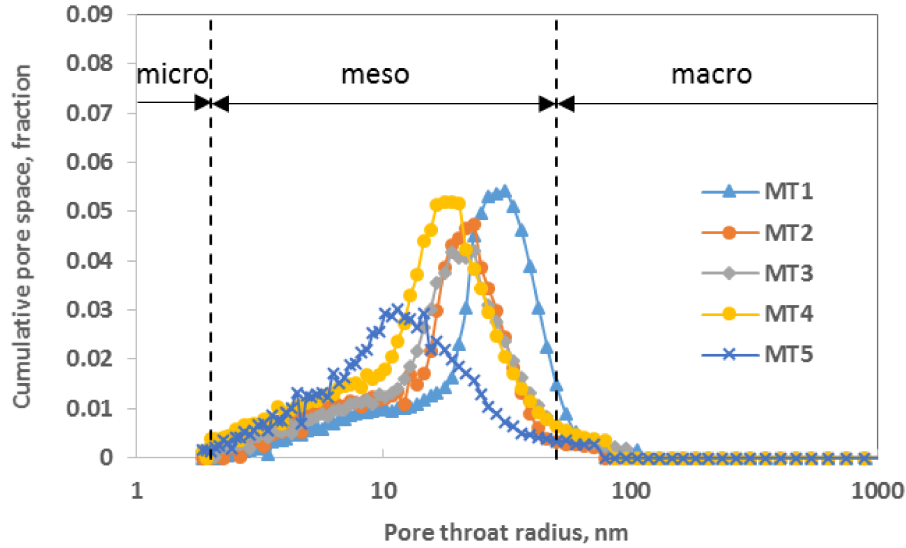


Figure 5. Pore size distribution of tight rock samples.

As the figure indicates, higher fraction of intra pores in the total porosity skews the MICP plots more to the left hand side of the mesopore window. MT5 is more skewed to the left and has lower peak pore throat and has a wider pore size distribution. Also, the distribution has a larger tail part. This indicates that dual-pore networks are more pronounced in MT5 compared with MT1, MT2, MT3, and MT4. Imbibition in these smaller pores leads to a three-region imbibition profile (i.e. type II). In mercury intrusion porosimetry, the amount of pressure required to intrude a pore is inversely proportional to the size of the pore. Maximum pressure applied to calculate pore size distribution of the samples was 414 MPa, corresponding to a theoretical limit of 1.86 nm pore-throat diameter. Thus MICP plots in figure 5, lack the distribution profile of pores smaller than 3.6 nm. Moreover, at such high pressure, blank effects from the heating and compression of the mercury[31], compressing of the rock structure, breaking the particles and opening closed pores[32, 33] may significantly affect the data.

SEM analysis

To further characterize rock samples, we performed Scanning Electron Microscopy/Energy Dispersive Spectroscopy (SEM/EDS) on the rock samples. Figure 6 shows the Secondary Electrons (SE) image and elemental mapping of MT5 using EDS analysis. SEM analysis reveals MT5 has two sets of pore networks. Inter pores are readily visible in Figure 6a. Figure 6b shows the intra-pores in the MT5 sample. Comparing scales of the figures 6a and 6b, inter pore is in micron size range while intra pores are in the nanometer range. Elemental mapping of MT5 in Figure 6c to 6f shows that the pores are surrounded by Quartz (Si & O) and Dolomite (Mg & Ca). Quartz is known to be water-wet while dolomite is oil-wet[34]. This observation explains the capacity of the samples to uptake both brine and oil.

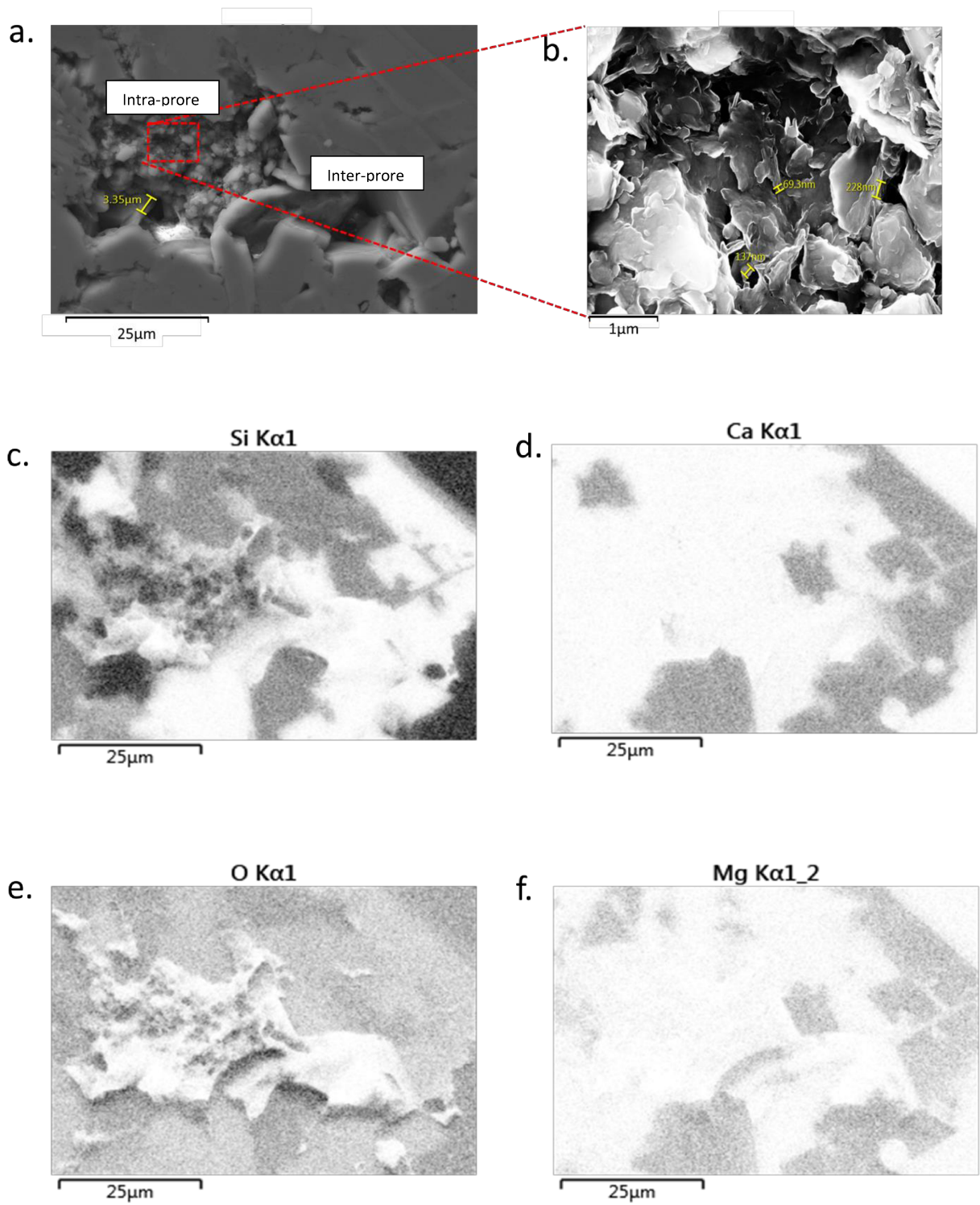


Figure 6. SEM images and elemental map of MT5 sample.

Decoupling imbibition model

In Figure 3 which plots the imbibed mass versus square root of time for MT5 sample we observe two different imbibition slopes. This observation does not match with classical imbibition models, such as Handy model, which predict a linear slope and a plateau region in the imbibition vs square root of time plot [33]. We call classical imbibition behavior as type I imbibition profile (spontaneous imbibition is mainly dominated by fluid flow in inter pores). Clearly type I imbibition profile cannot explain the imbibition behavior of MT5 sample. For MT5 sample we observe that the imbibition profile vs. square root of time increases linearly then breaks at break point and imbibition continues with a comparatively smaller linear slope until equilibrium is reached. We call this type of imbibition profile, type II (spontaneous imbibition occurs in both inter/intra pore-networks). In this type flow in intra pores compete with inter pores which leads to a distinct change in the slope of the imbibition profile. Figure 7 represents this characterization scheme. Samples that have a higher fraction of intra pores and better interconnectivity between inter and intra pore networks can potentially lead to type II imbibition profiles. Figure 7b shows how a type II imbibition profile can be decomposed into two distinct type I imbibition profiles. In Figure 7c we extend such decomposition scheme to MICP plots of a type II imbibition profiles. We assume as shown in Figure 7c the bell shaped part of the MICP plot is mostly represented by inter pores and the tail shaped part of the plot is mostly represented by the intra pores.

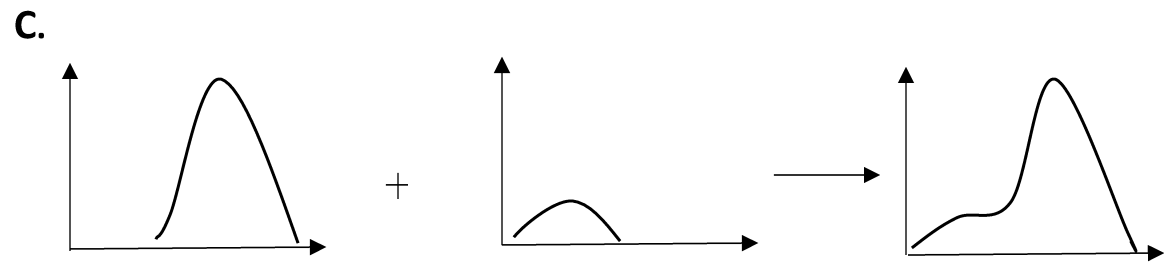
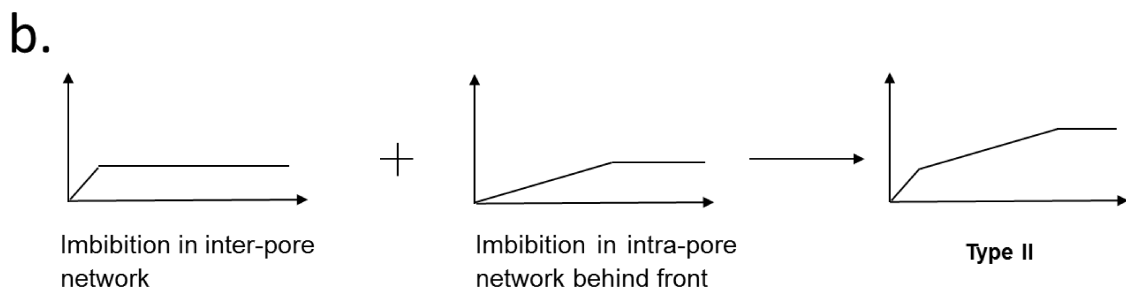
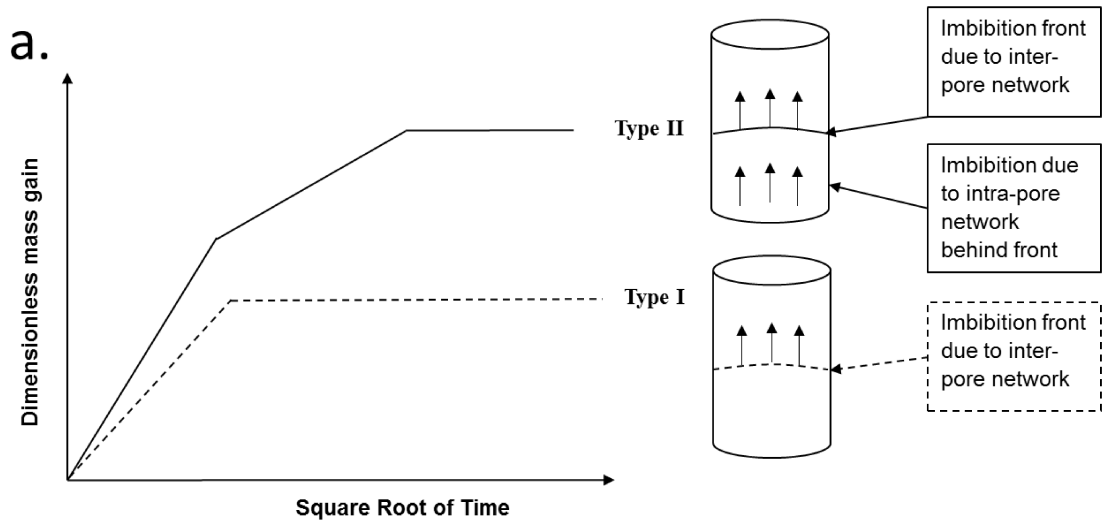


Figure 7. a. Schematics for imbibition characterization showing type I and II imbibition profiles, **b.** Type II profiles can be modelled into a combination of two type I profiles and **c.** Pore size distribution of type II profiles can be modelled as a combination of two pore-networks.

We attribute the initial slope of the imbibition profile to the imbibition into inter pores of the rock. The secondary slope in type II imbibition profile belongs mainly to the imbibition into the intra pore space.

Handy model assumes piston like imbibition in core samples [35] which assumes that all pores of the rock have the same size. Type I imbibition profiles can be sufficiently be described by Handy model. However, for type II imbibition profiles this assumption is not valid as imbibition in intra pore space of these rock samples can lead to dual flow behaviour. behind the imbibition front. A modification of Handy model is required to model flow in type II pore network. Figures 7, 8 and following derivations represent this modification. In Figure 4.b, we schematically illustrated spontaneous imbibition in rock sample type II imbibition profile.

From Handy model for co-current spontaneous imbibition into a rock sample, we have:

$$M = \sqrt{\frac{2A\phi K\rho^2 S_{wf} P_c}{\mu}} \sqrt{t} = \alpha_1 \sqrt{t} \quad (1)$$

Where M is the imbibed mass of wetting fluid, A is the cross-sectional area of the core plug perpendicular to the flow direction, ϕ is the total porosity, ρ is fluid density, S_{wf} is saturation at the front, P_c is capillary pressure, and t is the imbibition time. For a rock sample with a type II imbibition profile, as presented in Figure 7b, we assume imbibition into the intra pore network behind the imbibition front effects the flow leading to dual fluid flow behaviour. For type II imbibition profile, the total imbibed mass is the sum of fluid mass imbibed in both inter pore network M_1 and intra pore network M_2 . Figure 8, represents schematics of type II imbibition with its decoupled components (two type I imbibition profiles). A type II imbibition profile consists of three regions; Region one where we assume both inter/intra pore networks (with porosities of ϕ_1 and ϕ_2 respectively) get filled up with imbibing fluid at the same time. This region ends at T_s where the imbibition front reaches the top surface of the samples and imbibition in inter-pore network stops. Region two starts after T_s . In this region we assume we only have imbibition in intra-pore network (with porosity of ϕ_2) until we reach equilibrium at T_e . Region three is the equilibrium region, where both inter and intra pore networks are saturated with the imbibing fluids and imbibition process has terminated. The following equation represents the conditional function describing type II imbibition profile.

$$M = \begin{cases} \alpha_3\sqrt{t} & t < T_s \\ \alpha_3\sqrt{T_s} + \alpha_2\sqrt{(t - T_s)} & T_s < t < T_e \\ M_{eq} & t > T_e \end{cases} \quad (3)$$

Where T_s is the time when the inter-pore network imbibition front reaches the tope surface of the rock sample. For MTB5 $T_s=130$ hours as observed in Figure 3. After this time, we only have spontaneous imbibition in intra-pore network until we reach equilibrium. T_e is the time after which the plateau region begins.

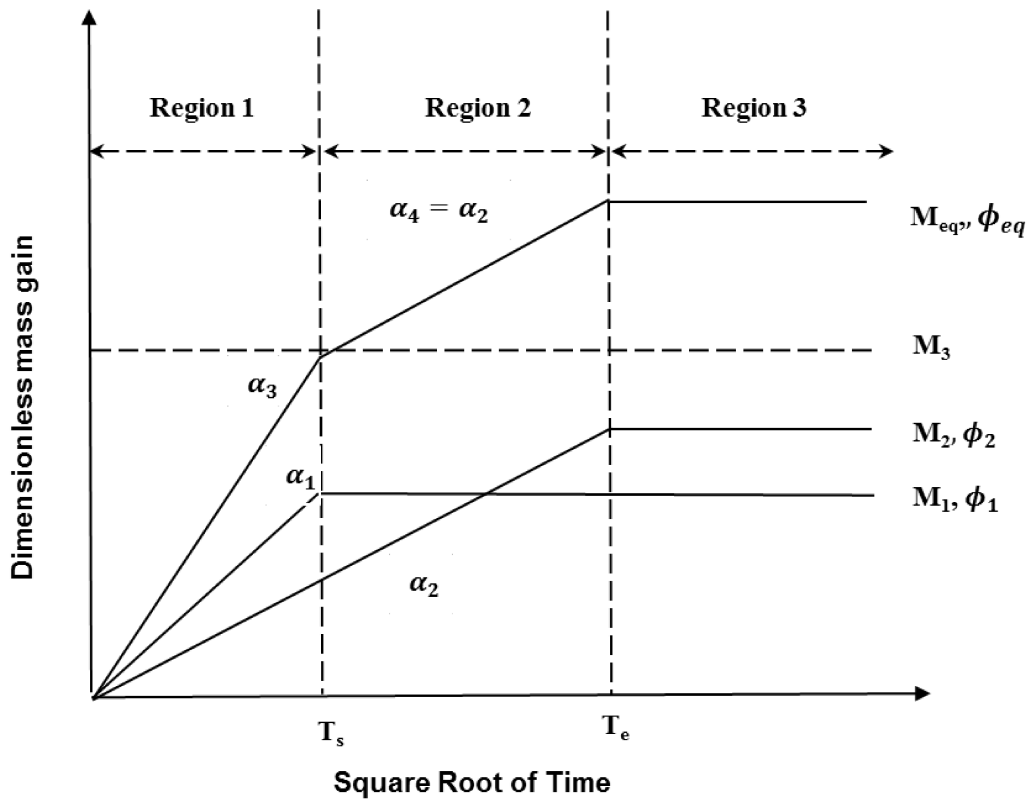


Figure 8. Schematics of the decoupling model for MT5. Note that $\phi_{eq} = \phi_1 + \phi_2$.

Summary of results

In this study we characterized fluid flow in unconventional rock samples from Montney formation based on their spontaneous imbibition profile, SEM images, and elemental maps. We categorize the pore network of samples into two types. In rock samples with type I imbibition profiles, imbibition is mainly dominated

in inter-pore network while in samples with type II imbibition profiles, imbibition occurs both in inter and intra pore networks. Type I imbibition profiles have a two region profile which is well-explained by conventional capillary driven imbibition models such as Handy. On the other hand, type II imbibition profiles results in a three region imbibition profile. We have developed relevant equations for both type I and type II imbibition profiles. Table 4, summarizes different properties of type I and type II imbibition profiles and Table 5 summarizes different imbibition slopes for the five twin samples based on Figure 8.

Table 4. Summary of decoupling scheme.

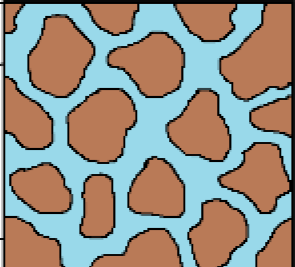
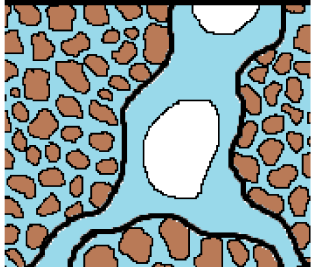
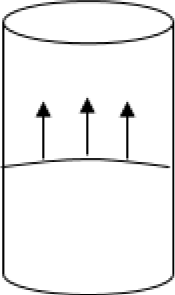
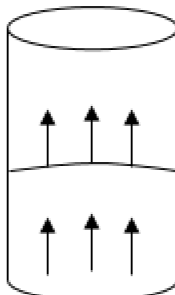
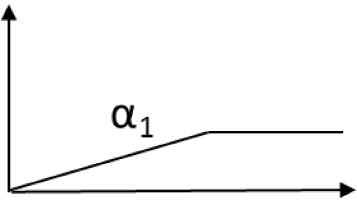
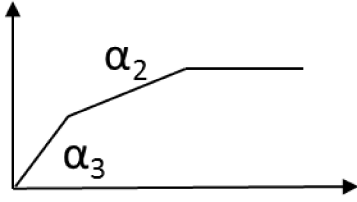
| Type I | Type II |
|---|--|
|  |  |
|  |  |
|  |  |
| $M = \begin{cases} \alpha_1 \sqrt{t} & t < T_e \\ M_{eq} & t > T_e \end{cases}$ | $M = \begin{cases} \alpha_3 \sqrt{t} & t < T_s \\ \alpha_3 \sqrt{T_s} + \alpha_2 \sqrt{(t - T_s)} & T_s < t < T_e \\ M_{eq} & t > T_e \end{cases}$ |

Table 5. Imbibition slope of different core samples

| | Oil imbibition slope, [hr ^{-0.5}] | | | Brine imbibition, [hr ^{-0.5}] | | |
|-------------|---|----------------------|----------------------|---|----------------------|----------------------|
| | α_1 | α_2 | α_3 | α_1 | α_2 | α_3 |
| MTB1 | -- | -- | -- | 5.7×10^{-4} | -- | -- |
| MTO1 | 5.2×10^{-4} | -- | -- | -- | -- | -- |
| MTB2 | -- | -- | -- | 4.0×10^{-4} | -- | -- |
| MTO2 | 2.5×10^{-4} | -- | -- | -- | -- | -- |
| MTB3 | -- | -- | -- | 5.0×10^{-4} | -- | -- |
| MTO3 | 5.5×10^{-4} | -- | -- | -- | -- | -- |
| MTB4 | -- | -- | -- | 3.8×10^{-4} | -- | -- |
| MTO4 | 1.8×10^{-4} | -- | -- | -- | -- | -- |
| MTB5 | -- | -- | -- | -- | 5.8×10^{-5} | 3.6×10^{-4} |
| MTO5 | -- | 7.1×10^{-5} | 3.8×10^{-4} | -- | -- | -- |

Conclusions

In this research we proposed a new pore-network characterization scheme based on spontaneous imbibition profiles results in twin core plugs. Such characterization scheme categorizes the samples based on their spontaneous imbibition profiles into type I and II. We proposed a decoupling model, which quantifies the characterization scheme. Based on the model we assumed flow in type I imbibition profiles is mainly dominated in inter pores while in type II imbibition profiles, fluid flow occurs both in inter and intra pores. Hence in core samples with type II imbibition profiles we assume there are two different pore networks which is in agreement with prior studies [34, 35]. One pore network lies within inter granular pores and the other one is extended into the intra granular pores. The results of the MICP data backs up such assumptions. Type II rock samples have a pore size distribution shifted into mesopore window of the MICP data, which suggests presence of intra pores. The SEM images support presence of inter and intra pore networks both of which are dual wet. Imbibition profile, pore size profile, SEM, and elemental mass of the core samples with type II imbibition profile are in agreement with the assumptions of the decoupling model.

References

- [1] L. Fan, J.W. Thompson, J.R. Robinson, Understanding gas production mechanism and effectiveness of well stimulation in the Haynesville Shale through reservoir simulation, in: Canadian Unconventional Resources and International Petroleum Conference, Society of Petroleum Engineers, 2010.
- [2] G.E. King, Hydraulic fracturing 101: what every representative, environmentalist, regulator, reporter, investor, university researcher, neighbor and engineer should know about estimating frac risk and improving frac performance in unconventional gas and oil wells, in: SPE Hydraulic Fracturing Technology Conference, Society of Petroleum Engineers, 2012.
- [3] H. Dehghanpour, E. Kuru, J.S. Parmar, Drainage against gravity: factors impacting the load recovery in fractures, in: SPE Unconventional Resources Conference-USA, Society of Petroleum Engineers, 2013.
- [4] J. Parmar, H. Dehghanpour, E. Kuru, Unstable displacement: a missing factor in fracturing fluid recovery, in: SPE Canadian Unconventional Resources Conference, Society of Petroleum Engineers, 2012.
- [5] J. Parmar, H. Dehghanpour, E. Kuru, Displacement of water by gas in propped fractures: Combined effects of gravity, surface tension, and wettability, *Journal of Unconventional Oil and Gas Resources*, 5 (2014) 10-21.
- [6] H. Dehghanpour, H. Zubair, A. Chhabra, A. Ullah, Liquid intake of organic shales, *Energy & Fuels*, 26 (2012) 5750-5758.
- [7] H. Dehghanpour, Q. Lan, Y. Saeed, H. Fei, Z. Qi, Spontaneous imbibition of brine and oil in gas shales: effect of water adsorption and resulting microfractures, *Energy & Fuels*, 27 (2013) 3039-3049.
- [8] B. Roychaudhuri, T. Tsotsis, K. Jessen, An experimental and numerical investigation of spontaneous imbibition in gas shales, paper presented at SPE Annual Technical Conference and Exhibition, Soc. of Pet, in, Eng, 2011.
- [9] K. Makhanov, A. Habibi, H. Dehghanpour, E. Kuru, Liquid uptake of gas shales: A workflow to estimate water loss during shut-in periods after fracturing operations, *Journal of Unconventional Oil and Gas Resources*, 7 (2014) 22-32.
- [10] S.A. Holditch, Factors affecting water blocking and gas flow from hydraulically fractured gas wells, *Journal of Petroleum Technology*, 31 (1979) 1,515-511,524.
- [11] J. Mahadevan, D. Le, H. Hoang, Impact of capillary suction on fracture face skin evolution in waterblocked wells, in: Paper SPE presented at SPE Hydraulic Fracturing Technology Conference, The Woodlands, Texas, 2009.
- [12] D.B. Bennion, F.B. Thomas, Formation damage issues impacting the productivity of low permeability, low initial water saturation gas producing formations, *Journal of energy resources technology*, 127 (2005) 240-247.
- [13] J.R. Shaoul, L.F. van Zelm, C. De Pater, Damage mechanisms in unconventional-gas-well Stimulation-a new look at an old problem, *SPE Production & Operations*, 26 (2011) 388-400.
- [14] A. Settari, R. Sullivan, R. Bachman, The modeling of the effect of water blockage and geomechanics in waterfracs, in: SPE Annual Technical Conference and Exhibition, Society of Petroleum Engineers, 2002.

- [15] Y. Cheng, Impact of water dynamics in fractures on the performance of hydraulically fractured wells in gas-shale reservoirs, *Journal of Canadian Petroleum Technology*, 51 (2012) 143-151.
- [16] M. Sharma, S. Agrawal, Impact of liquid loading in hydraulic fractures on well productivity, in: SPE hydraulic fracturing technology conference, Society of Petroleum Engineers, 2013.
- [17] C.H. Sondergeld, K.E. Newsham, J.T. Comisky, M.C. Rice, C.S. Rai, Petrophysical considerations in evaluating and producing shale gas resources, in: SPE Unconventional Gas Conference, Society of Petroleum Engineers, 2010.
- [18] R.G. Loucks, R.M. Reed, S.C. Ruppel, U. Hammes, Spectrum of pore types and networks in mudrocks and a descriptive classification for matrix-related mudrock pores, *AAPG bulletin*, 96 (2012) 1071-1098.
- [19] K. Bohacs, Q. Passey, M. Rudnicki, W. Esch, O. Lazar, The Spectrum of Fine-Grained Reservoirs from 'Shale Gas' to 'Shale Oil'/Tight Liquids: Essential Attributes, Key Controls, Practical Characterization, in: IPTC 2013: International Petroleum Technology Conference, 2013.
- [20] L. Handy, Determination of effective capillary pressures for porous media from imbibition data, *Trans. AIME*, 219 (1960) 75-80.
- [21] Zolfaghari A. and Piri M., "Pore-scale Network Modeling of Three-phase Flow based on Thermodynamically Consistent Threshold Capillary Pressures. I. Cusp Formation and Collapse," *Transport in Porous Media* 116 (3), pp 1093-1137, 2017
- [22] Zolfaghari A. and Piri M., "Pore-scale Network Modeling of Three-phase Flow based on Thermodynamically Consistent Threshold Capillary Pressures. II. Results," *Transport in Porous Media* 116 (3), pp 1139–1165, 2017
- [21] J.-P. Zonneveld, R.B. MacNaughton, J. Utting, T.W. Beatty, S.G. Pemberton, C.M. Henderson, Sedimentology and ichnology of the Lower Triassic Montney Formation in the Pedigree-Ring/Border-Kahntah River area, northwestern Alberta and northeastern British Columbia, *Bulletin of Canadian Petroleum Geology*, 58 (2010) 115-140.
- [22] B. Markhasin, Sedimentology and stratigraphy of the Lower Triassic Montney Formation, subsurface of northwestern Alberta, University of Calgary, 1997.
- [23] K. Sing, Everett. DH, Haul RAW, Moscou L, Pierotti RA, Rouquérol J and Siemieniowska T 1985, *Pure Appl. Chem*, 57 603.
- [24] R.F. Sigal, A methodology for blank and conformance corrections for high pressure mercury porosimetry, *Measurement Science and Technology*, 20 (2009) 045108.
- [25] D. Penumadu, J. Dean, Compressibility effect in evaluating the pore-size distribution of kaolin clay using mercury intrusion porosimetry, *Canadian Geotechnical Journal*, 37 (2000) 393-405.
- [26] J.T. Comisky, M. Santiago, B. McCollom, A. Buddhala, K.E. Newsham, Sample size effects on the application of mercury injection capillary pressure for determining the storage capacity of tight gas and oil shales, in: Canadian unconventional resources conference, Society of Petroleum Engineers, 2011.

Chapter 4

Investigating Imbibition Oil Recovery in Dual-Wettability Media: A Montney Case Study

Abstract

Previous studies demonstrate that the Montney rock samples have a dual-wettability pore network. Recovery of the oil retained in small hydrophobic pores is a unique challenge. In this study, we apply dual-core imbibition (DCI) method on several Montney core plugs and introduce imbibition-recovery (IR) trio to investigate the recovery mechanisms in rocks with dual-wettability pore network. First, we evaluate the wetting affinity of five twin core-plugs from the Montney Formation by measuring spontaneous imbibition of reservoir oil and brine, and by measuring equilibrium contact angle. We place one plug of each pair in the oil and the other in the brine, and measure the weight change periodically. Second, we place the oil-saturated samples in the brine to visualize the expelled oil droplets and measure volume of the recovered oil. We comparatively analyze the spontaneous imbibition data from the first step and the recovery data of the second step in one imbibition-recovery trio (oil imbibition, brine imbibition, and imbibition oil recovery). The results of air-liquid contact angle and spontaneous imbibition on dry samples suggest that the affinity of the samples to oil is higher than that to brine, in an air-liquid system. However, the results of liquid-liquid contact angle and counter-current imbibition tests suggest that the affinity of the samples to water is higher than that to oil, in a liquid-liquid system. For each twin set, the oil recovery curve follow the trend of brine imbibition curve, and the final oil recovery is always less than the equilibrated water uptake of dry samples. This observation indicates that water can only access the hydrophilic part of the pore network initially saturated with oil. Finally, we introduce a porosity-based model to analyze recovery data.

Introduction

Recent developments in multi-stage hydraulic fracturing have motivated industry to ramp up hydrocarbon production from unconventional reservoirs ¹. Tight sandstone alongside shale reservoirs and coal bed methane are three major classes of unconventional reservoirs ². “Tight” sandstones have low connected porosity (<10%) ³, low gas permeability (<0.1 mD) ⁴, and very high sensitivity to confining pressure ⁵ since pore-network of tight sandstone is often made up from interconnected network of micro-cracks ⁶. Until recently, interest in tight and shale reservoirs was limited due to lack of well-developed technology for development and characterization of such reserves ⁷. Investigating hydrocarbon production from tight/shale reservoirs relies on a full characterization of their petrophysical properties such as porosity, permeability and wettability.

Spontaneous imbibition of aqueous phases (water, brine, or surfactant solutions) in fractured sandstone has been studied as a possible mechanism for enhanced oil recovery ⁸⁻¹⁰. Extensive experimental and mathematical investigations have been conducted for relating the imbibition rate and total oil recovery to the capillary and gravity forces and the geometrical parameters ^{11, 12}. However, rock-fluid interactions in tight and shales reservoirs is more complicated than that in conventional reservoirs. In addition to capillary forces, organic materials ¹³ and reactive clay minerals ¹⁴ can influence the fluid flow and storage in the small pores of low-permeable rocks. In particular, affinity of reservoir rock to a fluid depend on rock mineralogy and properties of the organic matter that coats and fills the pores ¹⁵.

Previous comparative imbibition tests show that the affinity of the Montney samples to oil is significantly higher than that to water ¹³. This behaviour was explained by the presence of water-repellant pores within or coated by solid bitumen/pyrobitumen. In this paper, we focus on imbibition oil-recovery of samples cored from the Montney formation and investigate the role of rock fabric complexities such as dual-wettability characteristics on oil recovery by water imbibition. This paper is structured as follow: First, we discuss materials used in the spontaneous imbibition and oil-recovery tests including rock and fluid properties. Next, we describe the methodology and results of the three-stage tests: contact angle,

spontaneous imbibition and oil-recovery tests. Finally, we discuss the significance and application of this study followed by concluding remarks.

Recent years many studies are conducted to understand different parameters effecting imbibition oil recovery of rocks. Testing different rock types cored from different formations of interest with varying sample shapes and boundary conditions [1], measurement of recovery curves, quality of oil and aqueous phases [2] and pressures acting during spontaneous imbibition process [3] are of particular interest for researchers in this area of study. Other topics of interest in this field are scaling of imbibition recovery curves [4] with focus on porosity and permeability of core plugs under investigation, role of interfacial tension on spontaneous imbibition and recovery process, effect of viscosity ratio on recovery [5] and predicting trend of recovery curves [6]. Uncovering nature of induction time [7] and role of residual oil [8] on recovery curves are studied by other researchers as well. Some studies have gone further and applied advanced imaging techniques such as micro X-ray tomography, MRI [9], gamma ray attenuation [10] and neutron scattering [11] to detect and study the imbibition front in the core plugs during spontaneous imbibition process.

Among different parameters mentioned above, recovery curves are of high. Topics under investigation on recovery curves are: effect of boundary conditions on recovery curves [12], recovery trends plotted versus square root of time [13] coupled with relevant analytical modelling, effect of viscosity of wetting and non-wetting phases on oil recovery and effect of residual oil on recovery trends and final recovered volume. Although many aspects of recovery imbibition is still under study, few scientific works so far can reveal whether recovery rates are dependent upon spontaneous imbibition of water or rate of injection of fracturing fluids. In this study, we present a methodology that covers this gap. The results indicate that for Montney tight oil rock samples the rate of imbibing fluids follow the exact trend of oil recovery curves.

The rest of this paper is structured as follow: First we discuss materials used in the spontaneous imbibition and recovery tests such as rock and fluid properties. Next, we talk about methodology and results of the three-staged experimental tests: contact angle, spontaneous imbibition and recovery. Finally, we discuss the significance and application of this study followed by concluding remarks.

Materials

Rock properties

Geological background and minerology

The core plugs are dry-cut from the cores of the Montney Formation in the zone of 2100-2200 m. The plugs are well-preserved and uncontaminated. Montney Formation is a stratigraphical unit of Lower Triassic age in the Western Canadian Sedimentary Basin in British Columbia and Alberta ¹⁶. It is one of the largest natural gas resource plays in North American ¹⁷. The Montney is a tight, low permeability siltstone reservoir ¹⁸. This formation is divided into Upper Montney and Lower Montney. The Upper Montney is characterized by light brown siltstones interlaminated with fine grained sands. The Lower Montney is a dark grey, dolomitic siltstone with interbedded shales ¹⁹. The plugs are cored from a well located in Gordondale area of the formation.

The results of XRD analysis of the samples are listed in Table 1. The samples are mainly composed of quartz (40%-45%), k-feldspar (9%-15%), plagioclase (10%-16%), dolomite (14%-22%), and clay (9%-14%). Clay and TOC content of the core samples are listed in Table 2. The clay content does not vary much (9%-14%) and the amount of total organic carbon is very low (<1%). The clays are mainly composed of chlorite (35%-48%) and illite (51%-65%).

Table 1. XRD minerology analysis of the five sets of twin plugs.

| Mineralogy | MT1 | MT2 | MT3 | MT4 | MT5 |
|-------------------|------------|------------|------------|------------|------------|
| Quartz | 40.4 | 40.4 | 44.8 | 41.6 | 43.1 |
| Anhydrite | 0.0 | 0.8 | 0.5 | 0.4 | 0.0 |
| K-Feldspar | 9.0 | 12.1 | 10.0 | 14.9 | 12.8 |
| Plagioclase | 13.6 | 15.1 | 10.9 | 14.0 | 11.6 |
| Calcite | 3.9 | 3.0 | 5.7 | 0.0 | 2.0 |

| | | | | | |
|------------------------|-------|-------|-------|-------|-------|
| Dolomite & Fe-Dolomite | 22.5 | 14.0 | 14.2 | 14.5 | 16.5 |
| Pyrite | 1.2 | 1.5 | 1.5 | 1.4 | 1.7 |
| Total Clay (wt %) | 9.5 | 13.1 | 12.3 | 13.2 | 12.3 |
| Relative Clay Data | | | | | |
| Illite (wt %) | 51.2 | 56.3 | 52.3 | 64.6 | 58.0 |
| Chlorite (wt %) | 48.8 | 43.8 | 47.7 | 35.4 | 42.0 |
| Sum Bulk | 100.0 | 100.0 | 99.9 | 100.0 | 100.0 |
| Sum Clay | 100.0 | 100.1 | 100.0 | 100.0 | 100.0 |

Table 2. Clay and TOC content of the five twin plugs.

| Rock number | Depth (m) | Clay content (wt %) | TOC content (wt %) |
|-------------|-----------|---------------------|--------------------|
| MT1 | 2138 | 9.1 | 0.22 |
| MT2 | 2144 | 13.1 | 0.2 |
| MT3 | 2149 | 12.3 | 0.24 |
| MT4 | 2174 | 13.2 | 0.32 |
| MT5 | 2192 | 12.3 | 0.44 |

Fluid properties

Reservoir brine and oil are used as aqueous and oleic phases, respectively, for investigating the wetting affinity of the samples, and their properties are listed in Tables 3 and 4. The brine is highly saline water with total dissolved solids of 126 gr/L- 130 gr/L and total hardness of 22 gr/L which is relatively high. Its viscosity is 1.18 at ambient temperature and its surface tension is 67 mN/m which is lower than surface tension of water (72 mN/m). Although the surface tension of sodium-based brines are known to increase with salt concentration ²⁰, in this case the surface tension is lower than 72 mN/m. This is due to the impurities present in the field sample as reservoir brine is contaminated with fracturing fluid which contains surfactants. Logarithmic patterns of dissolved ions are presented in Figure 1. The brine chemistry in the

Montney is Na-Ca-Cl with low SO₄ indicating a highly evolved brine. The brine is slightly alkaline with a pH of 6.89. Table 4 shows properties of the reservoir oil we used in spontaneous imbibition tests. The oil is light with API of 45.07, and is low in sulphur content which shows that oil is of high quality and requires little refinement.

Table 3. Brine properties.

| Property | Quantity |
|--|----------|
| Total Dissolved Solids (mg/L)-Measured | 126000 |
| Total Dissolved Solids (mg/L)-Calculated | 130000 |
| Relative Density | 1.101 |
| Surface Tension (mN/m) | 67 |
| Refractive Index | 1.356 |
| Conductivity (μS/cm) | 159000 |
| Resistivity (ohm-m) @25 ⁰ C | 0.06 |
| Total Hardness as CaCO ₃ (mg/L) | 22000 |
| Total Alkalinity as CaCO ₃ (mg/L) | 110 |
| Observed pH | 6.89 |
| H ₂ S Spot Test | Absent |
| Viscosity (cP) | 1.18 |

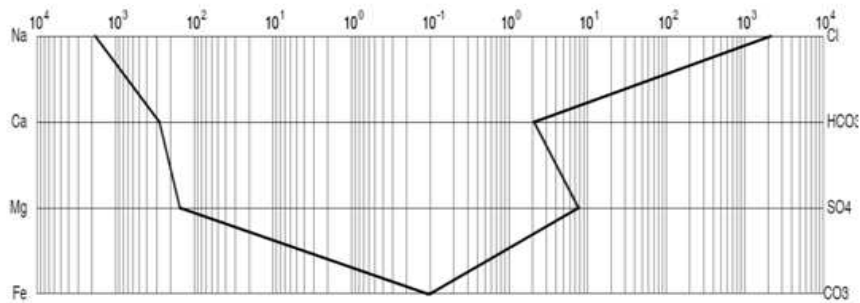


Figure 1. Logarithmic patterns of dissolved ions (meq/L).

Table 4. Oil properties.

| Property | Quantity |
|--|-----------------|
| Density of Clean oil @15 ⁰ C (ASTM D5002) | 1 |
| Relative Density | 0.8 |
| API | 45.07 |
| Surface tension (mN/m) | 28 |
| Absolute Density (kg/m ³) | 800.7 |
| Total Sulphur (mass percent) ASTM D4294 | 0.0796 |
| Viscosity(cP) | 1.87 |

Petrophysical properties

In order to understand fluid flow through fine-grained siliciclastic tight rocks, we need to have insight into the pore-structure of the rocks. In this study, we use porosity, permeability and pore-throat size to characterize petrophysical properties of the samples. Different researchers report different measures (geometric mean, arithmetic mean, median, and threshold) to represent the pore-throat size distribution ²¹. We use median pore-throat size as our measure in this study. Porosity of the samples are measured using helium gas. Permeability data are measured using air Swanson technique. The MICP plots are used to measure median pore-throat size of the samples. Figure 6 shows multivariate scatterplots of pore-throat radius (microns), permeability (mD) and porosity of seven core plugs from the same zone of interest, in the depth interval of 2100-2200 m. As evident from the plots, all variables follow power-law functions. The strength of the relationship is quantified by the R² values corresponding to each cross plot, displayed on its transverse side. The strongest correlation is observed in porosity-permeability correlation. Diagonal plots are univariate histograms of the three parameters, and off-diagonal scatterplots are bivariate cases.

In order to characterize the relationship between permeability and porosity, power law-based numerical models have been developed on a more or less empirical basis ²²⁻²⁵. Figure 7, shows the scatterplots of

logarithm of median pore-throat radius (microns), permeability (mD) and porosity. Previous studies show that in fine-grained clastic sediment, permeability is roughly related to porosity by log-linear functions ²⁶. Also, permeability in tight reservoirs is controlled more by pore size rather than porosity. Consistently, here we observe $R^2= 0.99$ for permeability vs. pore-throat size in Figure 2. All three variables follow a linear trend. The strength of the correlations between porosity, permeability and pore-throat size suggest that the samples are fine-grained. In this study, we investigate how oil and brine interact with and flow in the pore structure of the rocks, and examine the parameters effecting water imbibition and oil recovery.

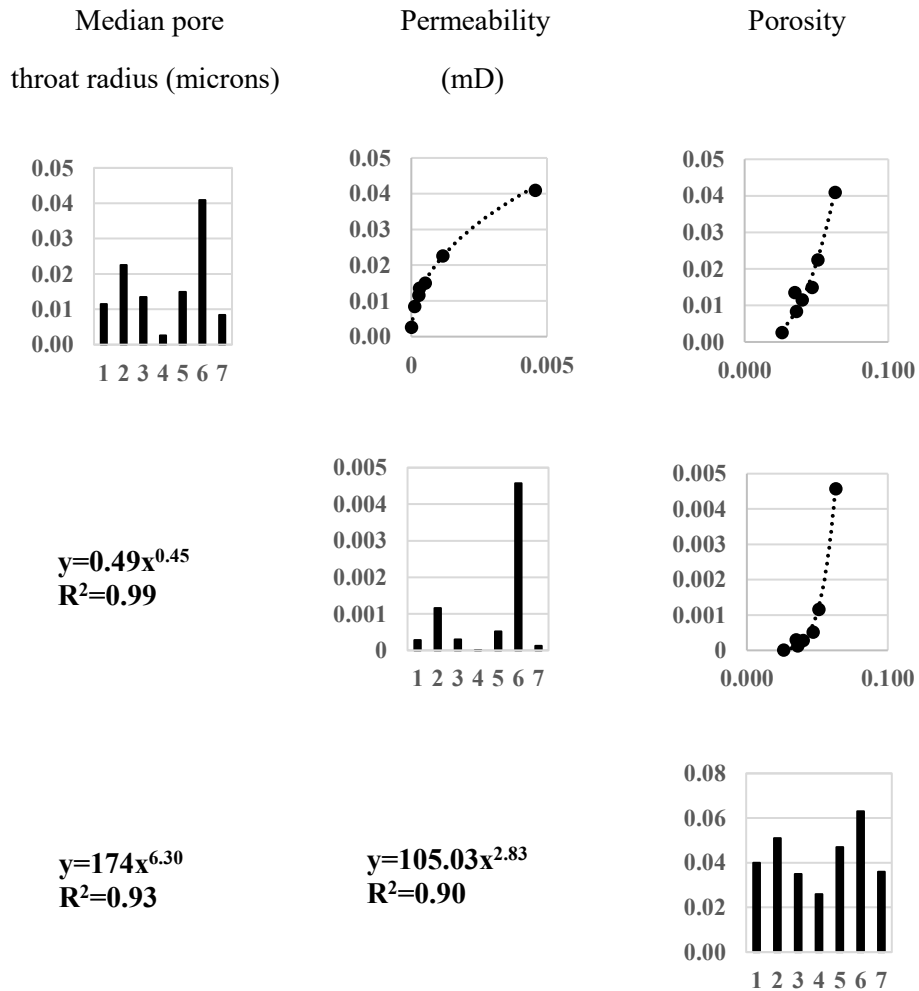


Figure 2. Multivariate scatterplots for three petrophysical parameters: porosity, permeability and median pore-throat size.

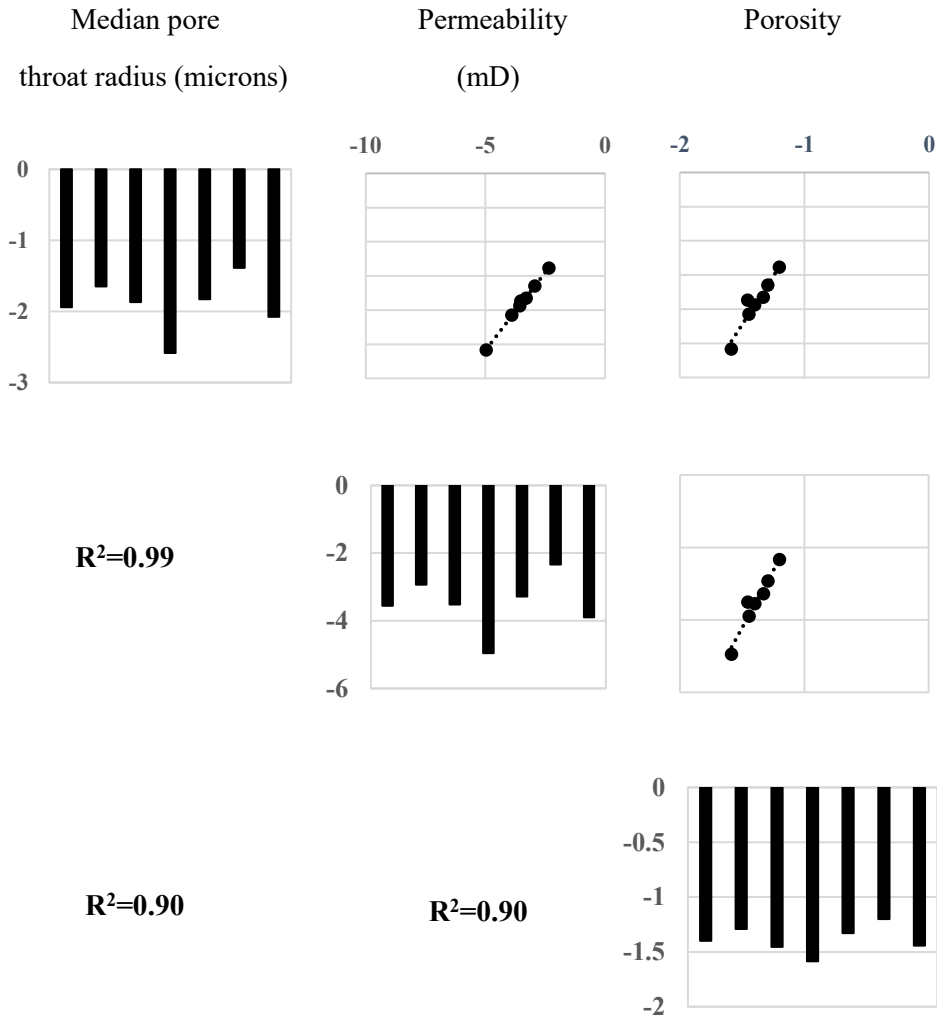
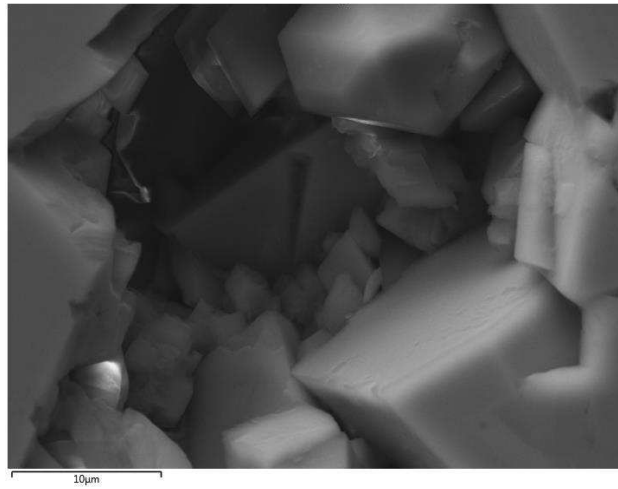


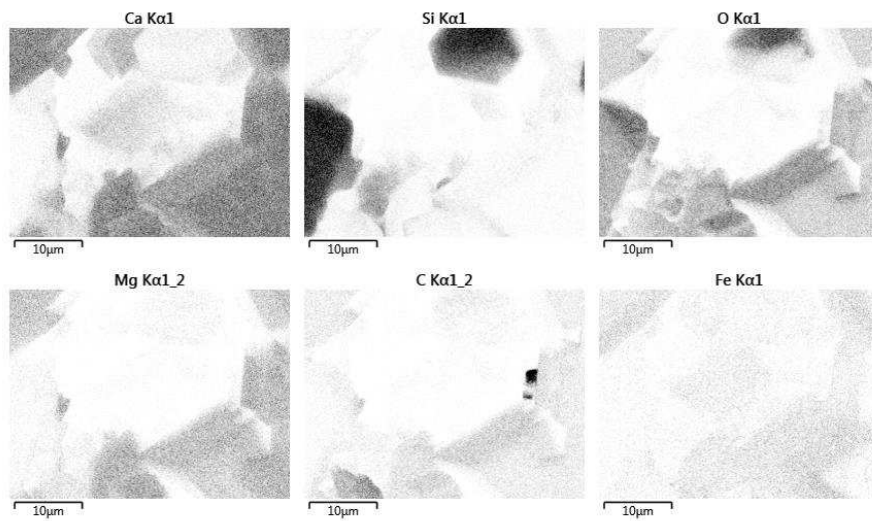
Figure 3. Multivariate scatterplots for logarithm of porosity, permeability, and median pore-throat size.

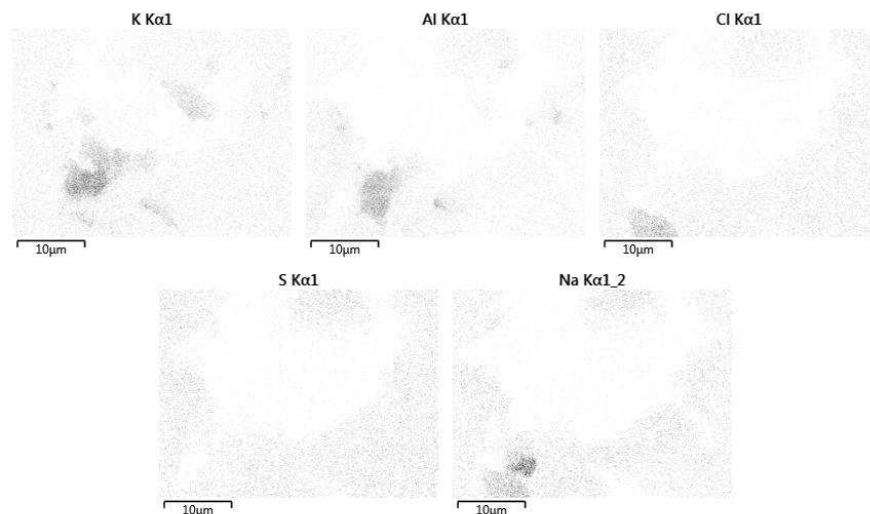
To characterize mineralogy of the plugs and possible reasons for affinity of samples to oil and brine, we performed Scanning Electron Microscopy/Energy Dispersive Spectroscopy (SEM/EDS) on the rock samples. Figure 4 shows the Secondary Electrons (SE) image and elemental mapping a sample using EDS analysis. SE images provide topographical information. Figure 4a shows a pore throat in MT1 and Figure 4b shows the corresponding elemental map. Comparing the two shows that the pore is made up mostly of Si elements (silica components) and Ca, Mg (carbonate components). This mixed distribution suggests that

quartz and carbonate components (dolomite) are mixed with each other. Quartz is known to be water-wet while dolomite tends to be oil-wet ²⁷.



(a)





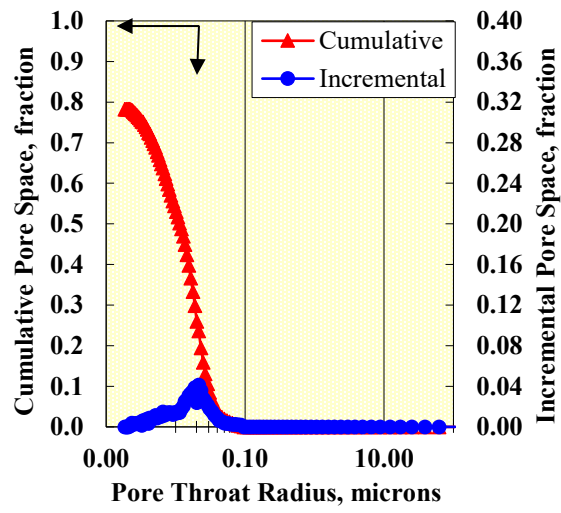
(b)

Figure 4. Sample MT1 under (a) SE beam (b) EDS analysis.

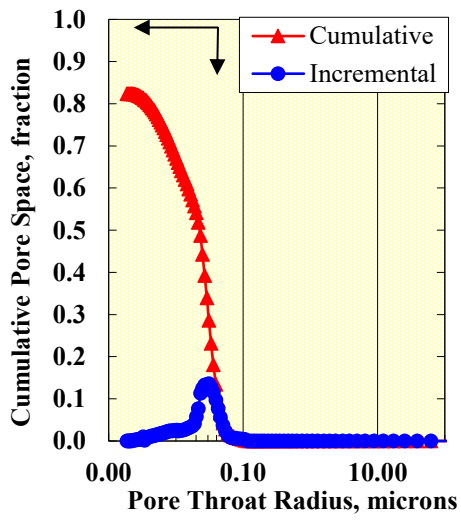
Figure 5 shows pore-throat size distributions of MT1 (a), MT2 (b), MT3 (c), MT4 (d) and MT5 (e). International Union of Pure and Applied Chemistry (IUPAC)²⁸ suggests pores can be categorized according to their pore-throat size as:

1. Micropores: pores < 2 nm
2. Mesopores: 2 nm < pores < 50 nm
3. Macropores: pores > 50 nm

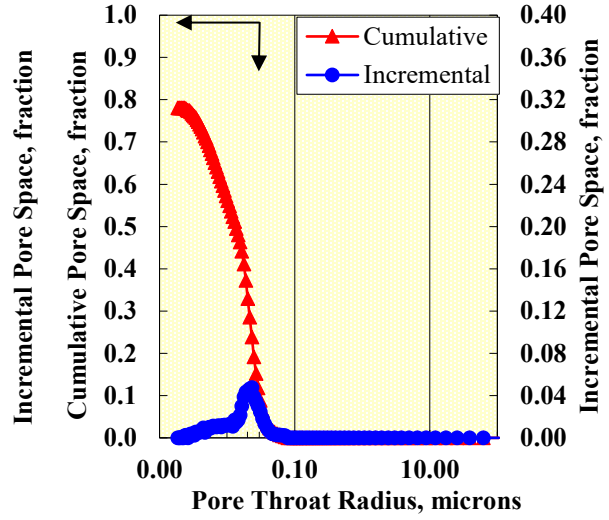
According to this classification and Figure 5, all tested samples have a considerable volume (70-80%) of their pore space in mesopores.



(a)



(b)



(c)

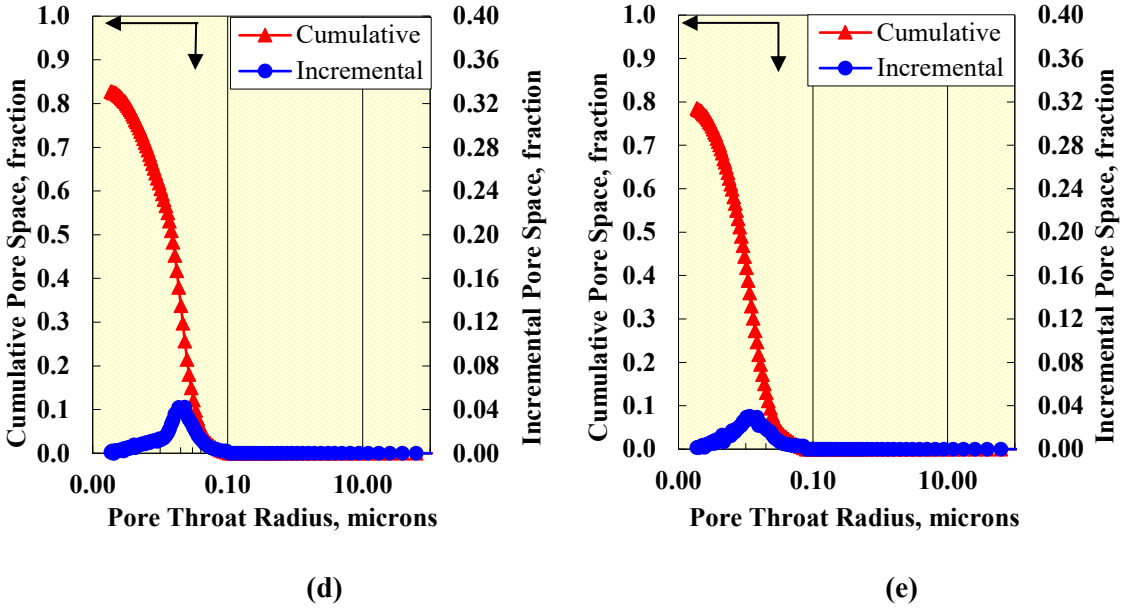


Figure 5. Pore-throat size distribution of five rock samples (a) MT1 (b) MT2 (c) MT3 (d) MT4 (e) MT5. The distributions show all samples have considerable volume of their pore space in mesopores.

Methodology, Results and Discussions

We conduct three sets of comparative tests on five twin core plugs, which were dry-cut from the Montney Formation cores. The samples are characterized by measuring mineral concentration, TOC content, porosity, and permeability. Figure 6 shows the procedure for conducting the tests. First, we measure contact angles of oil and brine droplets equilibrated on the surface of all plugs (Figure 6a). Surface roughness can have significant effect on the wetting angle²⁹; Hence samples are first polished and then air-dried before conducting contact angle tests. The samples were polished on a graded wheel plate using 240 grit sandpapers. Acetone was used to remove dirt from the surface and clean it, hence making the contact angle results more representative.

Next, one plug of each twin set is placed in a cell partly filled with brine and the other plug is placed in a cell partly filled with oil (Figure 6b). Only the bottom face of the plugs is exposed to the imbibing fluid. The weight of each plug is measured periodically with time and recorded. The imbibition cells are sealed

to avoid liquid evaporation. The experiments are halted once the mass gain of each sample reaches to the equilibrium conditions. Finally, the oil-saturated sample is placed in an Amott cell filled with reservoir oil and the volume of recovered oil is measured periodically until reaching to the equilibrium (Figure 6c). In order to avoid entrapment of oil droplets at the bottleneck of the cell, we use a shaker to make sure all recovered oil droplets accumulate the top of the cell. The cell is sealed to avoid evaporation of recovered oil.

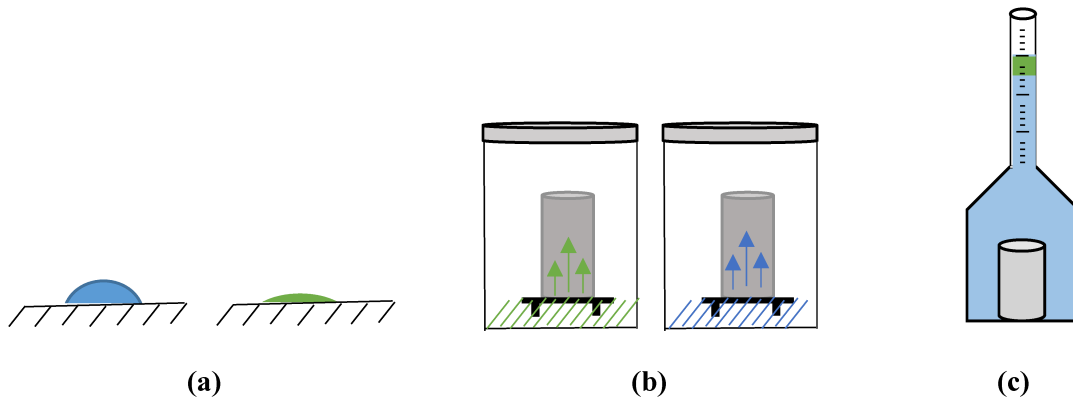


Figure 6. Schematic illustration of the setups for (a) comparative contact angle tests, (b) comparative oil/brine spontaneous imbibition tests and (c) counter-current oil-recovery tests.

Results and Discussions

In this section, we present and discuss the results for contact angle, spontaneous imbibition and oil-recovery tests.

I. Contact angle tests

Figure 7a shows oil and brine droplets equilibrated on the surface of a Montney core plug. Oil droplet completely spreads on all samples, while the brine droplets equilibrate with a non-zero contact angle. We observed similar trends for all five plugs. Figures 7b and 7c show liquid-liquid contact angles. Comparing Figures 7b and 7c show that, in a liquid-liquid system, the affinity of the sample to brine is higher than that to oil, and similar trends was observed for all samples. We plot the liquid-liquid contact angles for all five samples in an affinity chart as presented in Figure 8. X axis shows the values of contact angle for oil droplets on samples immersed in brine, and y axis shows the values of contact angles for brine droplets on

samples immersed in oil. The region to the right of the diagonal line represents water-wet behavior and the region to the left of the line represents oil-wet behavior. According to the results of air/liquid contact angle tests the samples are fully oil-wet and partially brine-wet. However, according to liquid-liquid contact angle tests, the samples are brine-wet. The results of imbibition tests show that liquid-air contact angle results are consistent with the results of water and brine imbibition tests in air-saturated samples, and the liquid-liquid contact angle results are consistent with the results of soaking tests which show oil production from the oil-saturated samples by spontaneous water imbibition.

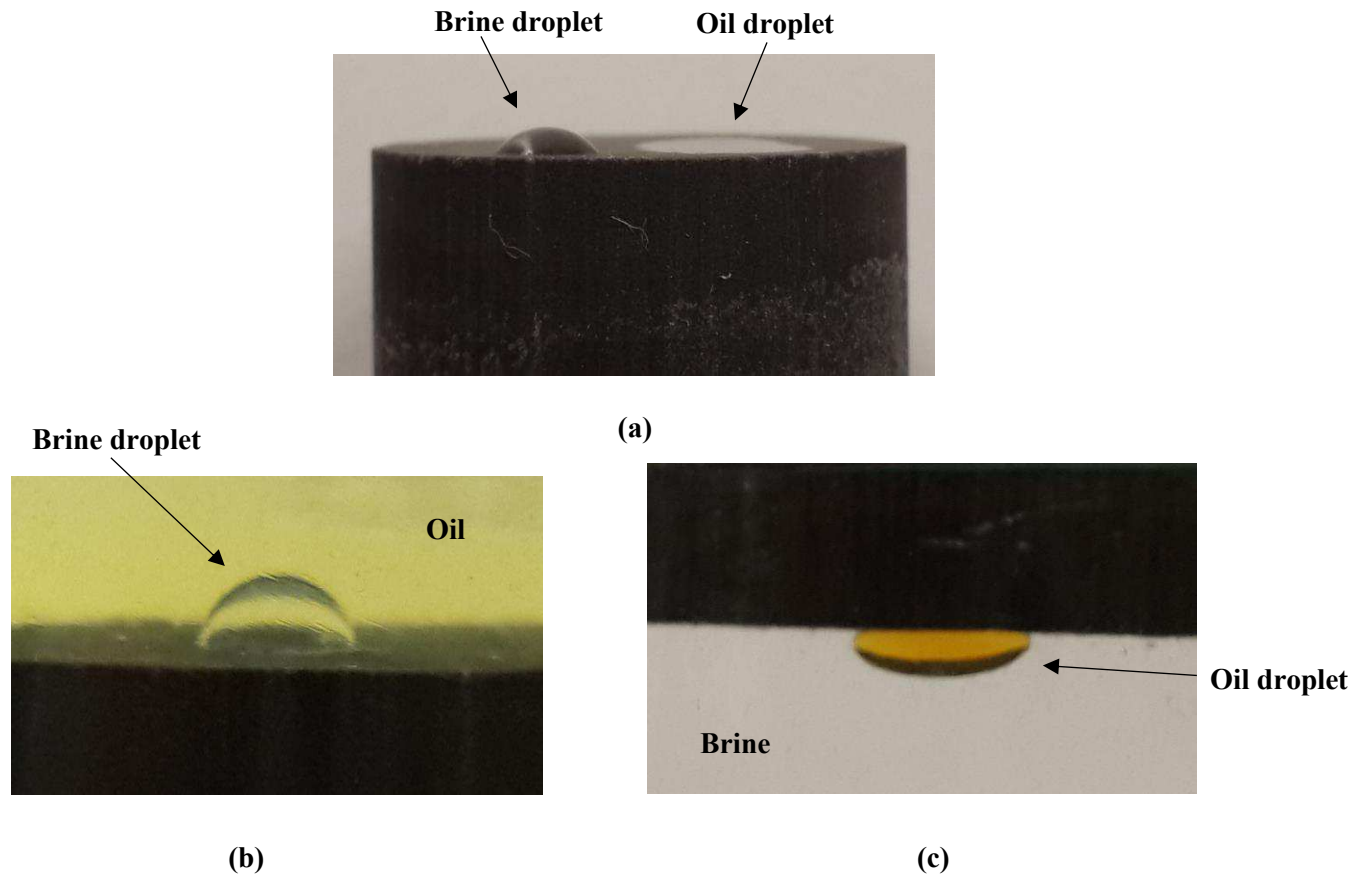


Figure 7. a) Oil and brine droplets equilibrated on the surface of a core plug in air at ambient conditions, b) a brine droplet equilibrated on the surface of a core plug immersed in reservoir oil, and c) an oil droplet equilibrated on the surface of a core plug immersed in reservoir brine.

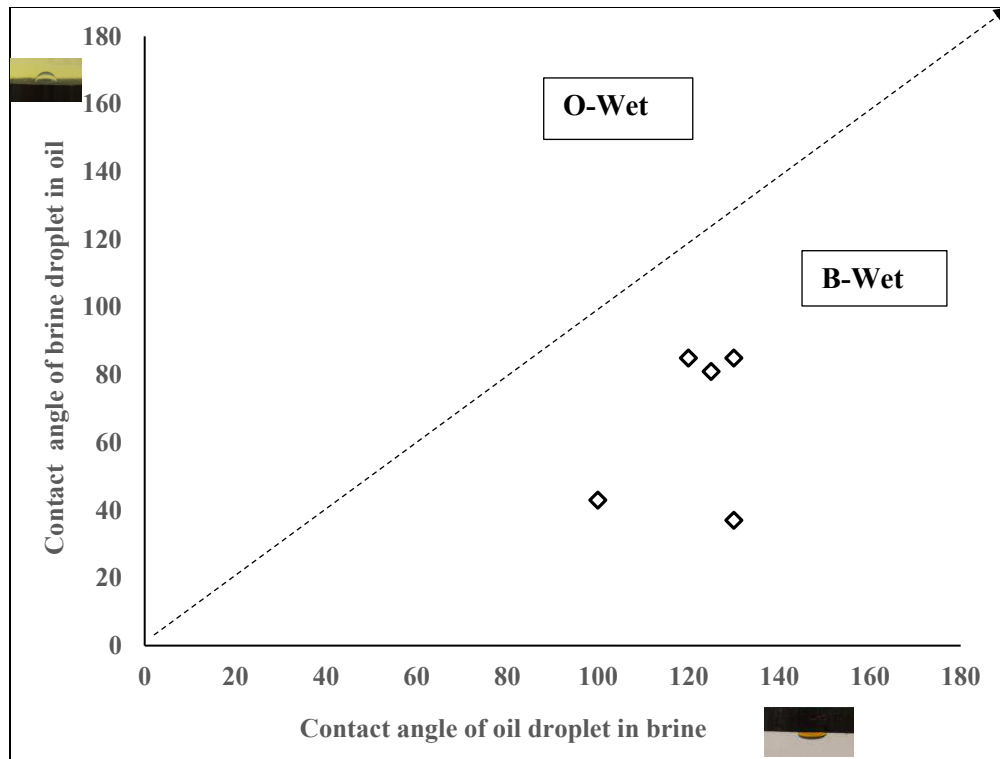
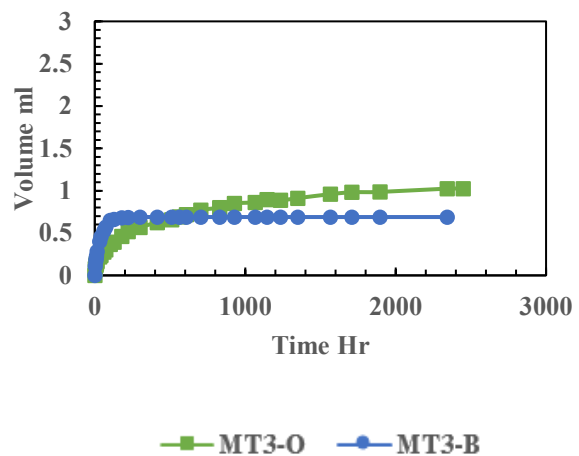
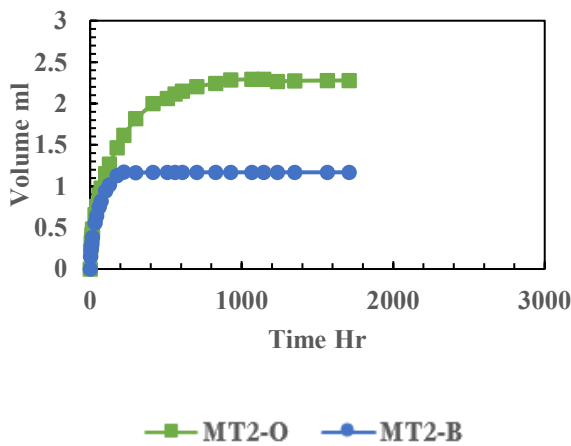
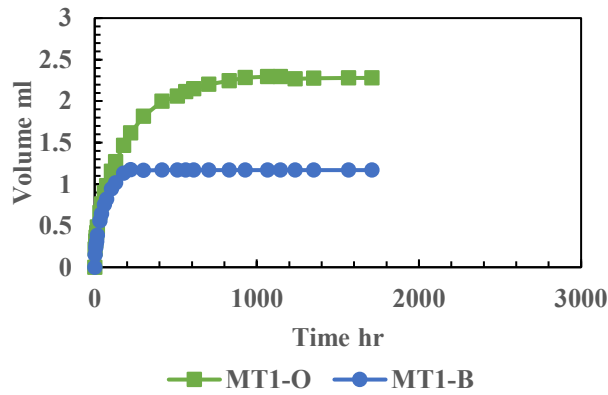


Figure 8. Affinity chart for the five sets of twin plugs. The results indicate all plugs are water-wet in a liquid-liquid system.

II. Spontaneous imbibition tests

Figure 9 plots the imbibed volume of oil and brine versus time during the co-current imbibition tests on dry core plugs. The imbibed volume of oil and brine are calculated by dividing the total imbibed mass by the fluid density. By comparing imbibition curves for both oil and brine, we observe consistently that the oil curves reach to equilibrium later than brine curves and the total imbibed volume of oil is significantly higher than that of brine. In general, brine imbibes faster than oil for all samples but brine curves plateau earlier than the oil curves. Considering porous media as a bundle of tubes, the liquid flow is slower in pores with smaller diameters³⁰. According to Figure 9, brine imbibition stops after 200-300 hours for all samples, while oil imbibition continues for more than 1000 hours for all samples. This behavior suggests that there is a significant number of small pores that have low affinity towards brine and high affinity towards oil. The rock matrix is comprised of organic matter and inorganic minerals such as quartz, feldspar, dolomite,

plagioclase, and clays. There are two general observations from results: 1) oil imbibition continues suggesting that imbibes into small-scale pores that have low affinity towards water and high affinity towards oil. 2) SEM image shows that there are small-scale pores within large-scale pores. So, we can conclude that the Montney core plugs show a dual porosity and dual wettability behavior, and small scale pore have a higher affinity to oil over brine. Although TOC content of core plugs is small (<1%), organic materials cover the surface area of pores. Organic matter is known to have high affinity towards oil³¹ while inorganic matter is mostly hydrophilic, especially in the presence of clay minerals³². The total clay content of all samples is 9-14%; and majority of inorganic material is quartz 40-45%.



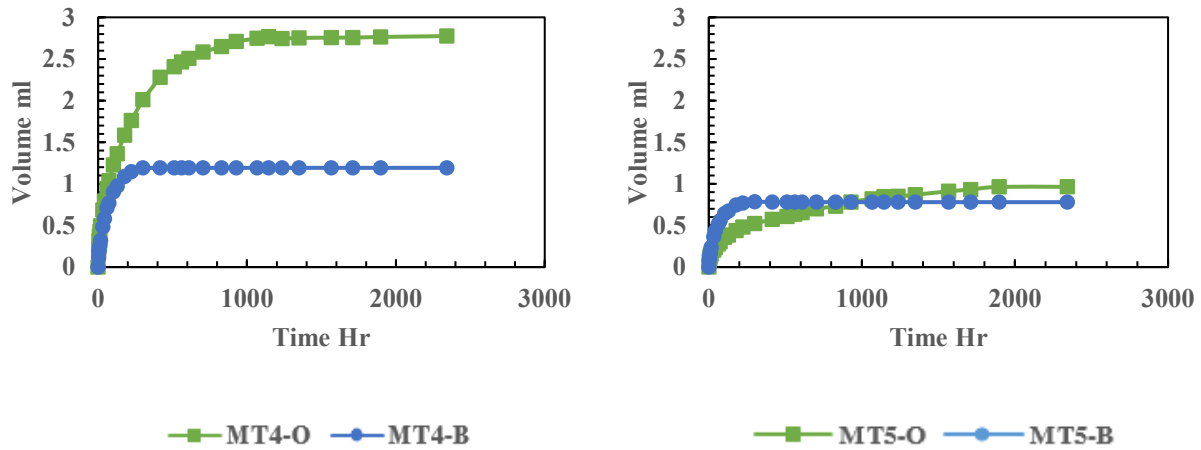


Figure 9. Spontaneous imbibition of oil and brine versus time for the five sets of twin plugs.

III. Imbibition oil-recovery tests

In the previous stage, we did co-current spontaneous imbibition tests on fresh core samples. In this stage, we place the oil-saturated samples in imbibition cells filled with brine. These tests are called imbibition recovery tests in this paper. The oil expelled by brine imbibition is collected at the top of the cells. The volume of produced oil is measured at different times. We also immersed brine-saturated samples in oil, but did not observe brine production for all samples. This observation is consistent with liquid-liquid contact angle tests. Figure 10 shows recovered oil droplets for MT4. As the imbibition process continues, oil droplets detach from the rock surface and accumulate at the top of the cell. In order to get accurate data, cells need to be physically shaken to help the recovered oil droplets to detach from rock surface or prevent them from sticking to the bottleneck of the cell.

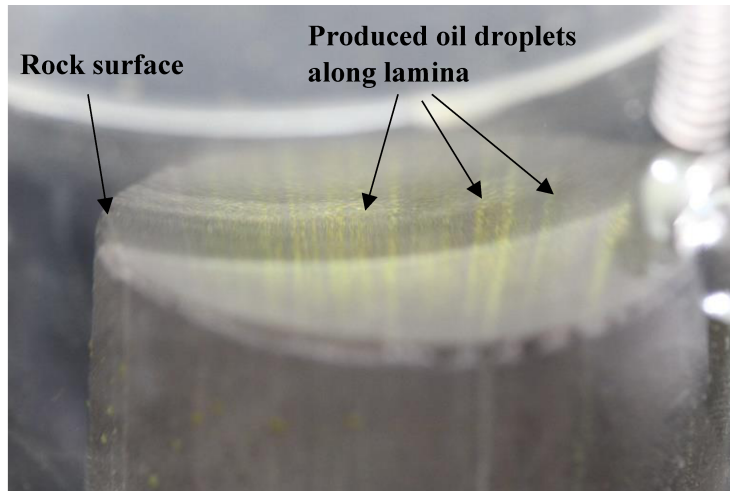
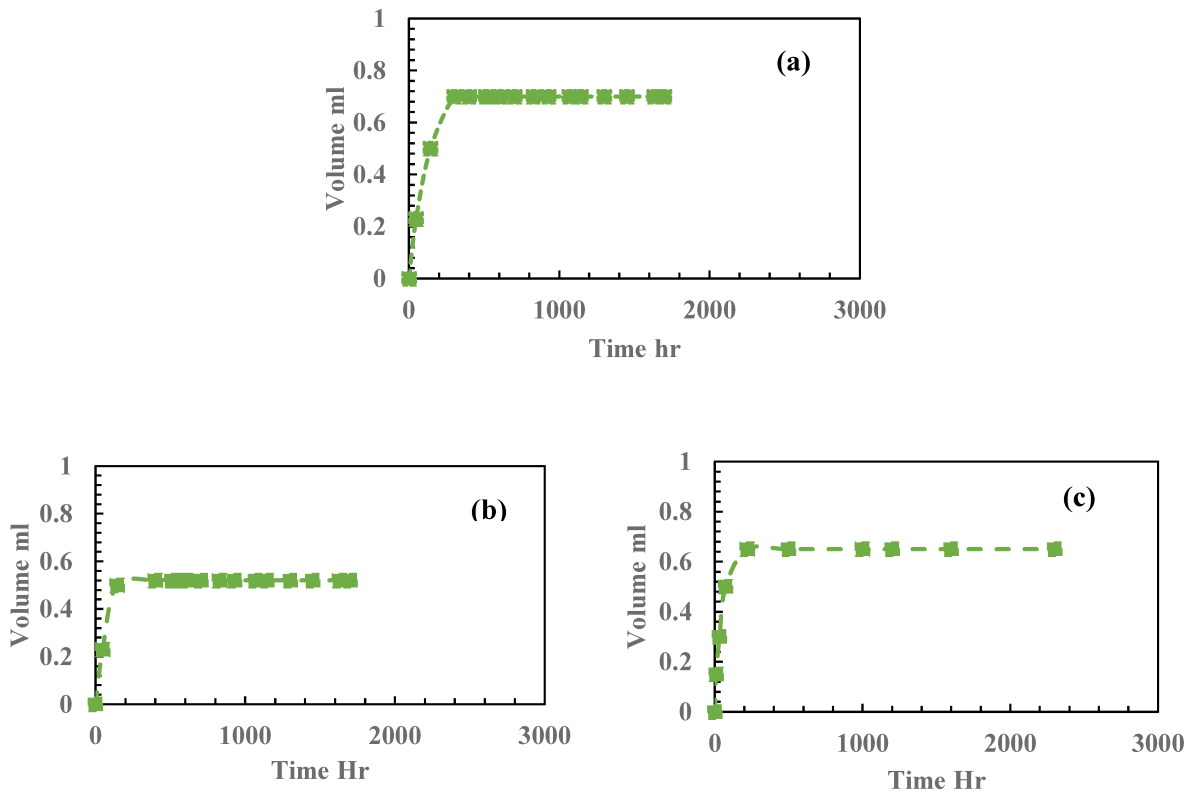


Figure 10. Recovered oil (yellow droplets lined up at the surface of the sample) is observed along the depositional laminations of an oil-saturated sample immersed in brine.

Figure 11 shows recovery plots of the five sets of twin plugs from the imbibition recovery tests. Although all recovery plots show similar trends, they plateau at varying final values.



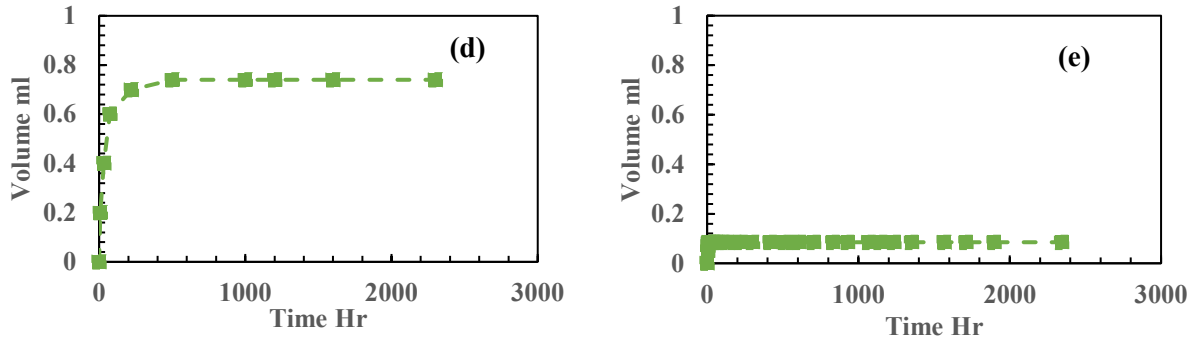


Figure 11. Oil-recovery plots for the five oil-saturated plugs immersed in brine for MT1 (a), MT2 (b), MT3 (c), MT4 (d) and MT5 (e).

In order to analyze the oil-recovery results, we introduce imbibition recovery (IR) trio. As presented in Figure 12, each IR trio consists of three curves. Oil and brine imbibition curves related to dry samples, and oil-recovery curves related to oil-saturated samples immersed in brine. One immediate observation from Figure 12 is that oil-recovery curve follows the trend of brine imbibition curve. Brine curves reach equilibrium at 200-300 hours. Recovery curves reach equilibrium almost at the same time; unlike oil imbibition curves which reach equilibrium at 1000-2000 hours. Moreover, the amount of recovered oil is always less than the amount of brine imbibed during the imbibition tests on dry samples. All five IR trios for the five sets of twin plugs are presented in Figure 13. We observe similar trends for all sets of twin plugs: 1) brine imbibition curves reach equilibrium faster than oil curves and the final imbibed volume of brine is lower than that of oil, 2) oil-recovery curves reach equilibrium almost at the same time as brine imbibition curves for all samples, and 3) final volume of recovered oil in oil-recovery tests is always less than the final volume of imbibed brine in imbibition tests. These observations suggest that the oil produced during the soaking tests mainly comes from the hydrophilic part of the pore-network. The non-recovered oil may be trapped in 1) small-scale pores which tend to be water-repellent based on the imbibition test results, and 2) parts of the hydrophilic pores due to snap-off mechanism.

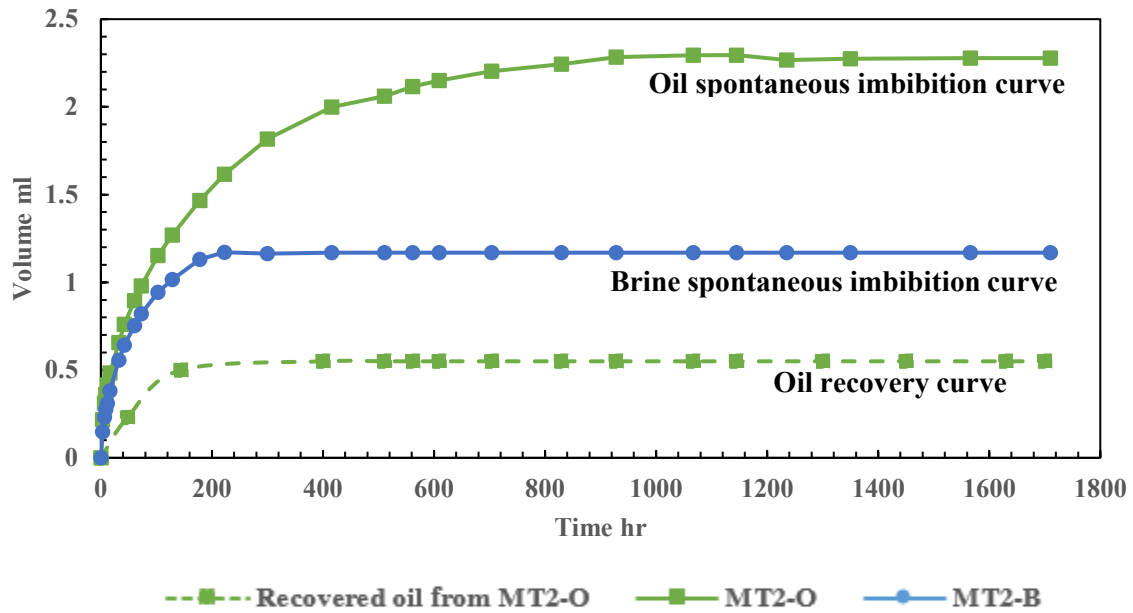
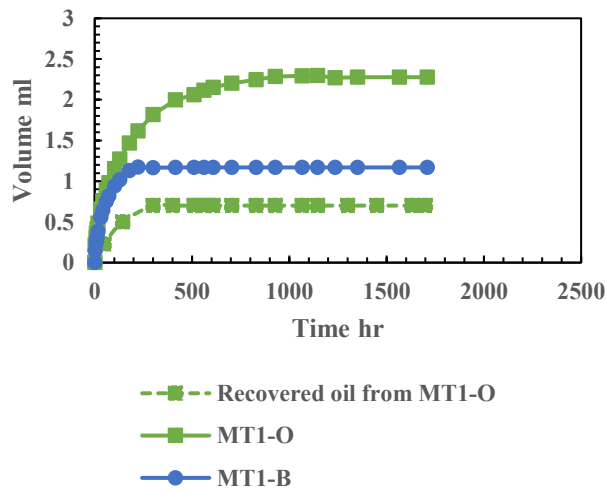


Figure 12. Imbibition-recovery (IR) trio consists of three curves. Oil imbibition curve, brine imbibition curve, and oil-recovery curve, plotted versus time. For twin plugs, oil-recovery curves and brine imbibition curves reach equilibrium almost at the same time, and the volume of total recovered oil is always less than the total water volume imbibed into the dry sample.



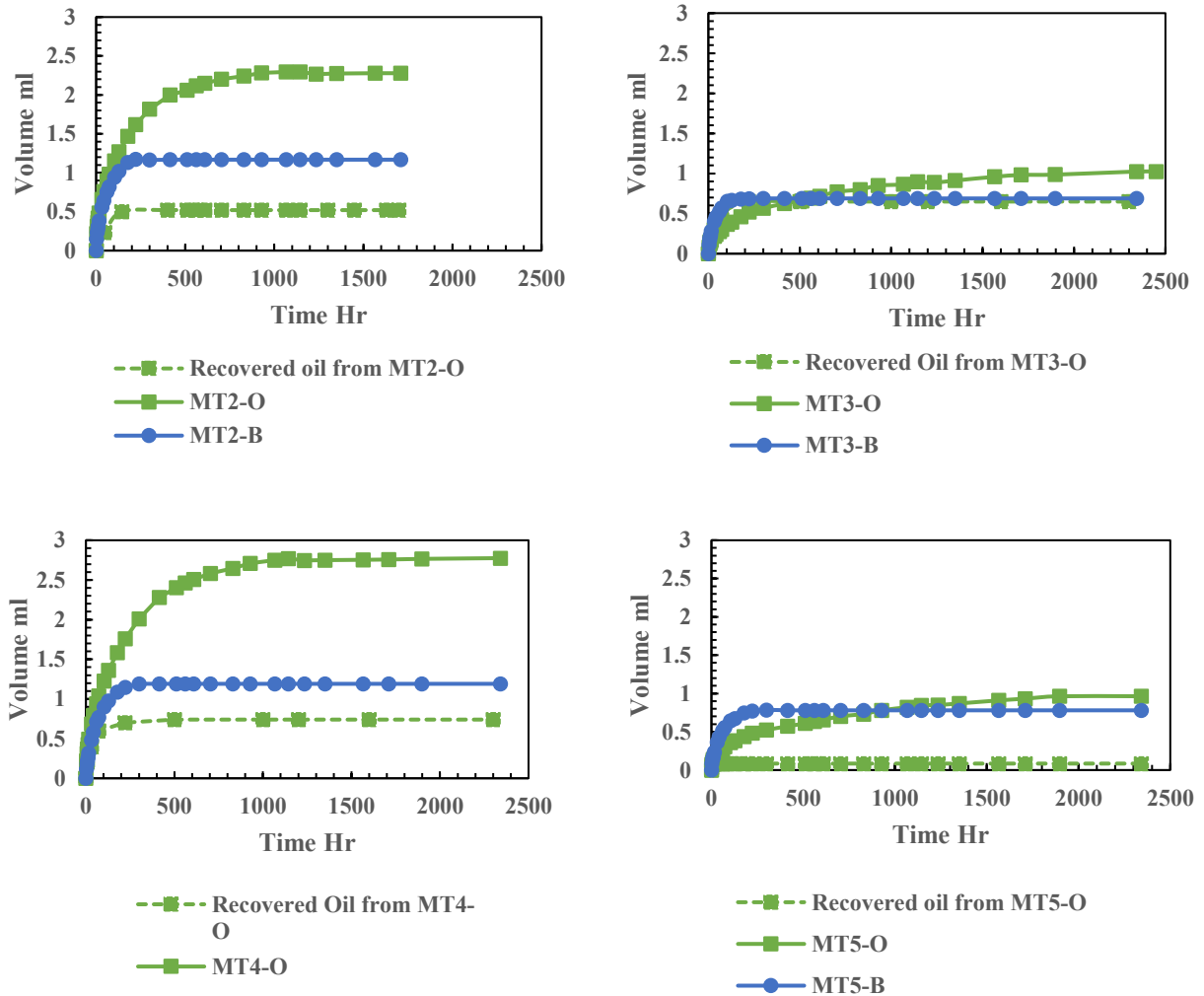


Figure 13. Imbibition-recovery (IR) trios for the five twin plugs.

The similarities between oil-recovery and brine imbibition curves suggest that capillarity is the main driving force for oil-recovery. Fluid displacement during spontaneous imbibition is dominated by two main driving forces: capillary force and gravity force. We use inverse Bond number^{33, 34} to comparatively investigate the effect of capillary and gravity forces during a counter-current imbibition process:

$$N_B^{-1} = C \frac{\delta \cos \theta \sqrt{\frac{\phi}{K}}}{(\Delta \rho) g H}$$

Where $C=0.4$ if we assume pores are a bundle of capillary tubes, $(\Delta\rho)$ is the difference in density of water and oil (Kg/m^3), δ is interfacial tension (N/m), g is gravity (m/s^2), H is height of the core (m), φ is porosity and K is absolute permeability (m^2). If $N_B^{-1} > 5$ capillary forces dominate; if $0.2 < N_B^{-1} < 5$ both capillary and gravity forces are effective and if $N_B^{-1} < 0.2$ gravity forces are dominate ³⁵. Table 5 lists the calculated inverse Bond numbers for all five samples. The results are much higher than 5 for all samples, confirming the dominance of capillary forces in the soaking tests.

Table 5. Inverse Bond numbers calculated for the five soaking tests.

| Sample | MT1 | MT2 | MT3 | MT4 | MT5 |
|---------------|------------|------------|------------|------------|------------|
| N_B^{-1} | 123 | 328 | 245 | 343 | 511 |

IV. Parameters effecting recovery

We define recovery index as recovered oil during recovery tests divided by sample pore volume.

$$RI = \frac{\text{Recovered oil (ml)}}{\text{Sample pore volume (ml)}}$$

In the next three sections, we investigate the role of petrophysical properties (porosity, permeability and wettability) on the recovery index of the core plugs.

Porosity

Figure 14 shows the values of recovery index on the primary axis versus porosity for the five tested samples. Initial normalized oil (amount of saturated oil during spontaneous oil imbibition process divided by the pore volume) in samples is shown on the secondary axis. According to Figure 14 both recovery index and initial normalized oil in samples increase with porosity. Samples with higher porosity imbibe more oil and subsequently produce more oil. Recovery index of each sample is always less than the initial normalized oil in of the sample. Initial normalized oil in samples increase linearly versus porosity; however, recovery index versus porosity shows a weaker linear trend. A closer investigation reveals that recovery index for fractured samples (MT1 and MT3) are higher than intact sample (MT2, MT4, MT5). Recovery index of the

intact samples also show a linear trend with a porosity threshold where there's zero recovery for samples with lower porosity than the threshold. Recovery index of the fractured samples are higher than recovery index of intact samples (baseline) and lower than initial normalized oil in samples (top line). We name this zone as favourable recovery zone. Figure 13 shows there is a porosity threshold (0.025) for recovery index of intact samples. In these experiments, recovery tests are done at atmospheric pressure and temperature.

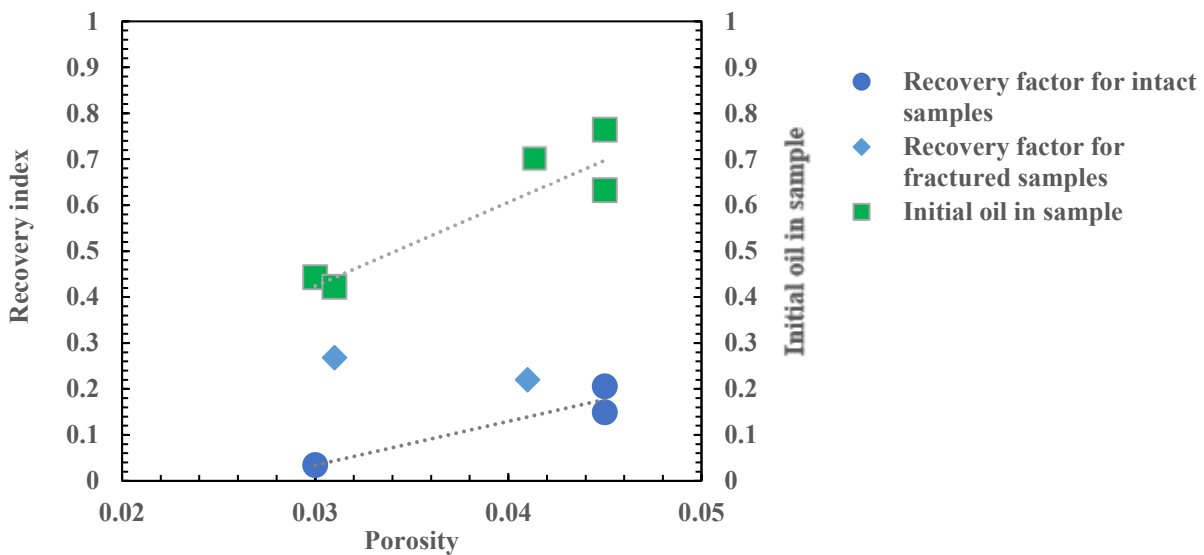


Figure 14. Recovery index versus porosity for the five samples are shown on the primary vertical axis. Recovery index for fractured samples (MT1 and MT3) are higher than that for intact samples (MT2, MT4, MT5). Initial normalized oil in samples are shown on secondary vertical axis. Intact samples have a cut-off recovery threshold of 0.025.

Permeability

In this section, we apply a permeability transformation approach to the results of Figure 14 to infer recovery index versus permeability for both intact and fractured samples. Pore-network of tight sandstone rocks are often made up from interconnected pores at the presence of a network of micro-cracks around quartz grains^{5, 36-39}. Figure 15 shows a micro-crack with a length of 20 microns on the surface of MT1. The length of the

micro-crack is almost 1000 times the median pore throat size of the rock sample. During spontaneous imbibition of wetting fluid, induction of such cracks or enlargement of the existing microfractures can enhance total rock permeability¹⁴. Subsequently, such permeability enhancement of the rock can enhance hydrocarbon recovery from low-permeability rocks. Figures 16 (a) and (b) show the expelled oil droplets show recovered oil droplets along a natural fracture at two different times. Such fractures create a preferential path for oil production by water imbibition.

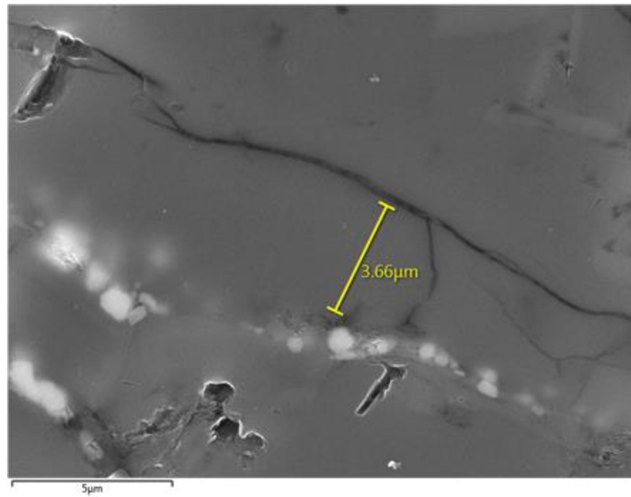


Figure 15. A micro-crack captured on the surface of MT1.

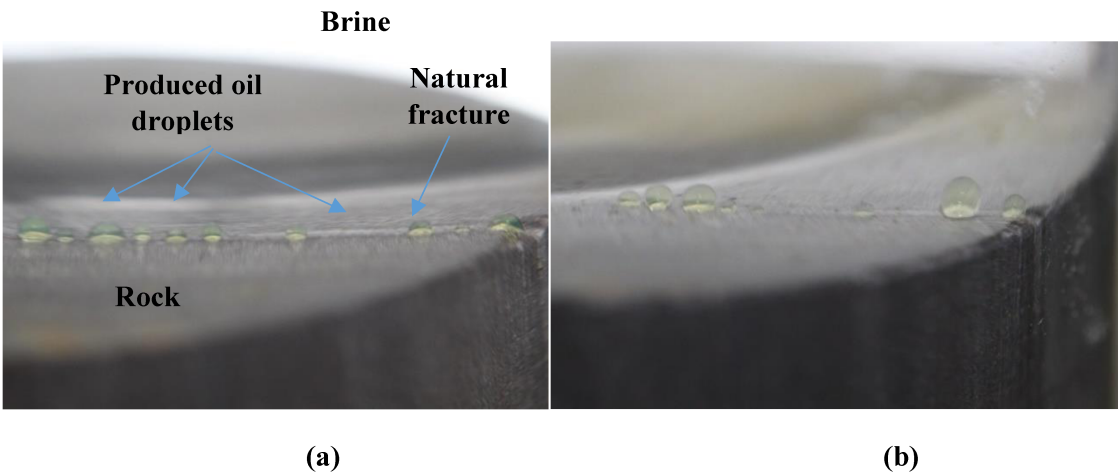


Figure 16. (a) Recovered oil along a fracture line of MT1 at after $t=10$ days (b) Recovered oil along a fracture line of MT1 after $t=20$ days.

Such micro-cracks/fractures can significantly enhance the rock permeability, even though these cracks might only have limited influence on total porosity. In Figure 14, we showed recovery index versus porosity for both intact and fractured samples. We also showed that fractured samples have higher recovery index. Enhanced recovery index of fractured samples (MT1 and MT3) are due to enhanced permeability and rock-fluid interface. By using permeability-porosity relationship from multivariate scatterplots of Figure 2, we transform recovery-porosity plots to recovery-permeability plots. Figure 17 schematically illustrates the procedure for such transformation for both fractured and intact rock samples. 1 refers to an intact sample (with porosity P_1 , permeability K_1 and recovery index R_1) and 2 refers to a fractured sample (with recovery index R_2). For the intact samples, the corresponding permeability is calculated using the permeability-porosity crossplot. In order to find equivalent permeability (K_2) for a fractured sample, we use the baseline (recovery index versus porosity for intact samples) to calculate the equivalent porosity and permeability of a fractured sample. As Figure 17 shows, calculated equivalent permeability of the fractured sample (K_2) is higher than the calculated permeability of the intact sample (K_1).

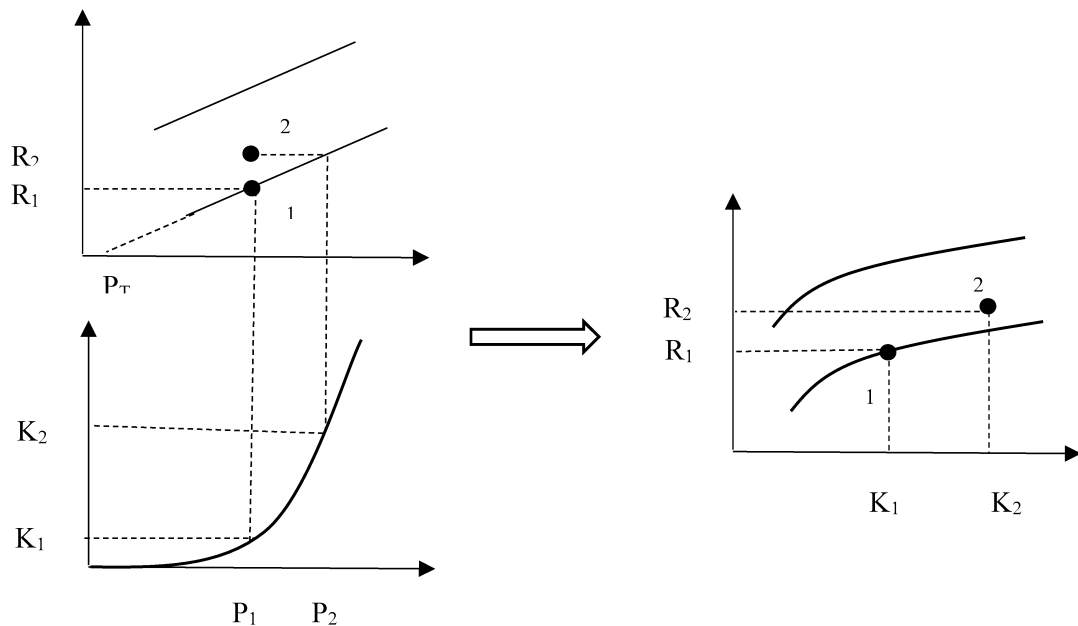


Figure 17. Transforming recovery vs. porosity plot to recovery vs. permeability plot using permeability-porosity relationship from multivariate scatterplots.

We apply the permeability transformation approach to the results of Figure 14 to infer recovery index versus permeability. Figure 18 shows the results of the permeability transformation. Similar to figure 14, we have a baseline which is recovery index versus permeability for intact samples. The permeability baseline is calculated by combining the recovery index versus porosity correlation for intact samples from Figure 14 and permeability versus porosity from multivariate crossplots of Figure 2. The permeability topline is calculated by combining the initial normalized oil in samples versus porosity correlation from Figure 14 and permeability versus porosity from multivariate crossplots of Figure 2. The calculated equivalent permeability of the fractured samples MT1 and MT3 lies between the baseline permeability and the top line.

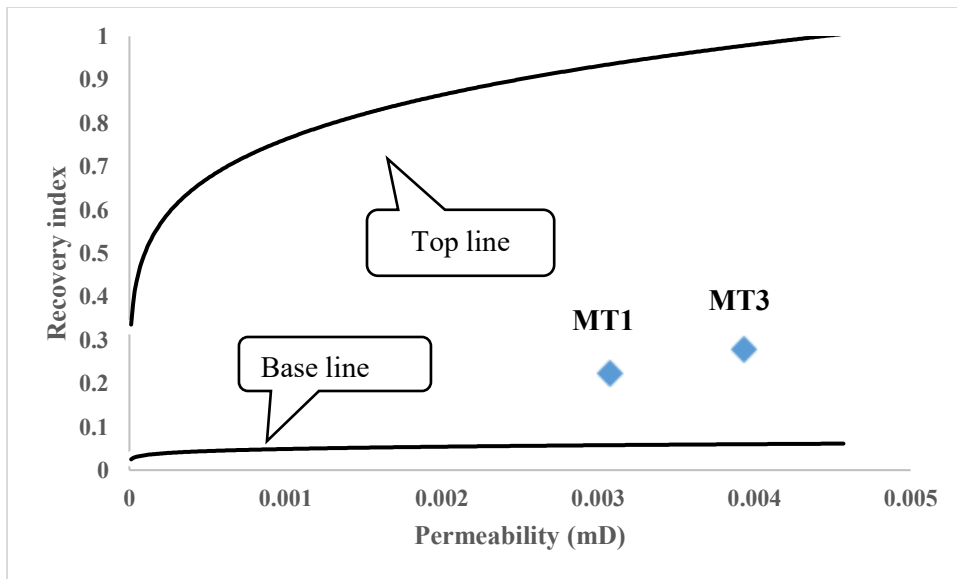


Figure 18. The result of the permeability transformation. The permeability of the fractured samples MT1 and MT3 lies between the baseline permeability and the top line permeability.

Median pore throat size

The objective of this section is to evaluate effect of pore-throat size on oil recovery. According to IR-trios from recovery tests, for each twin set, the oil recovery curve follows the trend of brine spontaneous imbibition curve, and the final oil recovery is always less than the equilibrated water uptake. This interesting observation indicates that water can only access the hydrophilic part of the pore network initially saturated with oil. MICP results (Figure 5) of the samples show that mercury cannot access pores $< 2\text{nm}$ and these pores form 20% of the pore space. The results of oil-recovery versus porosity show that the recovery index of the samples with lower porosity is lower. Multivariate plots of Figure 2 show that samples with lower porosity have lower median pore throat size and the relationship is in the form of power law. So, one can argue that oil recovery from the samples with smaller median pore size is lower. There can be two reasons for this observation: 1) Samples with lower porosity have less available pore space to imbibe oil during spontaneous oil imbibition and subsequently produce less oil during recovery tests 2) There is more trapped oil (per pore volume) in small-scale pores. In Table 2 we reported TOC of the samples measured from Rock-Eval tests. Organic matter is oil-wet and hence may lead to dual-wettability characteristics of the rock samples. Recovery of the oil retained in small hydrophobic pores is a unique challenge. Pores covered with organic matter are smaller. We also showed that there is a cut-off porosity (porosity is correlated to median pore-throat size from multivariate scatterplots of Figure 2) and subsequently a corresponding median pore throat size for oil recovery. So, we conclude that small pores are hydrophobic and tend to imbibe less brine/water and subsequently recover less oil.

Conclusions

In this research, we applied dual core imbibition technique (DCI) to five sets of twin plugs cored from the Montney Formation. First, we did contact angle tests. Next, we did spontaneous imbibition tests by putting one plug of each pair in oil and the other pair in brine and measured the weight gain of each pair during spontaneous imbibition process until equilibrium is reached. Finally, placed the oil-saturated

samples from the previous stage in brine, and measured the volume of recovered oil with respect to time. We compared the oil-recovery profiles with the imbibition profiles of oil and brine, obtained from the imbibition tests. The results can be summarized as follows:

- 1- Contact angle tests: According to air/liquid contact angle tests, the samples are fully oil-wet and partially brine-wet, consistent with the results of imbibition tests on dry core plugs. According to liquid-liquid tests, the samples are brine-wet, consistent with the results of counter-current imbibition tests on oil-saturated samples.
- 2- Spontaneous imbibition tests: In general, brine imbibes faster than oil into the dry samples, but the brine imbibition profiles reach to the equilibrium state faster than the oil imbibition profiles. Furthermore, the final imbibed volume of brine is significantly lower than that of oil, suggesting that a significant part of the pore network is water repellent. Analysis of the imbibition profiles and SEM images indicate that the water-repellent pores are smaller than water-wet pores, mainly represented by the tail part of the MICP pore-throat size distribution profiles.
- 3- Oil-recovery tests: In general, the shape of imbibition oil-recovery profiles is similar to that of water imbibition profiles for dry samples. This observation indicates that the oil recovered during water imbibition into oil-saturated samples comes from the water-wet part of the pore-network, which can be accessed by water when the samples are soaked in water. In addition, the results suggest that there is an approximate porosity threshold of 0.025, below which, oil can hardly be produced by spontaneous imbibition of water.

References

- [1] R. Arabjamaloei, S. Shadizadeh, A new approach for specifying imbibition face boundary condition in countercurrent spontaneous imbibition, *Petroleum Science and Technology*, 28 (2010) 1855-1862.
- [2] H. Fischer, N.R. Morrow, Scaling of oil recovery by spontaneous imbibition for wide variation in aqueous phase viscosity with glycerol as the viscosifying agent, *Journal of Petroleum Science and Engineering*, 52 (2006) 35-53.
- [3] Y. Li, D. Ruth, G. Mason, N.R. Morrow, Pressures acting in counter-current spontaneous imbibition, *Journal of Petroleum Science and Engineering*, 52 (2006) 87-99.
- [4] K. Schmid, S. Geiger, Universal scaling of spontaneous imbibition for water-wet systems, *water resources research*, 48 (2012).
- [5] H.S. Behbahani, G. Di Donato, M.J. Blunt, Simulation of counter-current imbibition in water-wet fractured reservoirs, *Journal of Petroleum Science and Engineering*, 50 (2006) 21-39.
- [6] M. Shouxiang, N.R. Morrow, X. Zhang, Generalized scaling of spontaneous imbibition data for strongly water-wet systems, *Journal of Petroleum Science and Engineering*, 18 (1997) 165-178.
- [7] H. Behbahani, M.J. Blunt, Analysis of imbibition in mixed-wet rocks using pore-scale modeling, *SPE Journal*, 10 (2005) 466-474.
- [8] D. Wang, J. Cheng, Q. Yang, G. Wenchao, L. Qun, F. Chen, Viscous-elastic polymer can increase microscale displacement efficiency in cores, in: *SPE annual technical conference and exhibition*, Society of Petroleum Engineers, 2000.
- [9] E. Aspenes, G. Ersland, A. Graue, J. Stevens, B.A. Baldwin, Wetting phase bridges establish capillary continuity across open fractures and increase oil recovery in mixed-wet fractured chalk, *Transport in Porous Media*, 74 (2008) 35-47.
- [10] A. Ishakoğlu, A.F. Baytaş, Measurement and evaluation of saturations for water, ethanol and a light non-aqueous phase liquid in a porous medium by gamma attenuation, *Applied Radiation and Isotopes*, 56 (2002) 601-606.

- [11] M. Prodanović, W. Lindquist, R. Seright, Porous structure and fluid partitioning in polyethylene cores from 3D X-ray microtomographic imaging, *Journal of Colloid and Interface Science*, 298 (2006) 282-297.
- [12] G. Mason, H. Fischer, N. Morrow, D. Ruth, S. Wo, Effect of sample shape on counter-current spontaneous imbibition production vs time curves, *Journal of Petroleum Science and Engineering*, 66 (2009) 83-97.
- [13] S. Ma, N. Morrow, X. Zhang, Generalized scaling of spontaneous imbibition data for strongly water-wet systems, in: *Technical Meeting/Petroleum Conference of The South Saskatchewan Section, Petroleum Society of Canada*, 1995.
- [14] A. Habibi, H. Dehghanpour, M. Binazadeh, D. Bryan, G. Uswak, *Advances in Understanding Wettability of Tight Oil Formations: A Montney Case Study*, *SPE Reservoir Evaluation & Engineering*, (2016).
- [15] Y. Yang, A.C. Aplin, A permeability–porosity relationship for mudstones, *Marine and Petroleum Geology*, 27 (2010) 1692-1697.
- [16] P.H. Nelson, Pore-throat sizes in sandstones, tight sandstones, and shales, *AAPG bulletin*, 93 (2009) 329-340.
- [17] X. Zhou, N.R. Morrow, S. Ma, Interrelationship of wettability, initial water saturation, aging time, and oil recovery by spontaneous imbibition and waterflooding, *SPE Journal*, 5 (2000) 199-207.
- [18] Z. Tong, X. Xie, N.R. Morrow, Crude oil composition and the stability of mixed wettability in sandstones, *Petrophysics*, 44 (2003).
- [19] Q. Lan, H. Dehghanpour, J. Wood, H. Sanei, Wettability of the Montney tight gas formation, *SPE Reservoir Evaluation & Engineering*, (2015).
- [20] Javaheri A, Dehghanpour H, Wood J. Imbibition Oil Recovery from Tight Rocks with Dual-Wettability Pore-Network A Montney Case Study. In *SPE Unconventional Resources Conference 2017 Feb 15*. Society of Petroleum Engineers..
- [21] G. Tang, N.R. Morrow, Salinity, temperature, oil composition, and oil recovery by waterflooding, *SPE Reservoir Engineering*, 12 (1997) 269-276.

- [22] N. Loahardjo, N.R. Morrow, Oil recovery from Bentheim sandstone by sequential waterflooding and spontaneous imbibition, *Petrophysics*, 54 (2013) 547-553.
- [23] D.J. Ligthelm, J. Gronsveld, J. Hofman, N. Brussee, F. Marcelis, H. van der Linde, Novel Waterflooding Strategy By Manipulation Of Injection Brine Composition, in: EUROPEC/EAGE Conference and Exhibition, Society of Petroleum Engineers, 2009.
- [24] S. Wickramathilaka, J. Howard, J. Stevens, N. Morrow, G. Mason, Å. Haugen, A. Graue, M. Fernø, Magnetic resonance imaging of oil recovery during spontaneous imbibition from cores with two-ends open boundary condition, in: Proceeding of the International Society of Core Analysts Annual Meeting. September, 2011, pp. 18-21.

Chapter 5

Conclusions

In this research, we applied dual core imbibition technique (DCI) to the plugs cored from Montney formation. First, we did spontaneous imbibition tests by putting one plug of each pair in oil and the other pair in brine and measured the weight gain of each pair during spontaneous imbibition process until equilibrium is reached. Next, we did recovery tests by placing the oil saturated sample during spontaneous imbibition process from previous stage in brine. All samples start producing oil. We measured the amount of recovered oil by time. Finally we plotted the two spontaneous imbibition plots of oil and brine we obtained from spontaneous imbibition tests along with recovery plots we obtained from recovery tests in one recovery graph-trio plot. The IR trios of all pairs indicate recovery curves follow the exact trend of brine spontaneous imbibition curves. Next, we measured oil and brine uptake of twin plugs cored from the Montney formation. First, we parametrized imbibed quantities of oil and brine into each twin set. We defined two sets of affinity indices: slope affinity index and equilibrium affinity index. Through multivariate scatterplots, we investigated correlations between indices and other petrophysical properties such as porosity, permeability, gamma spectra and neutron porosity logs.

Next, we proposed a new characterization scheme based on spontaneous imbibition results. We proposed a decoupling model, which decouples the two different imbibition regions of imbibition profile by assuming there are two different pore network within this rock type, one associated with inter granular pores and other intra granular pores. We developed relevant analytical models for both types of imbibition profiles. Next, we analyzed pore size distribution of samples in one graph. Then we investigated SEM images of rock sample MT6. We can easily detect two different types of pores in the images which again is in agreement with our decoupling model.

The following results are inferred after analyzing experimental results:

- 4- In general, oil imbibes slower than brine in the samples, but finally reaches to equilibrium with a higher value compared to brine.
- 5- Both slope affinity and equilibrium affinity indices for the oil phase increase by increasing ϕ and k , with slope affinity showing a stronger correlation. This observation suggests that part of the pore network has a stronger affinity to oil than to water.
- 6- Air-liquid contact angle results suggest that the samples are preferentially oil-wet, as oil fully spreads on the rock surface while brine partially wets the surface.
- 7- Spontaneous imbibition process is the main mechanism behind recovery process of Montney tight rock samples.
- 8- The oil recovery curve follows the trend of brine spontaneous imbibition curve, and the final oil recovery is always less than the equilibrated water uptake. This interesting observation indicates that water can only access the hydrophilic part of the pore network initially saturated with oil.

Overall, this study demonstrates that porosity is a key parameter controlling the fluid uptake and subsequent recovery of tight rock core samples from the Montney formation. We also observed useful correlations between rock wettability and neutron porosity and spectral gamma ray logs. Such correlations can be applied for quick evaluation of rock wettability by using the commonly-available open-whole logs.

References

1. Balogun, A. S.; Kazemi, H.; Ozkan, E.; Al-Kobaisi, M.; Ramirez, B. A. In *Verification and proper use of water-oil transfer function for dual-porosity and dual-permeability reservoirs*, SPE Middle East Oil and Gas Show and Conference, 2007; Society of Petroleum Engineers: 2007.
2. Barzegar Alamdari, B.; Kiani, M.; Kazemi, H. In *Experimental and numerical simulation of surfactant-assisted oil recovery in tight fractured carbonate reservoir cores*, SPE Improved Oil Recovery Symposium, 2012; Society of Petroleum Engineers: 2012.
3. Bennion, D. B.; Thomas, F. B., Formation damage issues impacting the productivity of low permeability, low initial water saturation gas producing formations. *Journal of energy resources technology* **2005**, 127, (3), 240-247.
4. Bohacs, K.; Passey, Q.; Rudnicki, M.; Esch, W.; Lazar, O. In *The Spectrum of Fine-Grained Reservoirs from 'Shale Gas' to 'Shale Oil'/Tight Liquids: Essential Attributes, Key Controls, Practical Characterization*, IPTC 2013: International Petroleum Technology Conference, 2013; 2013.
5. Cai, J.; Yu, B., A discussion of the effect of tortuosity on the capillary imbibition in porous media. *Transport in Porous Media* **2011**, 89, (2), 251-263.
6. Carrier III, W. D., Goodbye, hazen; hello, kozeny-carman. *Journal of geotechnical and geoenvironmental engineering* **2003**, 129, (11), 1054-1056.
7. Cheng, Y., Impact of water dynamics in fractures on the performance of hydraulically fractured wells in gas-shale reservoirs. *Journal of Canadian Petroleum Technology* **2012**, 51, (02), 143-151.
8. Chilingar, G. V.; Yen, T., Some notes on wettability and relative permeabilities of carbonate reservoir rocks, II. *Energy Sources* **1983**, 7, (1), 67-75.

9. Clarkson, C. R.; Jensen, J. L.; Pedersen, P. K.; Freeman, M., Innovative methods for flow-unit and pore-structure analyses in a tight siltstone and shale gas reservoir. *AAPG bulletin* **2012**, 96, (2), 355-374.
10. Clarkson, C. R.; Wood, J.; Burgis, S.; Aquino, S.; Freeman, M., Nanopore-structure analysis and permeability predictions for a tight gas siltstone reservoir by use of low-pressure adsorption and mercury-intrusion techniques. *SPE Reservoir Evaluation & Engineering* **2012**, 15, (06), 648-661.
11. Comisky, J. T.; Santiago, M.; McCollom, B.; Buddhala, A.; Newsham, K. E. In *Sample size effects on the application of mercury injection capillary pressure for determining the storage capacity of tight gas and oil shales*, Canadian unconventional resources conference, 2011; Society of Petroleum Engineers: 2011.
12. David, C.; Wong, T.-F.; Zhu, W.; Zhang, J., Laboratory measurement of compaction-induced permeability change in porous rocks: Implications for the generation and maintenance of pore pressure excess in the crust. *Pure and Applied Geophysics* **1994**, 143, (1-3), 425-456.
13. Davies, G. R.; Moslow, T. F.; Sherwin, M. D., The lower Triassic Montney formation, west-central Alberta. *Bulletin of Canadian Petroleum Geology* **1997**, 45, (4), 474-505.
14. Dehghanpour, H.; Lan, Q.; Saeed, Y.; Fei, H.; Qi, Z., Spontaneous imbibition of brine and oil in gas shales: effect of water adsorption and resulting microfractures. *Energy & Fuels* **2013**, 27, (6), 3039-3049.
15. Dehghanpour, H.; Zubair, H.; Chhabra, A.; Ullah, A., Liquid intake of organic shales. *Energy & Fuels* **2012**, 26, (9), 5750-5758.
16. Donaldson, E. C.; Alam, W., *Wettability*. Elsevier: 2013.
17. Dong, J.-J.; Hsu, J.-Y.; Wu, W.-J.; Shimamoto, T.; Hung, J.-H.; Yeh, E.-C.; Wu, Y.-H.; Sone, H., Stress-dependence of the permeability and porosity of sandstone and shale from TCDP Hole-A. *International Journal of Rock Mechanics and Mining Sciences* **2010**, 47, (7), 1141-1157.

18. Duan, Z.; Davy, C. A.; Agostini, F.; Jeannin, L.; Troadec, D.; Skoczylas, F., Gas recovery potential of sandstones from tight gas reservoirs. *International Journal of Rock Mechanics and Mining Sciences* **2014**, *65*, 75-85.
19. Fan, L.; Thompson, J. W.; Robinson, J. R. In *Understanding gas production mechanism and effectiveness of well stimulation in the Haynesville Shale through reservoir simulation*, Canadian Unconventional Resources and International Petroleum Conference, 2010; Society of Petroleum Engineers: 2010.
20. Fu, X.; Agostini, F.; Skoczylas, F.; Jeannin, L., Experimental study of the stress dependence of the absolute and relative permeabilities of some tight gas sandstones. *International Journal of Rock Mechanics and Mining Sciences* **2015**, *77*, 36-43.
21. Ghabezloo, S.; Sulem, J.; Guédon, S.; Martineau, F., Effective stress law for the permeability of a limestone. *International Journal of Rock Mechanics and Mining Sciences* **2009**, *46*, (2), 297-306.
22. Ghiasi, M. M., Yarveicy, H., Arabloo, M., Mohammadi, A. H., & Behbahani, R. M. "Modeling of stability conditions of natural gas clathrate hydrates using least squares support vector machine approach." *Journal of Molecular Liquids* *223* (2016): 1081-1092.
23. Gilman, J. R. In *Practical aspects of simulation of fractured reservoirs*, International Forum on Reservoir Simulation, Buhl, Baden-Baden, Germany, 2003; 2003; pp 23-27.
24. Gruener, S.; Hermes, H. E.; Schillinger, B.; Egelhaaf, S. U.; Huber, P., Capillary rise dynamics of liquid hydrocarbons in mesoporous silica as explored by gravimetry, optical and neutron imaging: Nano-rheology and determination of pore size distributions from the shape of imbibition fronts. *Colloids and Surfaces A: Physicochemical and Engineering Aspects* **2016**, *496*, 13-27.

25. Habibi, A.; Dehghanpour, H.; Binazadeh, M.; Bryan, D.; Uswak, G., Advances in Understanding Wettability of Tight Oil Formations: A Montney Case Study. *SPE Reservoir Evaluation & Engineering* **2016**.
26. Handy, L., Determination of effective capillary pressures for porous media from imbibition data. *Trans. AIME* **1960**, 219, 75-80.
27. Hensen, E. J.; Smit, B., Why clays swell. *The Journal of Physical Chemistry B* **2002**, 106, (49), 12664-12667.
28. Holditch, S. A., Factors affecting water blocking and gas flow from hydraulically fractured gas wells. *Journal of Petroleum Technology* **1979**, 31, (12), 1,515-1,524.
29. Holditch, S. A., Tight gas sands. *Journal of Petroleum Technology* **2006**, 58, (06), 86-93.
30. Jinxing, D.; Yunyan, N.; Xiaoqi, W., Tight gas in China and its significance in exploration and exploitation. *Petroleum Exploration and Development* **2012**, 39, (3), 277-284.
31. Jones, F. O.; Owens, W., A laboratory study of low-permeability gas sands. *Journal of Petroleum Technology* **1980**, 32, (09), 1,631-1,640.
32. King, G. E. In *Hydraulic fracturing 101: what every representative, environmentalist, regulator, reporter, investor, university researcher, neighbor and engineer should know about estimating frac risk and improving frac performance in unconventional gas and oil wells*, SPE Hydraulic Fracturing Technology Conference, 2012; Society of Petroleum Engineers: 2012.
33. Kuru, E.; Parmar, J. S.; Dehghanpour, H. In *Drainage against gravity: factors impacting the load recovery in fractures*, SPE Unconventional Resources Conference-USA, 2013; Society of Petroleum Engineers: 2013.
34. Lan, Q.; Dehghanpour, H.; Wood, J.; Sanei, H., Wettability of the Montney tight gas formation. *SPE Reservoir Evaluation & Engineering* **2015**.

35. Lan, Q.; Xu, M.; Dehghanpour, H.; Wood, J. In *Advances in understanding wettability of tight and shale gas formations*, SPE Annual Technical Conference and Exhibition, 2014; Society of Petroleum Engineers: 2014.
36. Levorsen, A. I.; Berry, F. A. F., *Geology of petroleum*. WH Freeman San Francisco: 1967.
37. Loucks, R. G.; Reed, R. M.; Ruppel, S. C.; Hammes, U., Spectrum of pore types and networks in mudrocks and a descriptive classification for matrix-related mudrock pores. *AAPG bulletin* **2012**, 96, (6), 1071-1098.
38. Ma, S.; Zhang, X.; Morrow, N.; Zhou, X., Characterization of wettability from spontaneous imbibition measurements. *Journal of Canadian Petroleum Technology* **1999**, 38, (13).
39. Mahadevan, J.; Le, D.; Hoang, H. In *Impact of capillary suction on fracture face skin evolution in waterblocked wells*, Paper SPE presented at SPE Hydraulic Fracturing Technology Conference, The Woodlands, Texas, 2009; 2009.
40. Makhanov, K.; Habibi, A.; Dehghanpour, H.; Kuru, E., Liquid uptake of gas shales: A workflow to estimate water loss during shut-in periods after fracturing operations. *Journal of Unconventional Oil and Gas Resources* **2014**, 7, 22-32.
41. Markhasin, B., *Sedimentology and stratigraphy of the Lower Triassic Montney Formation, subsurface of northwestern Alberta*. University of Calgary: 1997.
42. Mitchell, A.; Hazell, L.; Webb, K. In *Wettability determination: pore surface analysis*, SPE Annual Technical Conference and Exhibition, 1990; Society of Petroleum Engineers: 1990.
43. Nasr-El-Din, H.; Al-Otaibi, M.; Al-Aamri, A.; Ginest, N. In *Surface tension of completion brines*, SPE International Symposium on Oilfield Chemistry, 2005; Society of Petroleum Engineers: 2005.

44. Novlesky, A.; Kumar, A.; Merkle, S. In *Shale Gas Modeling Workflow: From Microseismic to Simulation--A Horn River Case Study*, Canadian Unconventional Resources Conference, 2011; Society of Petroleum Engineers: 2011.
45. Ostensen, R., Microcrack permeability in tight gas sandstone. *Society of Petroleum Engineers Journal* **1983**, 23, (06), 919-927.
46. Parmar, J.; Dehghanpour, H.; Kuru, E. In *Unstable displacement: a missing factor in fracturing fluid recovery*, SPE Canadian Unconventional Resources Conference, 2012; Society of Petroleum Engineers: 2012.
47. Parmar, J.; Dehghanpour, H.; Kuru, E., Displacement of water by gas in propped fractures: Combined effects of gravity, surface tension, and wettability. *Journal of Unconventional Oil and Gas Resources* **2014**, 5, 10-21.
48. Penumadu, D.; Dean, J., Compressibility effect in evaluating the pore-size distribution of kaolin clay using mercury intrusion porosimetry. *Canadian Geotechnical Journal* **2000**, 37, (2), 393-405.
49. Rezaveisi, M.; Rostami, B.; Kharrat, R.; Ayatollahi, S.; Ghotbi, C., Experimental investigation of tertiary oil gravity drainage in fractured porous media. *Special Topics & Reviews in Porous Media: An International Journal* **2010**, 1, (2).
50. Ross, D. J.; Bustin, R. M., The importance of shale composition and pore structure upon gas storage potential of shale gas reservoirs. *Marine and Petroleum Geology* **2009**, 26, (6), 916-927.
51. Roychaudhuri, B.; Tsotsis, T.; Jessen, K., An experimental and numerical investigation of spontaneous imbibition in gas shales, paper presented at SPE Annual Technical Conference and Exhibition, Soc. of Pet. In Eng: 2011.
52. Schechter, D.; Zhou, D.; Orr, F., Low IFT drainage and imbibition. *Journal of Petroleum science and Engineering* **1994**, 11, (4), 283-300.

53. Settari, A.; Sullivan, R.; Bachman, R. In *The modeling of the effect of water blockage and geomechanics in waterfracs*, SPE Annual Technical Conference and Exhibition, 2002; Society of Petroleum Engineers: 2002.
54. Shaoul, J. R.; van Zelm, L. F.; De Pater, C., Damage mechanisms in unconventional-gas-well Stimulation--a new look at an old problem. *SPE Production & Operations* **2011**, 26, (04), 388-400.
55. Sharif, A., Tight gas resources in Western Australia. *Petroleum in Western Australia September* **2007**, 28-31.
56. Sharma, M.; Agrawal, S. In *Impact of liquid loading in hydraulic fractures on well productivity*, SPE hydraulic fracturing technology conference, 2013; Society of Petroleum Engineers: 2013.
57. Sigal, R. F., A methodology for blank and conformance corrections for high pressure mercury porosimetry. *Measurement Science and Technology* **2009**, 20, (4), 045108.
58. Sing, K., Everett. DH, Haul RAW, Moscou L, Pierotti RA, Rouquérol J and Siemieniowska T 1985. *Pure Appl. Chem* 57, 603.
59. Sondergeld, C. H.; Newsham, K. E.; Comisky, J. T.; Rice, M. C.; Rai, C. S. In *Petrophysical considerations in evaluating and producing shale gas resources*, SPE Unconventional Gas Conference, 2010; Society of Petroleum Engineers: 2010.
60. Strand, S.; Standnes, D. C.; Austad, T., Spontaneous imbibition of aqueous surfactant solutions into neutral to oil-wet carbonate cores: Effects of brine salinity and composition. *Energy & fuels* **2003**, 17, (5), 1133-1144.
61. Thomas, R. D.; Ward, D. C., Effect of overburden pressure and water saturation on gas permeability of tight sandstone cores. *Journal of Petroleum Technology* **1972**, 24, (02), 120-124.

62. Wang, Q.; Chen, X.; Jha, A. N.; Rogers, H., Natural gas from shale formation—the evolution, evidences and challenges of shale gas revolution in United States. *Renewable and Sustainable Energy Reviews* **2014**, 30, 1-28.
63. Warpinski, N.; Teufel, L., Determination of the effective-stress law for permeability and deformation in low-permeability rocks. *SPE formation evaluation* **1992**, 7, (02), 123-131.
64. Wood, J., Water distribution in the Montney tight gas play of the western Canadian sedimentary basin: significance for resource evaluation. *SPE Reservoir Evaluation & Engineering* **2013**, 16, (03), 290-302.
65. Yarveicy, H., Moghaddam, A. K., & Ghiasi, M. M.. "Practical use of statistical learning theory for modeling freezing point depression of electrolyte solutions: LSSVM model." *Journal of Natural Gas Science and Engineering* 20 (2014): 414-421.
66. Yarveicy, H., & Javaheri, A. "Application of Lauryl Betaine in enhanced oil recovery: A comparative study in micromodel." *Petroleum*(2017).
67. Yarveicy, H., & Haghtalab, A.. "Effect of amphoteric surfactant on phase behavior of hydrocarbon-electrolyte-water system-an application in enhanced oil recovery." *Journal of Dispersion Science and Technology* just-accepted (2017).
68. Yarveicy, H., & Ghiasi, M. M.. "Modeling of gas hydrate phase equilibria: Extremely randomized trees and LSSVM approaches." *Journal of Molecular Liquids* (2017).
69. Zhang, X.; Morrow, N. R.; Ma, S., Experimental verification of a modified scaling group for spontaneous imbibition. *SPE Reservoir Engineering* **1996**, 11, (04), 280-285.
70. Zheng, J.; Zheng, L.; Liu, H.-H.; Ju, Y., Relationships between permeability, porosity and effective stress for low-permeability sedimentary rock. *International Journal of Rock Mechanics and Mining Sciences* **2015**, 78, 304-318.

71. Zonneveld, J.-P.; MacNaughton, R. B.; Utting, J.; Beatty, T. W.; Pemberton, S. G.; Henderson, C. M., Sedimentology and ichnology of the Lower Triassic Montney Formation in the Pedigree-Ring/Border-Kahntah River area, northwestern Alberta and northeastern British Columbia. *Bulletin of Canadian Petroleum Geology* **2010**, 58, (2), 115-140.
72. Zou, C.; Zhu, R.; Liu, K.; Su, L.; Bai, B.; Zhang, X.; Yuan, X.; Wang, J., Tight gas sandstone reservoirs in China: characteristics and recognition criteria. *Journal of Petroleum Science and Engineering* **2012**, 88, 82-91.